LIÈGE université
Gembloux
Agro-Bio Tech

Winter Wheat Phenotyping Based on Unmanned Aerial Vehicle Remote Sensing and Machine Learning - From Yield Prediction to Growth Diagnosis

Yulin Shen

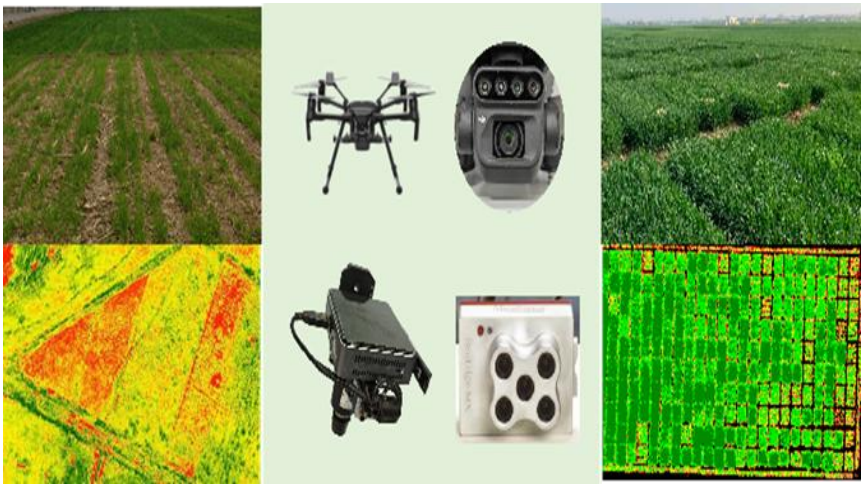

COMMUNAUTÉ FRANÇAISE DE BELGIQUE
UNIVERSITÉ DE LIÈGE — GEMBLOUX AGRO-BIO TECH

WINTER WHEAT PHENOTYPING BASED ON UNMANNED AERIAL VEHICLE REMOTE SENSING AND MACHINE LEARNING -FROM YIELD PREDICTION TO GROWTH DIAGNOSIS

Yulin Shen

Dissertation originale présentée en vue de l'obtention du grade de docteur en sciences agronomiques et ingénierie biologique

Promoteurs: Benoît MERCATORIS & Prof. Wensheng Wang

Année civile: 2026

Abstract

By 2050, global demand for wheat is expected to increase by 60%. As a major producer of winter wheat, China faces severe structural challenges such as water scarcity and low efficiency in nitrogen fertilizer utilization. Achieving a sustainable increase in winter wheat production is of critical importance to China. Given the inherent inefficiency of conventional agricultural monitoring methods, the emergence of unmanned aerial vehicle (UAV) remote sensing technology has brought about marked improvements. However, practical applications of this technology remain constrained by bottlenecks such as fragmented models and insufficient integration with crop physiological mechanisms. This research aims to systematically address a series of scientific problems from macro yield prediction to internal growth diagnosis through a gradually deepening technical path, providing a reliable and efficient technical solution for precision agriculture.

This research began by strengthening the predictive foundation. After that it utilized semi-supervised machine learning algorithms to overcome the limitation of data scarcity, and then analyzed key parameters to achieve collaborative inversion of coexisting parameters. Four steps were carried out as a systematic work.

The first step investigated the effectiveness of UAV remote sensing data for predicting winter wheat yield. A LSTM-random forest hybrid model based on the spectral characteristics of a single annual time series was constructed, which achieved reliable predictions of winter wheat yield. This verified the effectiveness of the time-series remote sensing method, but also revealed its dependence on the amount of labeled data.

To overcome the data constraints, multiple years of data with various experimental treatments were introduced in the second step, and a self-training semi-supervised learning strategy was adopted to automatically expand training dataset for yield prediction. The original spectral reflectance was directly used as input features. These approaches significantly enhanced the robustness and generalization ability of the yield prediction model.

By predicting the nitrogen content of the plants, the research in the third step was extended to the key internal physiological processes that drive yield formation. Based on the integration of high-dimensional spectral features, the plant nitrogen content was precise inverted, which opened up the "black box" of yield formation.

In the last stage, multi-task learning frameworks were introduced to solve the joint prediction problem of the biomass represented by dry weight and fresh weight which are two distinct but closely related components. This method effectively enhanced the training and prediction efficiency without reducing the overall prediction accuracy of biomass, thereby uncovered the intrinsic relationship between dry and fresh weights.

This study systematically constructed and validated a technical framework applicable to winter wheat growth monitoring. The monitoring system, progressing from "yield" to "nitrogen content" and then to "biomass components", achieved a shift from result prediction to process diagnosis. It provides a quantifiable technical tool for understanding the interactions among water, nitrogen, and biomass accumulation, holding significant theoretical value and application prospects.

The methodological system developed in this study provides core methodological support for promoting precision agriculture from single-point prediction to comprehensive diagnosis, and is significant for achieving optimal resource allocation and the strategic goal of food security.

Résumé

D'ici 2050, la demande mondiale de blé devrait augmenter de 60 %, tandis que des défis structurels tels que la pénurie d'eau et la faible efficacité de l'utilisation des engrais azotés entravent gravement la croissance durable de la production dans les principaux pays producteurs comme la Chine. Atteindre une augmentation durable de la production de blé d'hiver revêt une importance cruciale pour la Chine. Cependant, les méthodes traditionnelles de surveillance agricole sont inefficaces, et la technologie émergente de télédétection par drone reste confrontée à des goulots d'étranglement tels que des modèles isolés et une faible association avec les mécanismes physiologiques dans les applications pratiques. Cette recherche vise à résoudre systématiquement une série de problèmes scientifiques, allant de la prédiction macro du rendement au diagnostic interne de la croissance, grâce à une approche technique progressivement approfondie, fournissant ainsi une solution technique fiable et efficace pour l'agriculture de precision.

Cette recherche a commencé par renforcer les bases prédictives. Elle a utilisé des algorithmes d'apprentissage automatique semi-supervisés pour surmonter le problème de la rareté des données, puis a analysé des paramètres clés pour réaliser l'inversion collaborative de paramètres coexistants. Elle a été menée de manière systématique en quatre étapes:

Concernant la question de savoir "si les informations de télédétection par drone peuvent prédire efficacement le rendement du blé d'hiver", un modèle hybride LSTM-forêt aléatoire a été construit sur la base des caractéristiques spectrales d'une série temporelle annuelle unique, permettant de prédire avec succès le rendement. Cela a vérifié l'efficacité de la méthode de télédétection basée sur les séries temporelles, mais a également révélé sa dépendance à la quantité de données étiquetées.

Pour surmonter les contraintes liées aux données, des données pluriannuelles et diverses données de traitement expérimental ont été introduites, et une stratégie d'apprentissage semi-supervisé auto-formateur a été adoptée pour extraire directement les informations à partir de la réflectance spectrale originale, améliorant ainsi significativement la robustesse et la capacité de généralisation du modèle de prédiction du rendement.

En prédisant la teneur en azote des plantes, la perspective de recherche s'est étendue aux processus physiologiques internes clés qui déterminent la formation du

rendement. En intégrant des caractéristiques spectrales de haute dimension, l'inversion précise de la teneur en azote des plantes a été réalisée, ouvrant ainsi la "boîte noire" de la formation du rendement.

Pour le paramètre central qu'est la biomasse, un cadre novateur d'apprentissage multitâche a été introduit pour résoudre le problème de prédiction conjointe de deux composantes physiquement distinctes mais étroitement liées : le poids sec et le poids humide. Cette méthode améliore efficacement l'efficacité de l'entraînement et de la prédiction sans réduire la précision globale de la prédiction de la biomasse, en exploitant la relation intrinsèque entre les poids sec et humide.

Cette thèse a systématiquement construit et vérifié une approche technique applicable à la surveillance de la croissance du blé d'hiver, abordant successivement des problèmes clés tels que la modélisation des séries temporelles, l'apprentissage sur petits échantillons, l'inversion de caractéristiques de haute dimension et la prédiction collaborative multi-sorties ; elle a clarifié l'efficacité et les avantages de l'apprentissage multitâche dans la tâche spécifique d'inversion conjointe du poids sec et du poids humide de la biomasse, fournissant un exemple méthodologique pour traiter des groupes de paramètres de culture fortement corrélés ; le système de surveillance construit, allant du "rendement" à la "teneur en azote" puis aux "composantes de la biomasse", a non seulement permis d'approfondir la prédiction des résultats vers le diagnostic des processus, mais a également fourni un outil technique quantifiable pour comprendre la relation d'interaction entre l'eau, l'azote et l'accumulation de biomasse, et présente une valeur théorique et des perspectives applicatives importantes.

Le système méthodologique développé dans cette étude fournit un soutien méthodologique central pour faire évoluer l'agriculture de précision d'une prédiction ponctuelle vers un diagnostic complet, et revêt une grande importance pour atteindre une allocation optimale des ressources et l'objectif stratégique de sécurité alimentaire.

Acknowledgements

First and foremost, I would like to express my sincere gratitude to my promoters, Professor Benoît Mercatoris (University of Liege – Gembloux Agro-Bio Tech, Belgium) and Professor Wensheng Wang (Agricultural Information Institute, Chinese Academy of Agricultural Sciences, China) for their patient guidance, erudite knowledge, and valuable suggestions from the beginning to the end of this Ph.D. project.

I wish to extend my sincere appreciation to the members of my thesis committee and Jury members. Your expertise and perspectives have been instrumental in elevating the quality of my work.

My warm thanks also go to Professor Zhen Chen and his dedicated team at the Institute of Farmland irrigation, Chinese Academy of Agricultural Sciences (CAAS), for their unwavering expertise, insightful mentorship, and collaborative spirit throughout this research. Their scientific rigor and innovative approaches in irrigation studies have been instrumental to our experimental success. Special thanks also go to our experimental research base—a cornerstone of this project—for providing the cutting-edge facilities and operational support that transformed theoretical frameworks into actionable agricultural solutions.

I would like to wholeheartedly express my profound gratitude to my cherished family. To my parents, for stepping in to care for my children with such devotion when life left me stretched too thin. Your selflessness has been my anchor. To my husband, for your unwavering trust and support—you've been my rock through every challenge, and your belief in me fuels my strength. To my younger siblings, for your steadfast loyalty and the motherly warmth you've poured into my children. You've filled gaps I couldn't, and I'm endlessly thankful. To my incredible daughter and son, for your maturity beyond your years, your quiet understanding, and the trust you place in me even when life gets chaotic. You inspire me daily. I'm truly delighted that my daughter has come to understand the value of education this year and will complete her compulsory education next year. I'm so proud to see her mature and gain such awareness at this stage. I wholeheartedly wish her outstanding achievements in her exams and a smooth transition to her ideal high school! To all of you—your sacrifices, your belief in me, and the love that stitches our family together—you are my compass, my shelter, and the reason I strive to be better. Thank you for being my forever anchor.

The last but not the least, I would like to acknowledge that, apart from my own efforts, the success of this thesis relies largely on the encouragement and guidelines I have received from many others. I would like to take this opportunity to express my gratitude to all those who have generously offered their help and provided their best advice throughout this journey, including, but not limited to, my friends and colleagues.

Table of content

CHAPTER I: INTRODUCTION - 1 -

1. RESEARCH BACKGROUND -3-

2. PROBLEM STATEMENT AND RESEARCH GAP -4-

3. RESEARCH OBJECTIVES, AND RESEARCH METHODS -5-

4. RESEARCH SIGNIFICANCE -6-

5. THESIS OUTLINE -7-

CHAPTER II: LITERATURE REVIEW - 9 -

1. SYNOPSIS -11 -

2. THE EVOLUTION OF CROP PHENOTYPING -13 -

2.1 Traditional approach: limitations of destructive sampling -14 -

2.2 Satellite remote sensing: breakthroughs at the macro scale and inherent limitations -14 -

2.3 UAV remote sensing: the ideal platform for breaking the bottleneck -15 -

3. UAV-BASED REMOTE SENSING FOR WINTER WHEAT MONITORING: BRIDGING THE GAP BETWEEN PHENOTYPING AND MANAGEMENT -15 -

3.1 RGB imagery: structural phenotyping and color indices -17 -

3.2 Multispectral imagery for physiological monitoring -20 -

3.3 Hyperspectral imagery: high-fidelity spectral analysis -27 -

3.4 Thermal infrared imagery: water stress detection -29 -

4. MACHINE LEARNING ALGORITHMS USED IN WINTER WHEAT RESEARCH -29-

4.1 Using machine learning method for feature extraction -31 -
4.2 Using machine learning for building models -33 -

5. KEY RESEARCH APPLICATIONS AND FINDINGS -35 -
5.1 Winter wheat yield estimation -36 -
5.2 Winter wheat nitrogen content monitoring -36 -
5.3 Winter wheat biomass estimation -37 -
5.4 Disease detection, the case of yellow rust -38 -
5.5 Estimation of other growth indicators -39 -

6. CONCLUSION AND OUTLOOK: FROM LIMITATIONS TO INTEGRATION PATH -39-
6.1 Analysis of the Fundamental Limitations of the Methodology -40 -
6.2 Integrating the forward path: From diagnosing limitations to collaborative solutions -41 -
6.3 Synthesis and future perspectives -42-

CHAPTER III: RESEARCH METHODS AND EXPERIMENTAL DESIGN -43 -

1. EXPERIMENT DESIGN AND DATA ACQUISITION -45 -
1.1 Experimental site and rationale -45 -
1.2 Treatment structure and temporal scope -46 -
1.3 Weather variability in winter wheat growth -48 -
1.4 Multi-sensor UAV data acquisition -49 -
1.5 Ground truth data -51 -

2. RESEARCH METHODS -53 -

3. MODEL VALIDATION FRAMEWORK -55 -
3.1 Stratified cross-validation procedure -55 -
3.2 Validation strategy and performance metrics -56 -

CHAPTER IV: TEMPORAL YIELD PREDICTION USING AN LSTM-RF NETWORK -57 -

1. SYNOPSIS -59 -
2. MATERIALS AND DATA -59 -
2.1 Selection of spectral indices -61 -

3. METHOD: LSTM-RF -62 -
3.1 Long short-term memory network -62 -
3.2 Random forest regressor -63 -
3.3 LSTM-RF -64 -

4. RESULTS -65 -
4.1 Statistical description of grain yield -65 -
4.2 Correlations between vegetative indices and yield -66 -
4.3 Model performance evaluation -68 -

5. DISCUSSION -69 -
5.1 Physiological interpretation of feature-yield correlations -69 -
5.2 Synergistic advantages of the LSTM-RF framework -70 -
5.3 Limitations and future research directions -71 -

6. CONCLUSIONS -71 -

CHAPTER V: SEMI-SUPERVISED YIELD PREDICTION WITH SELF- TRAINING RANDOM FORESTS -73 -

1. SYNOPSIS -75 -

2. MATERIALS AND METHODS -76 -
2.1 Selection of spectral information -77 -
2.2 Pseudo label generation -77 -
2.3 Multi-scale joint prediction -78 -
2.4 Self-training random forest architecture -79 -

3. RESULTS -80 -
3.1 Winter wheat yield under different experiments -80 -
3.2 Correlation between multispectral information and winter wheat yield -82 -
3.3 Findings on the impact of threshold (δ) in pseudo label learning -84 -

3.4 Performance evaluation the yield prediction using multispectral information -85 -

4. DISCUSSION -87 -

4.1 Assessing the relationship between multispectral reflectance and winter wheat yield -87-

4.2 Challenges and performance factors in self-training random forest for yield prediction -88-

4.3 Enhancements in winter wheat yield prediction through self-training random forest -89-

5. CONCLUSIONS -89 -

CHAPTER VI: ROBUST ESTIMATION OF NITROGEN CONTENT -91 -

1. SYNOPSIS -93 -

2. MATERIALS AND METHODS -94 -

2.1 Experimental data for nitrogen modeling -94 -

2.2 Constructing high-dimensional composite features -95 -

2.3 Model building -97 -

3. RESULTS -98 -

3.1 Nitrogen content in jointing and booting stage -98 -

3.2 Nitrogen content prediction using VIs and multispectral reflectance -99 -

3.3 Nitrogen content prediction using high-dimensional composite features -100 -

3.4 The relationship between nitrogen content and yield -105 -

4. DISCUSSION -106 -

4.1 Dynamics of nitrogen content and implications for sensing -107 -

4.2 The value of high-dimensional feature engineering -107 -

4.3 Algorithm performance and practical considerations -108 -

4.4 Linking nitrogen status to final yield -108 -

5. CONCLUSIONS -108-

CHAPTER VII: MULTI-TASK LEARNING FOR JOINT BIOMASS ESTIMATION -111-

1. SYNOPSIS -113 -

2. MATERIALS AND METHODS -114 -
2.1 Spectral features construction -115 -
2.2 Multitask regression model -116 -
2.3 Stratified sampling for dataset division -117 -

3. RESULTS -119 -
3.1 Changes in dry and fresh weights of winter wheat -119 -
3.2 Combined prediction of dry and fresh weight -121 -
3.3 The relationship between biomass and yield -127 -

4. DISCUSSION -129 -
4.1 The advantage of multi-task learning for biomass prediction -129 -
4.2 The role of phenology in improving prediction accuracy -130 -
4.3 The contribution of thermal features to fresh weight estimation -130 -
4.4 Main sources of error in the models -130 -
4.5 Adaptability of the framework to other crops -131 -

5. CONCLUSIONS -131 -

CHAPTER VIII: GENERAL CONCLUSIONS AND DISCUSSION - 133 -

1. SYNTHESIS OF KEY FINDINGS AND RECONCILIATION WITH RESEARCH OBJECTIVES -135 -

2. IMPLICATIONS FOR PRECISION AGRICULTURE -136 -

3. LIMITATIONS AND GENERALIZABILITY -137 -

4. FUTURE RESEARCH DIRECTIONS -139 -
4.1 Advancing methodological sophistication -139 -
4.2 Bridging to practical application and edge computing -139 -

4.3 Ecosystem-Driven Scalability and Adoption *-140 -*
4.4 Ethical and environmental considerations *-140 -*

CHAPTER IX: REFERENCES **-143 -**

List of figures

Figure 1. Technical route of the research. 8

Figure 2. The concept map of winter wheat monitoring based on UAV remote sensing and machine learning. 12

Figure 3. Evolutionary chart of phenotyping technology 13

Figure 4. Winter wheat information collecting using UAV platform. 17

Figure 5. Spectral range of RGB camera. 18

Figure 6. Band distribution map of the camera RedEdge (MicaSense Inc., Seattle, WA, USA) 21

Figure 7. 125-band hyperspectral imaging. 28

Figure 8. The application of machine learning algorithm. 31

Figure 9. The research tasks of winter wheat. 35

Figure 10. Experimental field with irrigation facility. 45

Figure 11. Experimental area images captured by drone carrying sensors. 50

Figure 12. M210 quadrotor with multispectral and thermal cameras. 50

Figure 13. Stratified 5-fold cross-validation for different irrigation treatment in 2019-2020. 55

Figure 14. Methodological flowchart for crop yield prediction from the UAV imageries in combination with ground-based data. 60

Figure 15. Long short-term memory cell 62

Figure 16. How the random forest regressor works. 64

Figure 17. Structure of LSTM-RF. 65

Figure 18. Yield distribution at different irrigation. 66

Figure 19. Correlation analysis heat map in the heading stage, flowering stage and grain filling stage respectively. 67

Figure 20. Correlation analysis heat map between the extracted features of LSTM and yield. 67

Figure 21. The relationships between the measured and predicted values of -wheat yield based on the LSTM and LSTM-RF models. 69

Figure 22. Methodological flowchart for crop yield prediction from the UAV imageries in combination with ground-based data. 76

Figure 23. Multi-scale joint prediction. 79

Figure 24. Pseudo code of self-training random forest. 80

Figure 25. Winter wheat yield distribution under different experiments. 81

Figure 26. Winter wheat yield distribution under different irrigation treatments in 2022. 82

Figure 27. Correlation analysis heat map in filling stage respectively. 83

Figure 28. Yield distribution of learned pseudo labels. 85

Figure 29. The relationships between the ground-measured and predicted values of winter wheat yield obtained by RF. (a) Description of what is on test dataset; (b) Description of what is on validation dataset. 86

Figure 30. The relationships between the ground-measured and predicted values of winter wheat yield obtained by self-training random forest. (a) Description of what is on test dataset; (b) Description of what is on validation dataset.....87

Figure 31. KDE plots of nitrogen content by different treatment and growth stages. 98

Figure 32. The importance value of each input parameter from the RF regressor for nitrogen content prediction at the jointing stage.....103

Figure 33. The importance value of each input parameter from the RF regressor for nitrogen content prediction at the jointing stage.....104

Figure 34. The relationship between yield and plant nitrogen content at the jointing stage under water treatment in 2022, and nitrogen fertilizer treatment in 2022 and 2023. Note: the red and blue lines are the fitted curves of the linear plateau model and quadra. 105

Figure 35. The relationship between yield and plant nitrogen content at the booting stage under water treatment in 2022, and nitrogen fertilizer treatment in 2022 and 2023. Note: the red and blue lines are the fitted curves of the linear plateau model and quadra. 106

Figure 36. Methodological flowchart of the joint prediction of DW and FW. 114

Figure 37. Pearson correlation between features, and between features and dry-fresh weight. 118

Figure 38. Stratified sampling according to dry weight distribution. 119

Figure 39. Dry and fresh weights of winter wheat in different stages. 120

Figure 40. Water content during different stages. 121

Figure 41. The effect of removing the CWSI on DW and FW prediction.....125

Figure 42. The effect of phenology addition on DW and FW prediction. 127

Figure 43. The relationship between dry/fresh weight and yield during different stages. 128

Figure 44. Relationships between biomass and yield in grain filling stage. 129

List of tables

Table 1. Visible light spectral vegetation indices used in winter wheat monitoring. 19

Table 2. The multispectral vegetation indices. 22

Table 3. An overview of the water treatment for the 2019-2020 growing season.46

Table 4. Irrigation treatments in Field I. 47

Table 5. Nitrogen fertilizer treatments in Field II. 48

Table 6. An overview of the weather within the growing seasons. 48

Table 7. Summary of research method design. 54

Table 8. List of 7 vegetation indices which were examined in this study. 61

Table 9. Results of the estimation of the yield of winter wheat based on features extracted from three stages. 68

Table 10. Correlation index between multispectral indices and winter wheat yield. 83

Table 11. Vegetation indices and characteristic variables sensitive to nitrogen content. 96

Table 12. Performance of eight ML methods for winter wheat nitrogen content prediction using Vis and multispectral reflectance at jointing stage. 99

Table 13. Performance of eight ML methods for winter wheat nitrogen content prediction using VIS and multispectral reflectance at booting stage. 99

Table 14. Performance of eight ML methods for winter wheat nitrogen content prediction using high-dimensional composite features at jointing stage. 101

Table 15. Performance of eight ML methods for winter wheat nitrogen content prediction using high-dimensional composite features at booting stage. 101

Table 16. Vegetation index in winter wheat biomass estimation. 115

Table 17. Input feature set for winter wheat biomass prediction. 116

Table 18. The comprehensive evaluation results using multispectral and thermal infrared features of winter wheat canopy as input. 122

Table 19. The comprehensive evaluation results using multispectral features. 124

Table 20. The comprehensive evaluation results using spectral features and phenology. 125

List of abbreviations

AGB	Above ground biomass
ANN	Artificial Neural Network
CIR	Crop index ratio
CNN	Convolutional Neural Network
CWSI	Crop Water Stress Index
DL	Deep Learning
DN	Digital number
DW	Dry weight
FW	Fresh weight
GBR	Gradient Boosting Regression
GCP	Ground control points
GIS	Geographic information system
GNDVI	Green Normalized Difference Vegetation Index
KNN	K Neighbors
LAI	Leaf Area Index
LGBM	Light GBM
LSTM	Long short-term memory
MAE	Mean absolute error
MCARI	Modified chlorophyll absorption in reflectance index
ML	Machine Learning
MTVI2	Modified triangular vegetation index 2
NCP	North China Plain
NDRE	Normalised Difference Red Edge Index
NDVI	Normalised Difference Vegetation Index
NIR	Near-infrared
OSAVI	Optimized soil adjusted vegetation index
PNC	Plant nitrogen content
PPR	Normalized difference plant pigment ratio

RCBD	Randomized complete block design
RF	Random Forest
RGB	Red Green Blue —the three channels ofa colour image
RMSE	Root Mean Square Error
RVI1	Ratio vegetation index 1
SVR	Support Vector Regression
TIR	Thermal Infrared
UAV	Unmanned Aerial Vehicle
VHI	NDVI × CWSI
VI	Vegetation index

I

Introduction

1. Research Background

Winter wheat (Triticum aestivum L.) plays a vital role in ensuring China's food security, accounting for approximately 23% of national grain output and serving as the staple for over 1.4 billion people (National Bureau of Statistics, 2022). With the challenge of feeding 18% of the world's population on just 7% of its arable land (FAO, 2023), China's agricultural system faces unparalleled pressure to boost productivity sustainably. The North China Plain (NCP), a region that produces over 60% of the nation's winter wheat, faces the most acute manifestation of this challenge. The critical tension in this region between food production and resource limits makes it a priority for research focused on balancing higher yields with environmental protection.

The pursuit of higher wheat yields in the NCP is severely constrained by three interconnected pressures: water scarcity, nitrogen overuse, and climate extremes. Winter wheat yield is sensitive to droughts, especially occurring during booting and grain filling stage (Yang et al., 2020). The NCP wheat belt relies overwhelmingly on groundwater irrigation, extracting 120% of its sustainable yield annually (World Bank, 2020). Despite consuming 62% of the region's water resources, the application efficiency of irrigation is below 40%. (Haozhong et al., 2017). Chinese winter wheat farms apply nitrogen at an average rate of 220 kg/ha—nearly four times the global average—yet achieve a Nitrogen Use Efficiency (NUE) of only about 30% (Chinese Academy of Sciences, 2021). The excess nitrogen, driven by the prevalent but misguided belief that "more fertilizer guarantees higher yield," has led to severe soil degradation, including the acidification of 45% of NCP top soils, which undermines long-term soil health and productivity (Guo et al., 2010). Climate change amplifies these risks through rising temperatures and erratic precipitation. For instance, a 2022 spring drought combined with a 40°C heatwave during grain filling in Henan Province shortened the growth cycle and reduced yields significantly, highlighting the growing threat of thermal stress (National Meteorological Center, 2023).

Traditional methods for yield estimation and monitoring key physiological parameters, such as Plant Nitrogen Content (PNC), above-ground fresh biomass (indicative of real-time water status and structural growth), and above-ground dry biomass (representing accumulated carbon assimilation), are predominantly manual. These approaches are labor-intensive, inefficient, destructive and unsuitable for large-scale application, creating a major phenotyping bottleneck in modern plant science (Seishi et al., 2022). The Integration of remote sensing and information technology

offers a promising pathway to overcome these limitations. Satellite remote sensing can provide broad coverage remote sensing. The emergence of Unmanned Aerial Vehicles (UAVs) has enabled high-throughput, non-destructive crop monitoring at the field scale (Andrew et al., 2020). Machine Learning (ML) techniques, including Deep Learning (DL), have become indispensable for modeling the complex, non-linear relationships between the vast amounts of high-dimensional remote sensing data and key agronomic traits. (Frederik et al., 2017).

China's policy framework strongly supports this research. Since 2019, central policy (the annual "No. 1 Document") has consistently prioritized agricultural tech innovation. Key milestones include pushing drone commercialization (2019), emphasizing technology transfer from lab to field (2022), prioritizing water conservation (2023), promoting digital integration (2024), and finally calling for AI-powered "new quality productive forces" in agriculture (2025). This evolution provides a clear mandate for using UAVs and machine learning to address issues like precise water management.

2. Problem Statement and Research Gap

The prediction of winter wheat yield directly affects the national food security and the sustainability of resources. Accurate yield predictions can anticipate potential reductions in production due to drought and heat stress, providing a basis for macro-level food allocation and emergency management. Currently, most yield prediction models overlook temporal dynamics during growth stages (Alexis et al., 2022; Chaofa et al., 2022). However, the yield is an accumulation of the whole growing season. Zhang et al. (2023) emphasized in their study that time series data contain unique information about the response of crops to the environment, rather than merely being a collection of multiple snapshots. Bouras et al. (2023) through comparative experiments, proved that the crop model that integrates multiple time phases (sequences) of remote sensing data has significantly higher yield prediction accuracy than the model that only integrates data from a single critical time phase. This directly demonstrates the necessity of integrating information from different growth stages to improve the accuracy of yield prediction.

There is a significant imbalance between a large amount of UAV spectral data and scarce ground-truth measurements. Lobell (2015) in his landmark review on the application of remote sensing in yield prediction listed "availability of ground data" as one of the core challenges. He pointed out that it is difficult to obtain large-scale

and precise ground survey data for yield, which severely restricts the training and validation of complex statistical models and machine learning models, resulting in uncertainty in the generalization ability of the models. Weiss et al. (2020) when discussing agricultural remote sensing machine learning, explicitly proposed the term "ground truth bottleneck". They explained that although drones and satellites can quickly generate massive pixel data, the precise agronomic parameters (such as biomass, nitrogen content) corresponding to each pixel require destructive sampling and laboratory analysis, which is extremely costly and has resulted in a data-level imbalance.

The existing models for predicting winter wheat yields are mostly "black boxes" or statistical models, which directly establish the mapping relationship between environmental or remote sensing factors and the final yield. This paradigm has two major limitations: poor interpretability and low operability (Wang et al., 2023). Lobell (2015) pointed out yield itself is a complex integrated variable, and remote sensing cannot directly "see" yield. An effective monitoring system must first accurately quantify these physiological traits, and then link them to yield through crop growth models or statistical relationships. Nitrogen additions can enhance yield but must be managed efficiently to reduce pollution (Revill et al., 2021). Biomass is the ultimate manifestation of the accumulation of matter and energy during the growth process of crops, and it is the result of the combined effects of water, nutrients, climate, and management measures. The dynamic monitoring of biomass essentially serves as a direct measurement of the crop growth process and resource utilization efficiency. (Thenkabail et al., 2016). Lobell (2015) identifies biomass and nitrogen content as the "most crucial intermediate traits" that link remote sensing signals to final yield.

3. Research Objectives and Research Methods

The aim of this thesis is to establish a temporal awareness, data efficiency enhancement, and interpretable wheat yield prediction model, by integrating multi-temporal remote sensing of unmanned aerial vehicles and machine learning technology.

This goal is achieved through the following three interconnected research objectives:

Construction of a winter wheat yield prediction model incorporating multi-temporal remote sensing information to overcome the limitation of current models that ignore the dynamic growth process. We collected the canopy spectral sequence data of multiple critical growth stages of winter wheat. A time-series machine learning model

LSTM (Yu et al., 2019) was adopted to extract the temporal dynamic features. Based on the extracted dynamic features, we used a tree-based machine learning method random forest (Falv et al., 2022; Zongpeng et al., 2023b) to do yield prediction. This is a foundation that combines unmanned aerial vehicle remote sensing and machine learning to predict the yield of winter wheat.

To address the "bottleneck" problem between the scarcity of ground truth data and a large amount of remote sensing data, the research proposed a method combining semi-supervised deep learning algorithm self-training (Tuia, et al., 2016) and Random Forest (RF). It utilized a small amount of spectral data with ground yield truth labels for automatic labeling of the unlabeled data. And the feasibility and effectiveness of this labeling method were verified through a comparison experiment on yield prediction.

To address the "black box" problem of the model, machine learning algorithms (such as random forests, deep learning networks) were utilized to construct high-precision inversion models for aboveground fresh/dry biomass and plant nitrogen content. This aimed to verify the feasibility of using unmanned aerial vehicle (UAV) remote sensing to replace traditional destructive sampling, and to quantify the impact of different growth stages and different physiological parameters (biomass, nitrogen content) on the final yield prediction. To improve prediction accuracy of models, we designed high-dimensional composite input features. When doing DW and FW estimation, we used multi-task learning (Caruana, 1997) to enhance prediction efficiency.

4. Research Significance

This study combined the inversion of key crop physiological parameters with multi-temporal dynamic predictions to explore a new paradigm of "remote sensing inversion - process quantification - terminal prediction" for enhancing the mechanism of modeling. This helps deepen the understanding of the complex temporal relationships between remote sensing signals, crop physiology, and final yield, promoting the development of agricultural remote sensing from statistical correlations to mechanistic process explanations, and providing a theoretical framework for constructing the next generation of interpretable agricultural intelligent models. This study verified the effective of semi-supervised method for automatic labeling, reducing reliance on extensive labeled data while maintaining accuracy under variable irrigation and nitrogen regimes.

This research overcomes provides theoretical and technical support for precise water and nitrogen management and yield prediction of winter wheat in the North China Plain. The dynamic monitoring of biomass and nitrogen content can serve as a direct decision-making basis for variable irrigation and variable fertilization, achieving water and fertilizer savings. Accurate yield predictions help the agricultural sector to formulate grain storage and allocation plans in advance, ensuring food security. This research closely aligns with the policy demands of the "agricultural digitalization" and "AI-enabled new quality productive forces" of the country, and has significant application and promotion value.

5. Thesis structure

This thesis is divided into seven chapters. In **Chapter I**, based on China's relevant agricultural policies and national conditions, addresses the three major bottlenecks in predicting winter wheat yield in the North China Plain, namely the neglect of the dynamic process of growth period, the scarcity of ground truth data, and the poor interpretability of the model. It proposes and constructs a new framework for yield prediction that integrates multi-temporal unmanned aerial vehicle (UAV) remote sensing and machine learning, aiming to enhance data utilization efficiency and model interpretability. **Chapter II** is a comprehensive review of key studies related to unmanned aerial vehicle (UAV) remote sensing, inversion of winter wheat physiological parameters, yield prediction, and machine learning models was conducted to provide a theoretical foundation for this research and to clarify the innovative positioning. **Chapter Ⅲ** aims to clearly explain the research methods, specific experimental plans and data analysis methods adopted to achieve the three research objectives.

Chapter IV introduces a yield prediction model based on temporal-dynamic long short-term memory (LSTM) method that can capture the growth process leading to yield formation, laying the foundation for using unmanned aerial vehicle remote sensing for winter wheat monitoring. **Chapter V** develops an advanced second yield prediction model based on a semi-supervised method that uses spectral and thermal data to conduct reliable yield predictions with a small amount of data and a single-stage winter wheat monitoring. **Chapter VI** and **Chapter VII** focus on estimating basic physiological parameters - plant nitrogen content and biomass, demonstrating the effectiveness of unmanned aerial vehicle agents in quantifying key yield components.

Chapter VIII provides a comprehensive discussion, summarizes the research results of all experimental chapters, explores the existing limitations, and points out the future research directions and practical application significance in the field of precision agriculture. **Figure 1** shows the research roadmap.

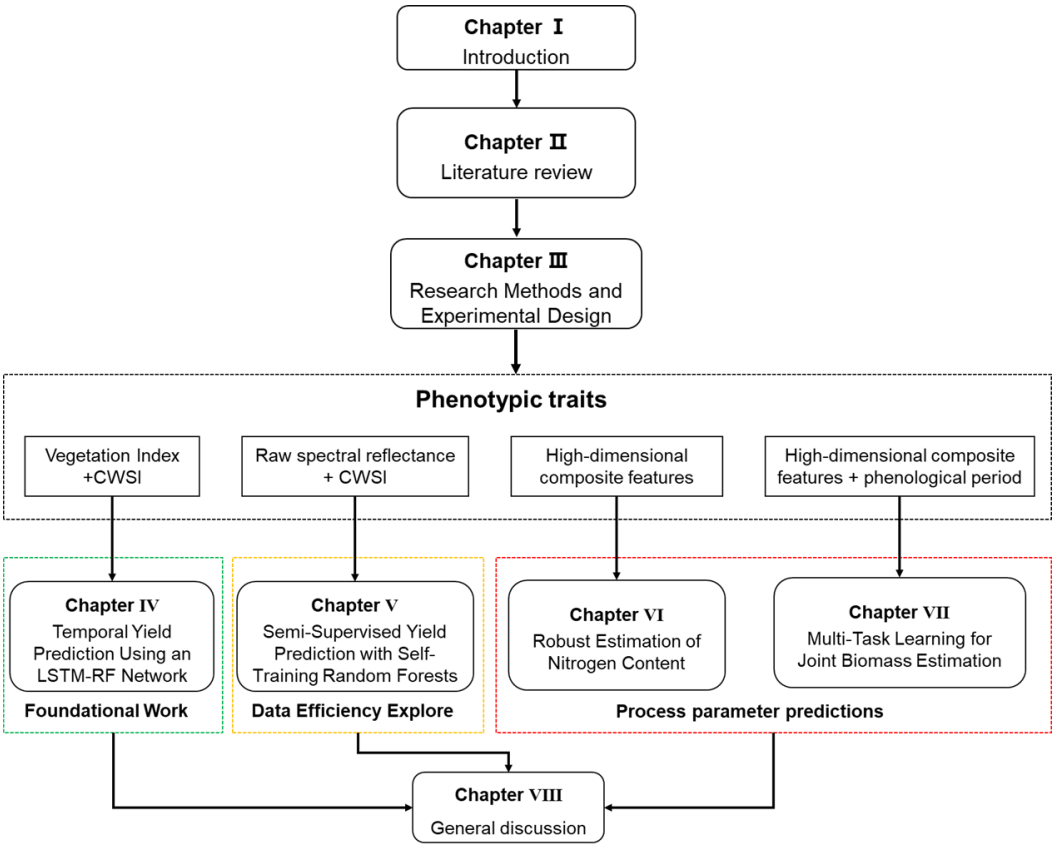

Figure 1. Technical route of the research.

II

Literature review

1. Synopsis

Accurate and efficient monitoring of winter wheat growth status is crucial for addressing global food security challenges and promoting the sustainable development of wheat production in China. However, traditional crop phenotyping methods are often hampered by inherent limitations such as high cost, low efficiency, and destructiveness, which have become key constraints in advancing modern plant science (Seishi, 2022; Kianoosh et al., 2023). In recent years, the integration of unmanned aerial vehicle (UAV) remote sensing with machine learning (ML) technologies has emerged as a revolutionary approach, enabling high-throughput, non-destructive field-based phenotyping and thereby overcoming these traditional bottlenecks (Liu et al., 2023; Anna et al., 2018; Shweta et al., 2023).

The impact of abiotic and biotic factors on global food production has become a key link in achieving global food security, which is a major scientific issue that urgently needs to be addressed by governments and academia today. For example, Drought and high-temperature are the most important abiotic stress limiting plant growth and crop productivity globally (Carolina et al., 2012; Rebecca et al., 2020). Salinity and drought stresses often occur simultaneously (Yuncai et al., 2017). Yellow rust in winter wheat is a widespread and serious fungal disease, resulting in significant yield losses globally (Xin et al., 2019). Stripe rust (Pst) is also a major disease of wheat crops leading untreated to severe yield losses (Michael et al., 2021).

To demonstrate the complete workflow of application of drone remote sensing and machine learning technology in winter wheat, based on the previous studies (Jose et al., 2020; Ryoya et al., 2023; Ghizlane et al., 2021; Rabi et a., 2024; Sumanta et al., 2021), the summarizes process of which is illustrated as shown in **Figure 2**.

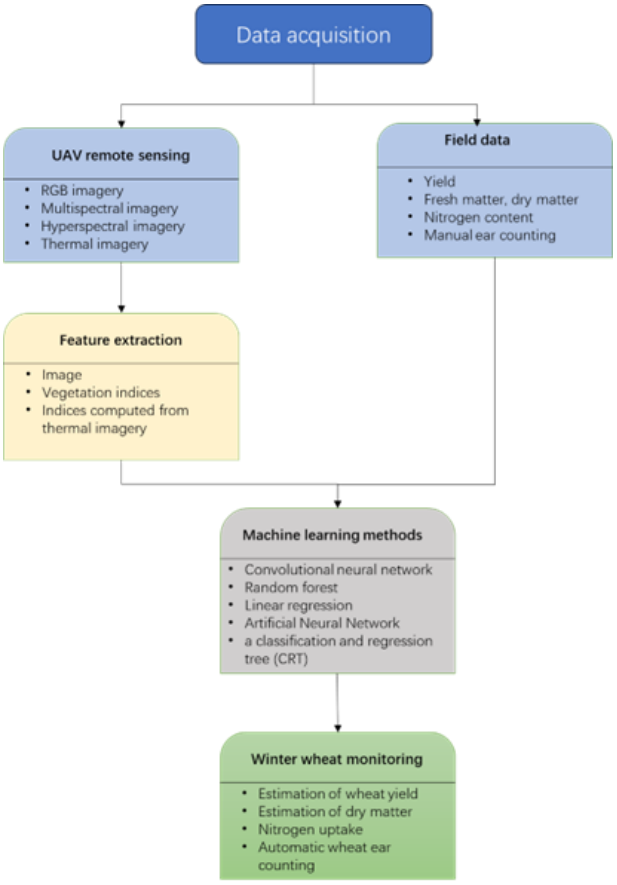

Figure 2. The concept map of winter wheat monitoring based on UAV remote sensing and machine learning.

To systematically review the research progress in this field and establish a theoretical foundation for the present study, this chapter will synthesize the literature from the following aspects: It begins by reviewing the evolution of UAV remote sensing platforms and their sensors in agricultural phenotyping research, analyzing their technical advantages. It then discusses the selection of spectral cameras, as well as the extraction and selection of spectral information from winter wheat canopies, such as spectral indices. Subsequently, the chapter explores the application status and challenges of machine learning methods in handling high-dimensional, non-linear remote sensing data to retrieve key agronomic parameters (e.g., biomass, nitrogen content, yield). Finally, based on the preceding synthesis, a critical analysis will be

conducted on the existing research gaps and shortcomings, particularly in areas such as temporal dynamic modeling, scarcity of ground-truth data, and model interpretability. This analysis will clearly define the academic positioning and innovative contributions of this study.

2. The evolution of crop phenotyping

Precise phenotyping plays a crucial role in monitoring crop responses to stresses such as drought and diseases, and in optimizing resource management including water and nitrogen fertilization. It is a key component for enabling smart agriculture and molecular breeding (Araus & Cairns, 2014). However, technological limitations have long hindered its advancement. The evolution of phenotyping technologies follows a clear track: from labor-intensive and destructive manual sampling, to large-scale satellite remote sensing, and ultimately toward unmanned aerial vehicle (UAV)-based remote sensing platforms that bridge the gap between genotypes and field-level phenotypes, as shown in **Figure 3**.

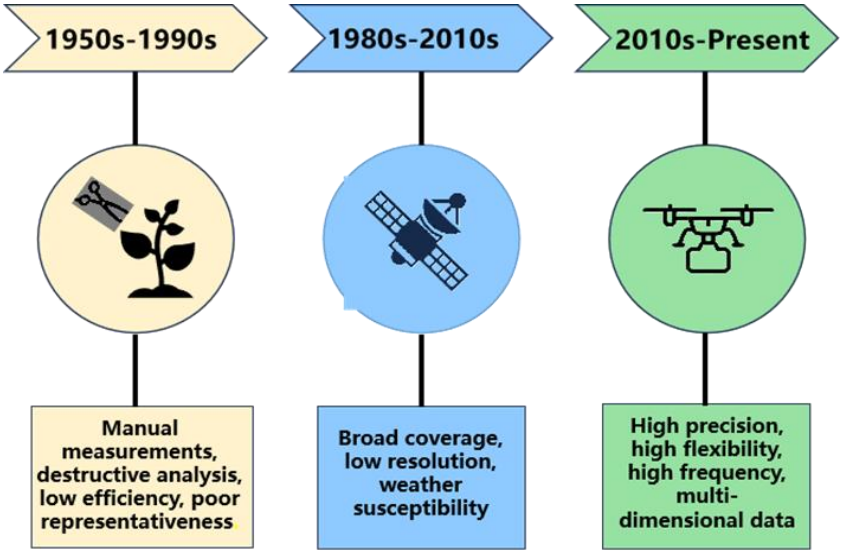

Figure 3. Evolutionary chart of phenotyping technology

2.1 Traditional approach: limitations of destructive sampling

Early crop phenotyping relied entirely on destructive sampling, which involves collecting plant samples and transporting them to a laboratory for biochemical or physical analysis. Although this method can yield accurate data, its drawbacks are substantial and have led to the well-known "phenotyping bottleneck" (Furbank & Tester, 2011).

The primary limitations include (i) low efficiency of manual sampling and subsequent analysis, which are time-consuming and labor-intensive, making large-scale field applications impractical, (ii) limited spatiotemporal representativeness, as point-based sampling fails to capture the inherent spatial heterogeneity in fields, resulting in poor data representativeness, and (iii) a significant time lag resulting from the prolonged cycle from sample collection to result acquisition, which prevents timely decision-making in response to field stresses.

These shortcomings show that traditional methods are inadequate for meeting the demands of modern high-throughput breeding and precision agriculture, both of which require vast amounts of real-time phenotypic data, thus driving the adoption of remote sensing technologies.

2.2 Satellite remote sensing: breakthroughs at the macro scale and inherent limitations

The introduction of satellite remote sensing technology has provided a revolutionary tool for regional-scale crop monitoring and phenotyping (Mulla, 2013). Its key advantages include extensive coverage capability—enabling periodic acquisition of crop growth information over large regions or even globally, and support through multispectral data—facilitating the retrieval of crop biophysical parameters through the calculation of vegetation indices such as NDVI.

However, satellite remote sensing faces significant limitations in field-based precision phenotyping applications (Yang et al., 2017). Its insufficient spatial and temporal resolution, caused by long revisit cycles (ranging from days to weeks) and limited spatial resolution (at the meter scale), prevents the detection of fine-scale variations within fields and short-term crop dynamics. Furthermore, its susceptibility to weather conditions—such as clouds, rain, and fog—frequently obstructs data acquisition by optical sensors and results in data gaps. Therefore, satellite remote sensing, while suitable for broad-scale agricultural surveys, lacks the capability to

support precision phenotyping at the individual plot level. This limitation has directly driven the emergence of more cost-effective and flexible remote sensing platforms.

2.3 UAV remote sensing: the ideal platform for breaking the bottleneck

The emergence of unmanned aerial vehicle (UAV) remote sensing technology has effectively addressed the core limitations of earlier methods, establishing it as an ideal bridge connecting genotype and field-based phenotyping (Yang et al., 2017). A first key advantage is the high spatial and temporal resolution. UAV platforms provide on-demand data at centimeter-scale spatial resolution and support high-frequency monitoring daily or even hourly, enabling precise capture of subtle changes in crop growth and early signs of stress (Gago et al., 2015). Secondly, drones give unparalleled flexibility. Missions are highly adaptable, allowing customized observation of specific fields, experimental plots, or individual plants. UAVs can also be equipped with various sensors, including multispectral, hyperspectral, thermal infrared, and LiDAR (Bai et al., 2016). Multi-dimensional phenotyping extraction is another underlying advantage of UAV-based imaging. Through the integration of multi-source sensor data, UAVs enable non-destructive, high-throughput extraction of a wide range of phenotypic traits such as plant height, biomass, leaf area index (LAI), canopy temperature, and 3D canopy structure (Yang et al., 2017).

In summary, by providing efficient, precise, and multidimensional data acquisition capabilities, UAV remote sensing has successfully addressed the long-standing phenotyping bottleneck, significantly accelerating progress in functional genomics research and smart agricultural management decisions.

The historical evolution of crop phenotyping technology—from destructive sampling to satellite remote sensing, and further to UAV-based platforms—represents a continuous pursuit of greater efficiency, higher precision, and increased intelligence. With its unique technical advantages, UAV remote sensing has become a core driving force in contemporary agricultural phenomics, providing indispensable technical support for decoding gene functions, selecting superior varieties, and enabling precise resource allocation.

3. UAV-based remote sensing for winter wheat monitoring: bridging the gap between phenotyping and management

Unmanned Aerial Vehicles (UAV) have emerged as a pivotal technology in precision agriculture, effectively bridging the gap between high-cost, low-resolution satellite imagery and labor-intensive ground-based measurements. Their operational flexibility, high spatial resolution (<10 cm), and on-demand data acquisition capability make them ideally suited for monitoring the dynamic physiological processes of winter wheat at the field scale. A critical advantage lies in the ability of UAVs to carry various lightweight sensors—including RGB, multispectral, hyperspectral, and thermal infrared (TIR) cameras—each capturing complementary aspects of crop status. The selection of these sensors involves a trade-off between information richness, cost, and operational complexity, which must be aligned with specific monitoring objectives, such as assessing water and nitrogen status.

The above ground phenotype of winter wheat is closely related to its growth and development. Spectral cameras with different spectral ranges that can be mounted on drones, provide the possibility of obtaining the required winter wheat phenotype information. The RedEdge Normalized Difference Vegetation Index (RENDVI) was been found had the most influence in predicting wheat crop height compared to the other predictor variables (Nduku, L., 2024). The outcomes from this study are beneficial for improving agronomic management within the season based on crop height trends. Hence, farmers can focus on using cost-effective Vis for monitoring particular areas experiencing crop stress. For example, quantifying the green area index (GAI) has become increasingly important as a crucial characteristic of crop canopies for modeling processes like transpiration, light interception, and growth (Josephine et al., 2019). By analyzing the selected literature, it can be seen that the spectral sensors and information collected by researchers vary depending on the research task and the required spectral information, as shown in **Figure 4**.

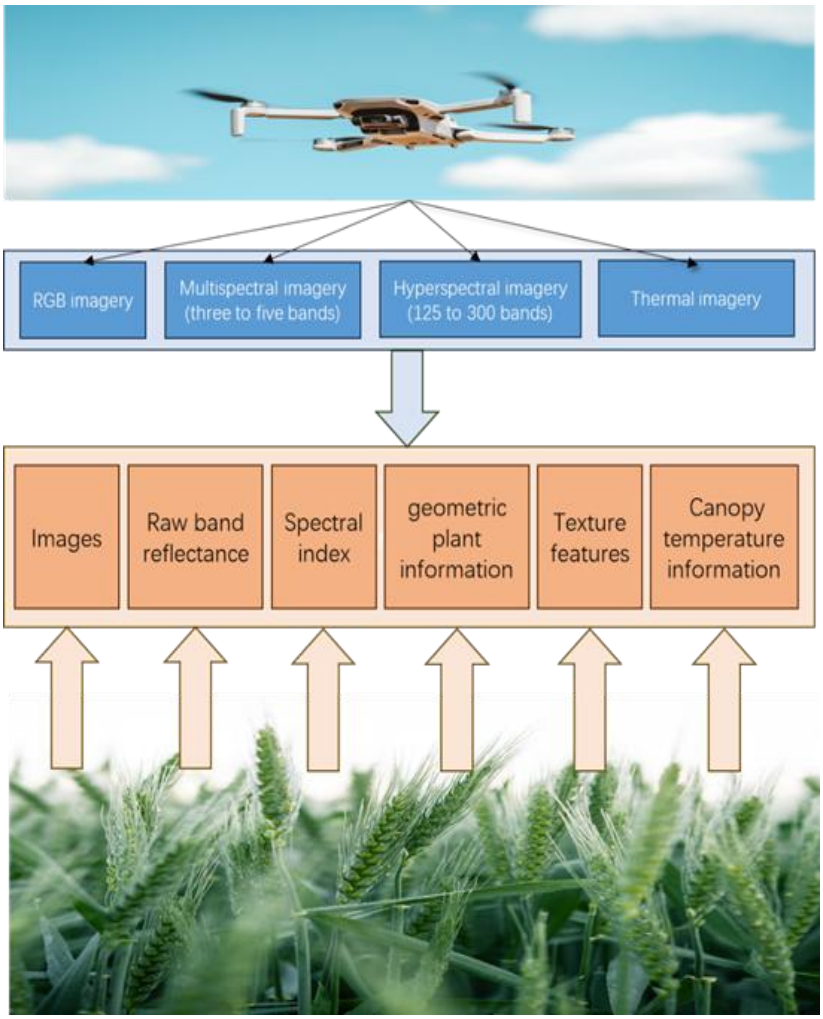

Figure 4. Winter wheat information collecting using UAV platform.

3.1 RGB imagery: structural phenotyping and color indices

Drones equipped with visible-light cameras covering the spectral range from 400 nm to 700 nm (**Figure 5**), researchers can acquire high-resolution aerial imagery (millimeter to centimeter-scale ground resolution) to monitor key crop traits across large agricultural fields—a critical advantage over ground-based sensing. The primary strength of RGB sensors lies in their high spatial resolution, which allows for the detailed extraction of morphological traits. For instance, advanced processing pipelines

can convert overlapping RGB images into 2D orthomosaics and 3D point clouds, from which plot-level traits such as plant height (PH), canopy cover (CC), and crop volume model (CVM) can be quantified with high accuracy (Zhengang et al., 2023; Guohui et al., 2023). This structural information is crucial for tracking biomass accumulation.

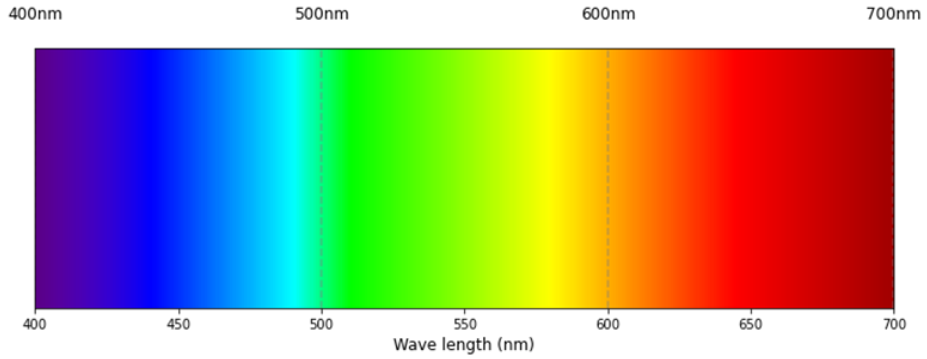

Figure 5. Spectral range of RGB camera.

Beyond structure, RGB imagery can be analyzed through color-based vegetation indices (VIs). By separating the image into its red, green, and blue channels, various indices can be calculated to assess canopy greenness and stress. Such as NGRDI (Normalized Green-Red Difference Index), which can minimize atmospheric effects and is sensitive to green vegetation fraction (Liao et al., 2023). NGBDI (Normalized Green-Blue Difference Index), which is useful for detecting flowering and senescence by mapping changes from vegetation to reproduction (Xiaofeng et al., 2021). VARI (Visible Atmospherically Resistant Index), can be used to assess canopy-level greenness using all three RGB bands (Yang et al., 2023).

Due to the numerous RGB vegetation indices, researchers have named them differently based on their own research findings. For example, The Normalized Green Blue Difference Index (NGBDI) in the study by Guohui and colleagues (2023) was referred to as the Normalized Difference Yellowness Index (NDYI) by Chaofa et al. (2022). Some equations have the same name for different RGB vegetation indices. Some RGB vegetation indices even have several names, for example, green-red vegetation index (GRVI) named by Quan et al., 2023b, was called normalized green-red variance index (NDRGI) by Wei et al., 2022, according to Weilong et al., 2023, it had another name normalized green red difference index (NGRDI), and it was referred to normalized difference index (NDI) in Yang et al., 2023. **Table 1** lists the visible light spectral vegetation indices that appear in the publications.

Table 1. Visible light spectral vegetation indices used in winter wheat monitoring.

Vegetation Index	Formula	Reference
Normalized pigment chlorophyll ratio index (NPCI/IKAW)	$\frac{R_r - R_b}{R_r + R_b}$	[Tanzeel U. R., 2019; Yuanyuan et al., 2023; Jianjun et al., 2021; Jing et al., 2023; Liao et al., 2023]
Normalized green blue difference index (NGBDI)	$\frac{R_g - R_b}{R_g + R_b}$	[Xiaofeng et al., 2021; Yuanyuan et al., 2023; Guohui et al., 2023; Chaofa et al., 2022]
Normalized green red difference Index (NGRDI)	$\frac{R_g - R_r}{R_g + R_r}$	[Zhengang et al., 2021; Chengxin et al., 2023; Quan et al., 2023a; Falv et al., 2022; Mengxi et al., 2023]
Green blue ratio (GBRI)	$\frac{R_g}{R_b}$	[Chaofa et al., 2022]
Green red ratio (GRRI)	$\frac{R_g}{R_r}$	[Zongpeng et al., 2023a; Jinya et al., 2021; Jianjun et al., 2021]
Red green ratio index (RGRI)	$\frac{R_r}{R_g}$	[Chengxin et al., 2023; Jianjun et al., 2021; Zongpeng et al., 2023b]
Red blue ratio index (RBRI)	$\frac{R_r}{R_b}$	[Chaofa et al., 2022; Zongpeng et al., 2023a]
Difference between green and blue (DifGB)	$R_g - R_b$	[Jianjun et al., 2021]
Red green difference vegetation index (RGD)	$R_r - R_g$	[Jinkang et al., 2022]
Normalized redness intensity (NRI)	$\frac{R_r}{R_r + R_g + R_b}$	[Zhengang et al., 2021; Jinya et al., 2021; Shuaipeng et al., 2023]
Normalized greenness intensity (NGI)	$\frac{R_g}{R_r + R_g + R_b}$	[Zhengang et al., 2021; Xiaofeng et al., 2021]
Normalized blueness intensity (NBI)	$\frac{R_b}{R_r + R_g + R_b}$	[Xiaofeng et al., 2021]
Red green-blue vegetable index (RGBVI)	$\frac{R_g^2 - R_r * R_b}{R_g^2 + R_r * R_b}$	[Chengxin et al., 2023; Yuanyuan et al., 2023; Yang et al., 2023; Weilong et al., 2023; Falv et al., 2022]
Modified green red vegetation index (MGRVI)	$\frac{R_g^2 - R_r^2}{R_g^2 + R_r^2}$	[Chengxin et al., 2023; Yuanyuan et al., 2023; Yang et al., 2023; Weilong et al., 2023]
Normalised difference index (NDI)	$\frac{R_g + R_r}{R_g + R_r + 0.1}$	[Zongpeng et al., 2023a; Yuanyuan et al., 2023]
Excess green minus excess red index (EXGR)	$3 * R_g - 2.4 * R_r - R_b$	[Yuanyuan et al., 2023; Yang et al., 2023; Weilong et al., 2023]

Vegetation Index	Formula	Reference
Excess green index (EXG)	$2 * R_g - R_r - R_b$	[Wei et al., 2022; Yan et al., 2022; Weilong et al., 2023]
Excess red index (ExR)	$1.4 * R_r - R_g$	[Yang et al., 2023; Jing et al., 2023; Weilong et al., 2023]
Excess blue index (ExB)	$1.4R_b - R_g$	[Weilong et al., 2023]
IPCA	$0.994\|R_r - R_b\| + 0.961\|R_g - R_b\| + 0.914\|R_g - R_r\|$	[Weilong et al., 2023]
Ground-level image index (GLI)	$\frac{2 * R_g - R_r + R_b}{2 * R_g + R_r + R_b}$	[Zhengang et al., 2021; Chengxin et al., 2023; Yang et al., 2023]
Hue index (HI)	$\frac{2 * R_r - R_g - R_b}{R_g - R_b}$	[Jianjun et al., 2021]
Vegetative index (VEG)	$\frac{R_g}{R_r^a * R_b^{(1-a)}}, a = 0.667$	[Yuanyuan et al., 2023; Weilong et al., 2023]
Visible atmospherical resistance index (VARI)	$\frac{R_g - R_r}{R_g + R_r - R_b}$	[Zongpeng et al., 2023a; Yuanyuan et al., 2023; Wei et al., 2022]
INT	$\frac{R_r + R_g + R_b}{3}$	[Weilong et al., 2023]
Redness index (RI)	$\frac{R_r^2}{R_b * R_g^3}$	[Jianjun et al., 2021]
Brightness index (BI)	$\sqrt{\frac{R_g^2 + R_r^2}{2}}$	[Jianjun et al., 2021]
Colouration index (CI)	$\frac{R_r - R_b}{R_r}$	[Zongpeng et al., 2023a; Zongpeng et al., 2023b]
Gray scale	$0.2126 * R_r + 0.7152 * R_g + 0.0722R_b$	[Liao et al., 2023]

3.2 Multispectral imagery for physiological monitoring

Multispectral cameras vary in the spectral ranges they capture, which typically include red, green, blue, red edge, and near-infrared (NIR) bands (**Figure 6** shows the band distribution of the camera RedEdge (MicaSense Inc., Seattle, WA, USA). But the blue band data was considered easily contaminated by residual atmospheric effects, some multispectral cameras contain four bands, including green, red, red edge and NIR light (Songlin et al., 2023; Guanghui et al., 2020; Jie et al., 2022; Jie et al., 2023a; Jie

et al., 2023b). The green band contributes to the biophysical change of vegetation and is beneficial to the remote sensing inversion of canopy spectral indices. Some multispectral cameras contain six bands, including two green bands, green, 530 nm and green, 570 nm (Ruhua et al., 2023). The inclusion of dual green bands allows these cameras to extract richer spectral information in complex environments, meeting the demands of high-precision analysis and specialized applications.

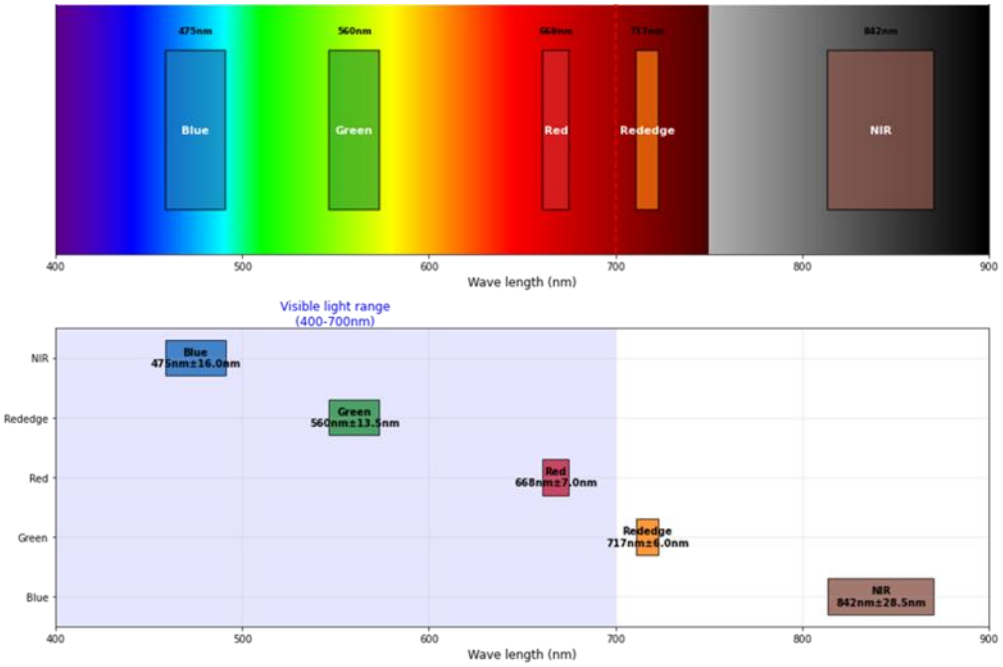

Figure 6. Band distribution map of the camera RedEdge (MicaSense Inc., Seattle, WA, USA)

Due to the presence of some visible spectral bands in the multispectral data, the original visible light reflectance and visible light spectral index of winter wheat canopy can also be obtained from the multispectral information of winter wheat canopy. In Tianxiang et al., 2021, wheat and non-wheat pixels are directly labelled according to on-site experiment and UAV RGB color image, where the RGB image is generated by using Red-Green-Blue bands of the multispectral image. In Jinya et al., 2021, Generating false-color RGB image from the calibrated red, green and blue bands. There were 10 visible color indices and 11 visible and near-infrared (Vis/Nir) spectral indices obtained from multispectral imagery (Xiaofeng et al., 2021).

The inclusion of red-edge and NIR bands provides a fundamental advantage over RGB for monitoring crop physiology, as these regions are highly sensitive to chlorophyll content, leaf internal structure, and biomass. This enables the calculation of powerful vegetation indices that are robust proxies for key biophysical parameters: NDVI is widely used to estimate fractional vegetation cover and green biomass, though it saturates under dense canopies (Songlin et al., 2023). Indices such as GNDVI and NDRE improve sensitivity to chlorophyll and nitrogen dynamics, with NDRE performing particularly well in dense vegetation (Jinya et al., 2018; Liao et al., 2023). Meanwhile, RDVI effectively estimates Leaf Area Index (LAI), a crucial variable for growth modeling (Jinkang et al., 2022). A wider spectral range results in more spectral indices being calculated, as shown in the **Table 2**.

Table 2. The multispectral vegetation indices.

Vegetation Index	Formula	Reference
Green ratio vegetation index (GRVI)	$\frac{R_{NIR}}{R_g}$	[Zongpeng et al., 2023b]
Ratio blue index (RBI)	$\frac{R_{NIR}}{R_b}$	[Jie et al., 2023a]
SR-REG	$\frac{R_{NIR}}{R_{re}}$	[Falv et al., 2022]
Structure insensitive pigment index (SIPI)	$\frac{R_{NIR}-R_b}{R_{NIR}-R_r}$ $\frac{R_{NIR}-R_b}{R_{NIR}+R_b}$	[Liao et al., 2023; Falv et al., 2022] [Chengxin et al., 2023; Jie et al., 2023a; Shuaipeng et al., 2023]
Blue-wide dynamic range vegetation index (BWDRVI)	$\frac{0.1*R_{NIR}-R_b}{0.1*R_{NIR}+R_b}$	[Zongpeng et al., 2023b]
Blue normalized difference vegetation index (BNDVI)	$\frac{R_{NIR}-R_b}{R_{NIR}+R_b}$	[Xiaofeng et al., 2021; Zongpeng et al., 2023b; Falv et al., 2022]
Normalized difference red edge blue index (BNDREI)	$\frac{R_{re}-R_b}{R_{re}+R_b}$	[Xiaofeng et al., 2021]
Normalized difference red edge green index (GNDREI)	$\frac{R_{re}-R_g}{R_{re}+R_g}$	[Xiaofeng et al., 2021; Fan et al., 2022; Wei et al., 2022; Quan et al., 2023a; Falv et al., 2022]
CRI	$\frac{1}{R_g}+\frac{1}{R_{NIR}}$	[Weilong et al., 2023]

Vegetation Index	Formula	Reference
Anthocyanin reflectance index (ARI)	$\frac{1}{R_g} - \frac{1}{R_{re}}$	[Jinya et al., 2018; Jinya et al., 2021]
Anthocyanin reflectance index1 (ARI1)	$\frac{1}{R_g} - \frac{1}{R_{NIR}}$	[Xiaofeng et al., 2021]
Anthocyanin reflectance index2 (ARI2)	$\left[\frac{1}{R_g} - \frac{1}{R_{NIR}}\right] * R_{NIR}$	[Xiaofeng et al., 2021]
Green difference vegetation index (GDVI)	$R_{NIR} - R_g$	[Zongpeng et al., 2023a; Chengxin et al., 2023; Jianjun et al., 2021; Falv et al., 2022]
Normalized blue–green band difference vegetation index (GBNDVI)	$R_{NIR} + (R_g + R_b) * (1 - R_{NIR})$	[Yan et al., 2022]
ENDVI	$\frac{R_{NIR} + R_g - 2 * R_b}{R_{NIR} + R_g + 2 * R_b}$	[Ning et al., 2022]
Green normalized difference vegetation index (GNDVI)	$\frac{R_{NIR} - R_g}{R_{NIR} + R_g}$	[Fan et al., 2022; Quan et al., 2023b; Liao et al., 2023; Falv et al., 2022; Mengxi et al., 2023]
TVI	$\sqrt{\frac{R_{NIR} - R_r}{R_{NIR} + R_r} + 0.5}$	[Guanghui et al., 2020; Quan et al., 2023b; Jianjun et al., 2021]
Triangular vegetation index (TVI)	$60 * (R_{NIR} - R_g) - 100(R_r - R_g)$	[Chengxin et al., 2023; Jing et al., 2023; Falv et al., 2022]
CI-REG	$\frac{R_{NIR}}{R_{re}} - 1$	[Fan et al., 2022; Liao et al., 2023; Falv et al., 2022]
CI-RED	$\frac{R_{NIR}}{R_r} - 1$	[Falv et al., 2022]
ChlorophyII index-green (CIG)	$\frac{R_{NIR}}{R_g} - 1$	[Quan et al., 2023a; Weilong et al., 2023; Mengxi et al., 2023]
Soil adjusted vegetation index (SAVI)	$\frac{1.5 * (R_{NIR} - R_r)}{R_{NIR} + R_r + 0.5}$	[Shaohua et al., 2024b; Jie et al., 2023a; Jingjing et al., 2024; Xiu et al., 2023]
Green band optimized soil conditioning vegetation index (GOSAVI)	$\frac{R_{NIR} - R_g}{R_{NIR} + R_g + 0.16}$ $\frac{1.16 * (R_{NIR} - R_g)}{R_{NIR} + R_g + 0.16}$	[Zongpeng et al., 2023a; Falv et al., 2022] [Wei et al., 2022; Jingjing et al., 2024; Mengxi et al., 2023]
Generalised soil-adjusted vegetation index (GSAVI)	$\frac{1.5 * (R_{NIR} - R_g)}{R_{NIR} + R_g + 0.5}$	[Jie et al., 2022; Jie et al., 2023a; Jie et al., 2023b; Falv et al., 2022, Xiu et al., 2023]

Vegetation Index	Formula	Reference
Nonlinear vegetation index (NLI)	$\frac{1.5 * (R_{NIR}^2 - R_r)}{R_{NIR}^2 + R_r + 0.5}$	[Zongpeng et al., 2023a]
	$\frac{R_{NIR}^2 - R_r}{R_{NIR}^2 + R_r}$	[Shuaipeng et al., 2023; Weilong et al., 2023]
MNLI	$\frac{1.5 * (R_{NIR}^2 - R_g)}{R_{NIR}^2 + R_r + 0.5}$	[Falv et al., 2022]
Wide dynamic range vegetation index (WDRVI)	$\frac{0.2 * R_{NIR} - R_r}{0.2 * R_{NIR} + R_r}$	[Falv et al., 2022]
	$\frac{0.12 * R_{NIR} - R_r}{0.12 * R_{NIR} + R_r}$	[Fan et al., 2022; Quan et al., 2023a]
	$\frac{0.1 * R_{NIR} - R_r}{0.1 * R_{NIR} + R_r}$	[Chengxin et al., 2023; Jinkang et al., 2022]
Noval chlorophyll absorption ratio index (NCARI)	$(R_{re} - R_r) - 0.2 * (R_{re} + R_r)$	[Jianjun et al., 2021; Yan et al., 2022; Mengxi et al., 2023]
Normalized difference red edge red index (NDREI)	$\frac{R_{re} - R_r}{R_{re} + R_r}$	[Xiaofeng et al., 2021; Jinya et al., 2018; Jinya et al., 2021; Xiu et al., 2023]
Renormalized difference vegetation index (RDVI)	$\frac{R_{NIR} - R_r}{\sqrt{R_{NIR} + R_r}}$	[Quan et al., 2023b; Shuaipeng et al., 2023; Yan et al., 2022; Jing et al., 2023;]
Normalized difference red edge index (NDRE)	$\frac{R_{NIR} - R_{re}}{R_{NIR} + R_{re}}$	[Yan et al., 2022; Jing et al., 2023; Liao et al., 2023; Quan et al., 2023a; Mengxi et al., 2023]
Normalized difference vegetation index (NDVI)	$\frac{R_{NIR} - R_r}{R_{NIR} + R_r}$	[Yuanyuan et al., 2023; Chaofa et al., 2022; Jianjun et al., 2021; Liao et al., 2023]
Renormalized difference vegetation index for rededge (RERDVI)	$\frac{R_{NIR} - R_{re}}{\sqrt{R_{NIR} + R_{re}}}$	[Falv et al., 2022]
Simplified canopy chlorophyII content index (SCCCI)	$\frac{(R_{NIR} - R_{re})(R_{NIR} + R_r)}{(R_{NIR} + R_{re})(R_{NIR} - R_r)}$	[Chengxin et al., 2023; Fan et al., 2022; Jinya et al., 2018; Quan et al., 2023a; Falv et al., 2022]
NAVI	$1 - \frac{R_r}{R_{NIR}}$	[Falv et al., 2022]
Ratio vegetation index (RVI)	$\frac{R_{NIR}}{R_r}$	[Yang et al., 2023; Fan et al., 2022; Quan et al., 2023b]
RedEdge ratio index1 (RRI1)	$\frac{R_{NIR}}{R_{re}}$	[Zongpeng et al., 2023b; Jingjing et al., 2024]
RedEdge ratio index2 (RRI2)	$\frac{R_{re}}{R_r}$	[Zongpeng et al., 2023b]

Vegetation Index	Formula	Reference
ChlorophyII index-rededge (CIRE)	$\frac{R_{NIR}}{R_{re}} - 1$	[Yang et al., 2023; Jinya et al., 2018; Xiaokai et al., 2023]
Difference vegetation index (DVI)	$R_{NIR} - R_r$	[Jianjun et al., 2021; Jing et al., 2023; Liao et al., 2023;]
Red edge difference vegetation index (REDVI)	$R_{NIR} - R_{re}$	[Falv et al., 2022]
Adjusted transformed soil-adjusted vegetable index (ATSAVI)	$\frac{1.22 * (R_{NIR} - 1.22 * R_r - 0.03)}{1.22 * R_{NIR} + R_r + 0.16}$	[Chengxin et al., 2023]
	$\frac{1.22 * (R_{NIR} - 1.22 * R_r - 1.22}{1.22 * R_{NIR} + R_r - 0.0366 + 0.08 *}$	[Zongpeng et al., 2023b]
Optimized soil adjusted vegetation index (OSAVI)	$\frac{1.16 * (R_{NIR} - R_r)}{R_{NIR} + R_r + 0.16}$	[Liao et al., 2023; Jingjing et al., 2024; Mengxi et al., 2023]
	$\frac{R_{NIR} - R_r}{R_{NIR} - R_r + 0.16}$	[Yang et al., 2023; Fan et al., 2022; Quan et al., 2023a]
Red edge soil-adjusted vegetation index (RESAVI)	$\frac{1.16 * (R_{NIR} - R_{re})}{R_{NIR} + R_{re} + 0.16}$	[Falv et al., 2022]
Modified simple ratio index (MSR)	$\frac{\frac{R_{NIR}}{R_r} - 1}{\sqrt{\frac{R_{NIR}}{R_r} + 1}}$	[Shaohua et al., 2024b; Quan et al., 2023b; Shuaipeng et al., 2023; Wei et al., 2022]
Red edge modified simple ratio index (REMSR)	$\frac{\frac{R_{NIR}}{R_{re}} - 1}{\sqrt{\frac{R_{NIR}}{R_{re}} + 1}}$	[Falv et al., 2022]
Modified soil-adjusted vegetation index (MSAVI)	$\frac{2 * R_{NIR} + 1 - \sqrt{(2 * R_{NIR} + 1)^2 - 8}}{2}$	[Fan et al., 2022; Liao et al., 2023; Mengxi et al., 2023]
Modified soil-adjusted vegetation index2 (MSAVI2)	$\frac{2 * R_{NIR} + 1 - \sqrt{(2 * R_{NIR})^2 - 8 * (I}}{2}$	[Chaofa et al., 2022; Quan et al., 2023b]
Nitrogen reflectance index (NRI)	$\frac{R_g - R_r}{R_{NIR} - R_r}$	[Liao et al., 2023]
Structure intensive pigment index (SIPI)	$\frac{R_{NIR} - R_b}{R_{NIR} - R_r}$	[Yang et al., 2023; Jingjing et al., 2024]
Plant senescence reflectance index (PSRI)	$\frac{R_r - R_b}{R_{NIR}}$	[Shuaipeng et al., 2023; Weilong et al., 2023]
Enhanced vegetation index (EVI)	$\frac{2.5 * (R_{NIR} - R_r)}{R_{NIR} + 6 * R_r - 7.5R_b + 1}$	[Chengxin et al., 2023; Zongpeng et al., 2023b; Xiu et al., 2023]
Enhanced vegetation index1 (EVI1)	$\frac{2.5 * (R_{NIR} - R_r)}{R_{NIR} - 2.4 * R_r + 1}$	[Fan et al., 2022; Falv et al., 2022]

Vegetation Index	Formula	Reference
Enhanced vegetation index2 (EVI2)	$\frac{2.5 * (R_{NIR} - R_r)}{R_{NIR} + 2.4 * R_r + 1}$	[Ryoya et al., 2023; Jing et al., 2023; Mengxi et al., 2023]
Modified chlorophyll absorption in reflectance index (MCARI)	$\frac{R_{re} - R_r - 0.2(R_{re} - R_g)}{\frac{R_{re}}{R_r}}$	[Shaohua et al., 2024b]
	$\frac{R_{re} - R_r - 0.2(R_{re} - R_g)\frac{R_{re}}{R_r}}{\frac{R_{re}}{R_r}}$	[Jianjun et al., 2021; Liao et al., 2023; Quan et al., 2023a; Weilong et al., 2023]
Modified chlorophyll absorption in reflectance index1 (MCARI1)	$\frac{R_{NIR} - R_{re} - 0.2(R_{NIR} - R_g)}{\frac{R_{NIR}}{R_{re}}}$	[Jie et al., 2022; Jie et al., 2023a; Yuanyuan et al., 2023; Falv et al., 2022]
Modified chlorophyll absorption in reflectance index2 (MCARI2)	$1.2[2.5 * (R_{NIR} - R_r) - 1.3(R_{NIR} - R_g)]$	[Jinkang et al., 2022; Falv et al., 2022]
Triangular chlorophyll index (TCI)	$1.2(R_{re} - R_g) - 1.5(R_r - R_g)\sqrt{\frac{R_{re}}{R_r}}$	[Jianjun et al., 2021]
Transformed chlorophyll absorption and reflectance index (TCARI)	$3[(R_{re} - R_r) - 0.2(R_{re} - R_g)\frac{R_{re}}{R_r}]$	[Jinya et al., 2018; Shuaipeng et al., 2023; Weilong et al., 2023]
	$1.5[2.5(R_{re} - R_g) - 2.1(R_r - R_g)]$	[Falv et al., 2022]
Modified triangular vegetation index (MTVI)	$1.2[2.5(R_{NIR} - R_g) - 2.5(R_r - R_g)]$	[Zhengang et al., 2021; Jinkang et al., 2022; Chaofa et al., 2022]
Modified triangular vegetation index2 (MTVI2)	$\frac{1.5[2.5(R_{re} - R_g) - 2.5(R_r - R_g)}{\sqrt{2(R_{NIR} + 1)^2 - 6R_{NIR} + 5\sqrt{R_r} - 0}}$	[Shuaipeng et al., 2023; Weilong et al., 2023; Mengxi et al., 2023]
ChlorophyII vegetation index (CVI)	$\frac{R_{NIR}}{R_g} * \frac{R_r}{R_g}$	[Zongpeng et al., 2023a; Jinya et al., 2018; Shuaipeng et al., 2023; Jianjun et al., 2021]
RTVI-CORE	$100(R_{NIR} - R_{re}) - 10(R_{NIR} - R_g)$	[Falv et al., 2022]
GARI	$\frac{R_{NIR} - [R_g - 1.7(R_b - R_r)]}{R_{NIR} + [R_g - 1.7(R_b - R_r)]}$	[Chengxin et al., 2023; Falv et al., 2022]
Modified normalised difference index (MNDI)	$\frac{R_{NIR} - R_{re}}{R_{NIR} - R_g}$	[Zongpeng et al., 2023a]
Normalised NIR index (NNI)	$\frac{R_{NIR}}{R_{NIR} + R_{re} + R_g}$	[Zongpeng et al., 2023a]

Vegetation Index	Formula	Reference
Normalised red-edge index (NREI)	$\frac{R_{re}}{R_{NIR}+R_{re}+R_g}$	[Zongpeng et al., 2023a]
Single red-edge band chlorophyll index (SRCI)	$\frac{R_{NIR}-R_{re}}{R_{re}-R_r}$	[Liao et al., 2023; Weilong et al., 2023; Mengxi et al., 2023]
Leaf chlorophyll index (LCI)	$\frac{R_{NIR}-R_{re}}{R_{NIR}-R_r}$	[Jie et al., 2022; Jie et al., 2023a; Xiaokai et al., 2023]
	$\frac{R_{NIR}-R_{re}}{\sqrt{R_{NIR}+R_r}}$	[Yang et al., 2023]
MERIS terrestrial chlorophyll index (MTCI)	$\frac{R_{NIR}-R_{re}}{R_{re}+R_r}$	[Shuaipeng et al., 2023; Jianjun et al., 2021]

Due to the addition of a wider range of spectra, the calculated multispectral vegetation index has more numbers than visible light vegetation index, and there was the same vegetation index formula with different names. Ratio vegetation index (RVI) in Jinya et al., 2018, was named simple ratio (SR) in Jinkang et al., 2022. Enhanced vegetation index (EVI) in Jingjing et al., 2024, was called soil and atmospherically resistant vegetation index (SARVI) in Zongpeng et al., 2023b. while others have only different equations but same names. Such as modified chlorophyll absorption in reflectance index (MCARI) in Jianjun et al., 2021; Jinkang et al., 2022; Shaohua et al., 2024b and Guanghui et al., 2020, are different vegetation index. These papers are cited by different researchers, which leads to different results when comparing the effects of vegetation indices with the same name.

Multispectral data can also be used to generate false-color RGB composites for visual interpretation. Nevertheless, the fixed, broad bands of multispectral sensors limit their ability to detect subtle spectral features, which can be critical for precise quantification of biochemical constituents like nitrogen.

3.3 Hyperspectral imagery: high-fidelity spectral analysis

Hyperspectral imaging surpasses multispectral by capturing reflectance data across hundreds of narrow, contiguous spectral bands (e.g., 125–300 bands within 400–1000 nm), creating a continuous spectrum for each pixel (**Figure 7**). This high spectral

resolution (e.g., 4 nm) allows for precise identification of specific wavelengths that correlate with plant biochemical properties.

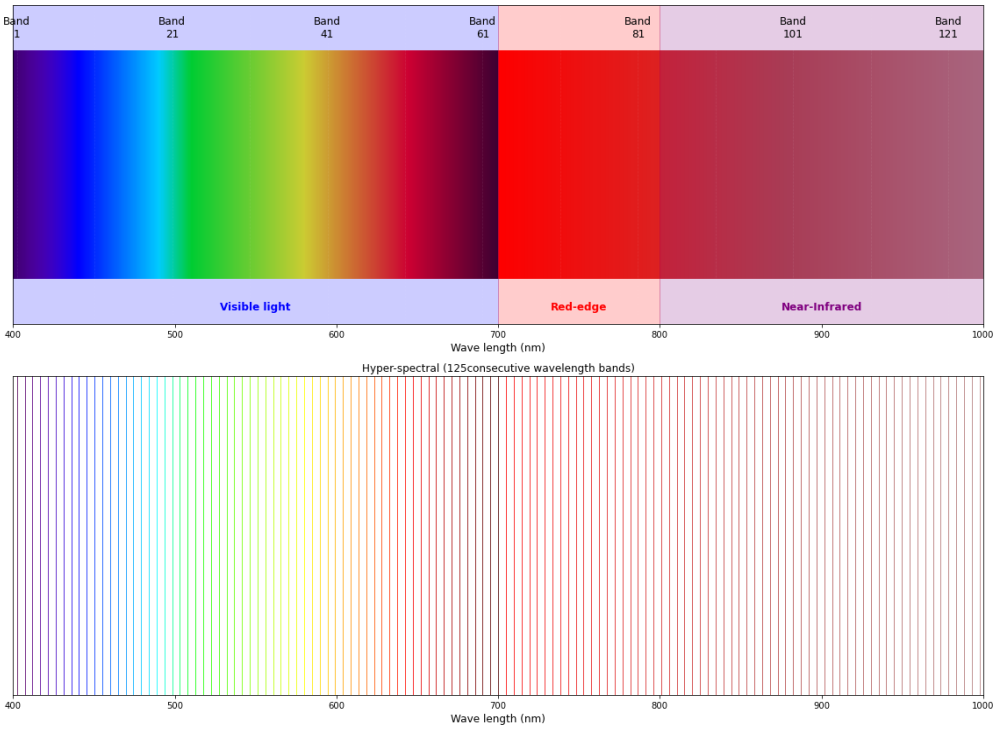

Figure 7. 125-band hyperspectral imaging.

Hyperspectral data offers significant technical advantages due to its high spectral resolution. One key benefit is enhanced precision in retrieving plant biochemical parameters, such as leaf nitrogen content (LNC) and chlorophyll concentration, as narrow-band indices—particularly at wavelengths like 458 nm, 492 nm, and 740 nm—have been demonstrated to achieve lower estimation errors compared to broad-band multispectral indices (Jinkang et al., 2022). Furthermore, hyperspectral imaging enables detailed spectral analysis, supporting advanced methodologies including the identification of specific spectral features such as the red-edge position, as well as the application of full-spectrum techniques like partial least squares regression. These approaches contribute to building more accurate predictive models for key vegetation traits, including leaf area index (LAI) and dry biomass (Zongpeng et al., 2022; Kaur, S., 2024).

However, these advantages come with challenges, including immense data volume, high computational demands for processing, and greater cost, which can limit its practical application in routine field scouting.

3.4 Thermal infrared imagery: water stress detection

TIR sensors measure radiation in the long-wave infrared spectrum (approximately 7.5-13.5 μm), which is directly related to the canopy's surface temperature. This provides a unique capability to monitor crop water status, as water-stressed plants typically have reduced transpiration and cooling, leading to higher canopy temperatures.

Key metrics derived from Thermal Infrared (TIR) imagery include canopy temperature (CT), which represents the average temperature measured at the plot level and serves as a fundamental indicator of plant thermal status (Zhengang et al., 2021). Another essential metric is the Crop Water Stress Index (CWSI), a normalized index that quantifies water stress levels by comparing canopy temperature to ambient atmospheric conditions (Jingjing et al., 2024). Additionally, the canopy-air temperature difference (CTD), calculated as the simple difference between canopy temperature and air temperature, provides insight into evaporative cooling and plant physiological activity (Shaohua et al., 2024b). These metrics are widely used for monitoring crop water status, stress responses, and irrigation management.

TIR data provides a direct physiological signal that is largely independent of the spectral information from other sensors, making it highly complementary for integrated stress assessment.

4. Machine learning algorithms used in winter wheat research

The application of machine learning (ML) is pivotal for translating UAV-derived spectral data into actionable agronomic insights. Numerous international studies have recently shown the real potential of such an approach. Fatemeh et al. (2024) developed a UAV-RGB-image workflow for yellow rust detection, utilizing feature extraction, ANOVA-based feature prioritization, and ML classification. Nduku et al. (2024) showed that gaussian process regression (GPR) applied to UAV multispectral vegetation indices (VIs) provides the most accurate prediction of winter wheat crop height (R^2 = 0.69-0.74), outperforming soil-integrated models

and offering a cost-effective solution for in-season stress and growth monitoring. Beltrame et al. (2024) proposed a scalable, explainable deep learning approach using reduced-resolution UAV multispectral imagery (60 meters height) for efficient yellow rust scoring (1-9 scale), achieving high accuracy with minimal bands (EVI, Red, GNDVI) and fewer time steps, enabling cost-effective large-scale phenotyping. Kaushal et al. (2024) demonstrated that integrating UAV-based high-throughput phenotyping (HTP) traits with deep neural networks (DNNs) significantly enhances phenomic prediction of grain yield (GY R^2=0.76), test weight, and protein content, yielding a 32% improvement in forward GY prediction using multi-location data; they also found HTP traits like ARI and GCI boost multi-trait genomic selection (MT-GS) accuracy beyond single-trait models.

Within China, research based on our reviewed literature indicates that winter wheat monitoring using UAV remote sensing primarily employs three algorithmic categories: linear models, traditional machine learning models, and neural network models. Illustrating this, Xiaokai et al. (2023) applied linear nonparametric regression and traditional ML methods to evaluate winter wheat plant nitrogen concentration. Similarly, Liao et al. (2023) leveraged high-precision UAV multispectral imagery, employing both traditional ML and neural network models to estimate critical biophysical parameters including leaf area index (LAI), canopy photosynthetic pigments (CPP - chlorophyll a, b, and carotenoids), and leaf nitrogen concentration (LNC).

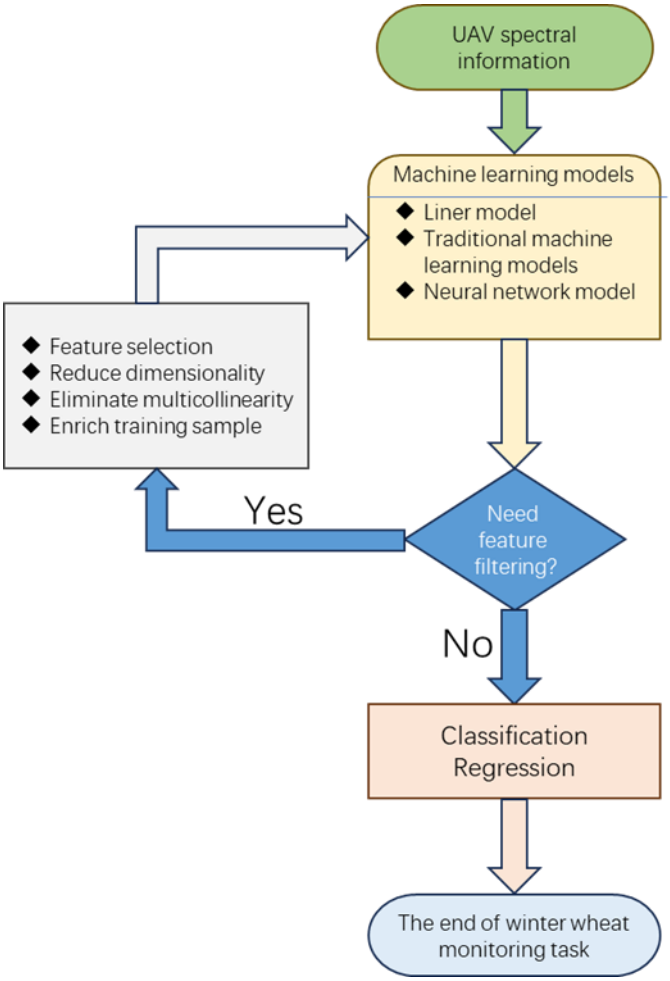

Figure 8. The application of machine learning algorithm.

This section systematically reviews the ML methodologies employed in winter wheat research, categorizing them into two interconnected processes: feature engineering and predictive modeling (**Figure 8**).

4.1 Using machine learning method for feature extraction

The choice of input features is as important as the choice of the algorithm to be used when building the model (Zongpeng et al., 2022). The high-dimensionality of UAV data (e.g., hundreds of hyperspectral bands, multiple vegetation indices) necessitates sophisticated feature engineering to enhance model performance and interpretability.

For doing feature filtering, there were four types methods, including feature selection, reduce dimensionality, eliminate multicollinearity and enrich training samples.

To identify features most relevant to winter wheat, multiple feature selection techniques have been employed. Methods such as recursive feature elimination (RFE), the Boruta algorithm, and Pearson correlation coefficient (PCC) have been used to filter spectral indices, reduce data dimensionality, and rank feature importance (Zongpeng et al., 2022). Competitive adaptive reweighted sampling (CARS) has also been applied to select features from reflectance data, vegetation indices, and texture metrics (Yan et al., 2022). Another study utilized K-means and genetic algorithms (GA) to identify 18 informative multispectral vegetation indices (Chengxin et al., 2023), while first derivative (FD), successive projections algorithm (SPA), CARS, and its hybrid CARS_SPA were effective in extracting characteristic bands related to leaf area index (LAI) from hyperspectral imagery (Juanjuan et al., 2021). Additional techniques such as Pearson correlation analysis coupled with multiple stepwise regression (MSR) helped identify optimal vegetation indices and red-edge parameters (Qi et al., 2023).

When excessive spectral information risks causing overfitting, dimensionality reduction becomes indispensable. For instance, principal component analysis (PCA) was applied to near-infrared bands (750–1000 nm), successfully compressing 75 original bands into three principal components while retaining critical information (Juncheng et al., 2023a).

Multicollinearity among features can undermine model stability, and machine learning methods have been introduced to mitigate this issue. The variance inflation factor (VIF) was used to screen vegetation indices (VIs) and texture features (TFs), resulting in a fused “graph–spectrum” index free from multicollinearity (Juanjuan et al., 2022).

Finally, the challenge of limited field-scale training samples has been addressed through innovative simulation and modeling frameworks. A split-merge methodology was proposed to alleviate sample scarcity (Juncheng et al., 2023b), and the CW-RF model incorporated a crop growth model (CERES-Wheat) to simulate ample training samples at the plot scale, thereby supporting random forest-based yield estimation (Siqi et al., 2021).

4.2 Using machine learning for building models

The selection of an appropriate machine learning algorithm is contingent upon the nature of the input data and the specific monitoring objective. The reviewed literature reveals a clear paradigm: traditional machine learning models excel with pre-engineered features (e.g., vegetation indices, texture metrics), while deep learning architectures are superior for processing raw, high-dimensional image data directly.

When dealing with tabular datasets derived from spectral information—such as vegetation indices, band reflectance, and texture features—ensemble and kernel-based machine learning methods often achieve significantly better performance than conventional linear regression. Among ensemble techniques, Random Forest (RF) is frequently identified as a top-performing model. Its robustness and excellent performance in high-dimensional feature spaces have made it one of the standard tools for agricultural remote sensing prediction (Fulv et al., 2022; Zongpeng et al., 2023b). It is capable of capturing complex nonlinear relationships while resisting overfitting, even with a large number of input variables; it has been shown to outperform methods like Support Vector Regression (SVR) in applications such as biomass estimation (Chiu, M.S., 2024). Gaussian Process Regression (GPR) is another powerful approach, recognized for high predictive accuracy in estimating traits like crop height ($R^2 = 0.69–0.74$) and yield. A major advantage of GPR is its ability to provide uncertainty estimates alongside predictions, making it particularly useful for risk-aware applications (Nduku, L., 2024; Chaofa et al., 2022). Other widely adopted algorithms include Support Vector Machines (SVM/SVR) and Partial Least Squares Regression (PLSR). Moreover, combining multiple vegetation indices with ensemble or kernel methods such as RF and PLSR has been proven to enhance prediction accuracy for plant traits beyond what is achievable with linear models (Kaur, S., 2024). More advanced techniques like Extreme Gradient Boosting (XGBoost) and Elastic Net Regression (ENR) are also gaining traction due to their robustness and performance (Shuaipeng et al., 2022). It is common practice to evaluate multiple algorithms—such as RF, SVR, GPR, and k-Nearest Neighbors (kNN)—on the same dataset to determine the best-performing model for specific tasks like yield prediction or leaf area index (LAI) estimation (Zongpeng et al., 2023b; Liao et al., 2023).

For tasks involving time dynamic modeling, such as capturing the growth status of key phenological stages, the advanced variant of the recurrent neural network (RNN), the long short-term memory (LSTM) network, has become the preferred method. Due to its outstanding gating mechanism, LSTM can effectively learn long-

term dependencies and has been successfully applied to extract crop growth dynamic features from time-series remote sensing data (Xu et al., 2020). Using recurrent neural networks directly enables the processing of sequences of input features (such as vegetation indices that change over time), and automatically extracts the phenological perception patterns that are crucial for yield prediction.

For tasks involving raw image inputs, deep learning models are indispensable due to their capacity to automatically learn discriminative spatial and spectral features directly from pixel data, eliminating the need for manual feature engineering. Convolutional Neural Networks (CNNs)—including standard architectures and deeper variants like EfficientNetV2—are widely used for both image classification and end-to-end regression tasks, such as predicting crop yield directly from RGB imagery (Juncheng et al., 2023b). For pixel-level classification applications like disease detection or ear counting, specialized segmentation models such as Fully Convolutional Networks (FCN) and U-Net have proven highly effective, generating detailed segmentation maps from multispectral or hyperspectral images (Jinya et al., 2021; Juncheng et al., 2020). More advanced strategies involve multi-modal and hybrid deep learning frameworks designed to integrate information from diverse sensors. For example, architectures like Multimodal Net combine features from RGB, hyperspectral, and thermal imagery to achieve state-of-the-art performance in yield prediction (Juncheng et al., 2023a). Additionally, 1D-CNNs have been used to model spectral signatures or temporal sequences of vegetation indices, in some cases outperforming traditional machine learning models even on tabular data derived from images (Zongpeng et al., 2023b).

To address the long-standing problem of scarce labeled data in agricultural applications, semi-supervised learning (SSL) technology offers a promising solution. These methods combine a small amount of labeled data with a large amount of unlabeled data to enhance the generalization ability of the model. The self-training algorithm generates pseudo labels for unlabeled data by using a model trained based on labeled data, thereby expanding the effective training set (Tuia et al., 2016). This makes it particularly outstanding in the field of remote sensing among various methods of semi-supervised learning.

Finally, in order to predict multiple related agronomic traits (such as fresh weight and dry weight), multi-task learning (MTL) can provide a framework that enhances prediction efficiency and do not decrease accuracy by sharing input features among related tasks. This concept has a solid theoretical foundation in the field of machine learning (Caruana, 1997).

In summary, the algorithmic landscape is not one of replacement but of complementarity. The choice hinges on the data representation. Traditional ML models provide powerful, interpretable tools for analyzing extracted features, while deep learning offers unparalleled capability for learning directly from complex image data, enabling more automated and comprehensive phenotypic analysis. Nevertheless, the challenge of data scarcity remains a significant bottleneck for the widespread application of deep learning in precision agriculture, solidifying the continued relevance of hybrid and strategically chosen models for most practical, field-scale applications.

5. Key research applications and findings

Based on our review of the selected literature, eighteen tasks of winter wheat monitoring have been researched based on UAV platform and machine learning algorithm. Among them, the number of publications on nitrogen content in winter wheat is the highest, followed by the number of publications on yield prediction of winter wheat plants. **Figure 9** illustrates the distribution of tasks.

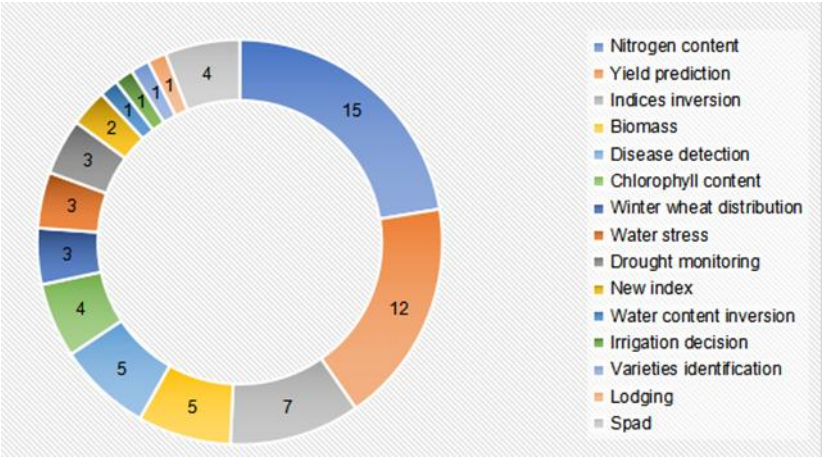

Figure 9. The research tasks of winter wheat.

This section synthesizes the principal research applications identified in the reviewed literature, detailing how UAV remote sensing and machine learning (ML) are deployed to address critical winter wheat monitoring tasks. The applications are categorized and analyzed below.

5.1 Winter wheat yield estimation

Yield prediction has evolved from single-source data analysis to sophisticated multi-sensor and multi-temporal fusion models. A promising approach involves direct image-based prediction using deep learning models. For instance, Juncheng et al. (2023b) demonstrated that high-resolution RGB imagery processed with an EfficientNetV2 architecture can achieve competitive prediction accuracy (R^2 = 0.6341, MAPE = 7.43%), with the grain-filling stage identified as particularly informative.

More commonly, vegetation indices (VIs) derived from multispectral or hyperspectral imagery are used as inputs for machine learning models. Among these, Gaussian Process Regression (GPR) has shown notably high performance, reaching R^2 values of 0.87–0.88 when integrating multi-temporal VI data, while ensemble methods combined with feature selection techniques such as Boruta have also yielded strong results (R^2 = 0.78) (Chaofa et al., 2022; Yang et al., 2023; Zongpeng et al., 2022).

Advanced modeling techniques continue to improve accuracy: 1D convolutional neural networks (1D-CNNs) applied to time-series VIs can outperform traditional machine learning models, and custom deep learning frameworks—such as MultimodalNet, which fuses RGB, hyperspectral, and thermal imagery—have achieved elevated prediction performance (R^2 = 0.74) by capturing complementary crop traits (Zongpeng et al., 2023b; Juncheng et al., 2023a).

Alternatively, some studies employ indirect yield estimation by first predicting intermediate physiological parameters like leaf area index (LAI) and leaf nitrogen content (LNC) from UAV data, then integrating these into crop models (e.g., CERES-Wheat) or machine learning algorithms such as Random Forest, offering another robust pathway for accurate yield forecasting (Siqi et al., 2021).

Although the accuracy has improved, currently many yield prediction models remain physiological blindness. They establish a direct spectral-yield correlation, but often lack a systematic analysis of physiological driving factors (for example, how nitrogen uptake at specific stages or biomass accumulation is transformed into final yield). Moreover, models that heavily rely on multi-temporal data encounter practical obstacles when applied to new regions or new varieties where there is a lack of historical marked yield data (Waldner et al., 2019).

5.2 Winter wheat nitrogen content monitoring

The non-destructive assessment of nitrogen status is essential for precision nutrient management, and machine learning (ML) models have demonstrated a strong capacity to integrate diverse data sources for this purpose. One particularly effective approach involves the fusion of spectral and texture features (TFs). Models combining vegetation indices (VIs) with TFs consistently outperform those using spectral information alone. For instance, a Ridge Regression (RR) model integrating both VIs and TFs achieved high accuracy in estimating Leaf Nitrogen Content (LNC), with an R^2 value of 0.87 (Juanjuan et al., 2020).

Advanced machine learning algorithms further enhance prediction performance for nitrogen-related traits. Methods such as Support Vector Regression (SVR) and Random Forest (RF) have proven especially effective in estimating Plant Nitrogen Concentration (PNC). These models can explain over 90% of the variability at critical growth stages, significantly surpassing the performance of traditional linear regression techniques (Xiaokai et al., 2023).

Multi-view and multi-sensor integration represents another frontier for improving estimation robustness. The use of multi-view imagery, which captures crop canopies from multiple angles, along with the fusion of data from diverse sensors—including multispectral, RGB, and thermal infrared—has been shown to substantially improve the accuracy and reliability of nitrogen status assessment (Ning et al., 2022; Fan et al., 2022).

However, high-performance nitrogen content prediction models usually require labor-intensive field measurement ground truth for calibration, which creates scalability bottlenecks (Cao et al., 2023).

5.3 Winter wheat biomass estimation

The estimation of Above-Ground Biomass (AGB) addresses a key challenge in precision agriculture which is the saturation of vegetation indices (VIs) during mid-to-late crop growth stages. Machine learning (ML) techniques offer an effective solution for mitigating this limitation. By combining multispectral data with algorithms such as Random Forest (RF) and Partial Least Squares Regression (PLSR), models can significantly improve AGB estimation accuracy. Research has shown that the heading stage is particularly suitable for AGB prediction, with RF models achieving notably high performance—reaching R^2 values of up to 0.93 (Falv et al., 2022).

To further enhance estimation accuracy, multi-modal data integration has been widely adopted. Combining vegetation indices with canopy structural parameters and temperature data can substantially improve the predictive ability of biomass

models. For instance, RF models utilizing such integrated data at the anthesis stage have yielded R^2 values as high as 0.897 (Shaohua et al., 2024b). Additionally, the inclusion of terrain factors such as slope helps account for field variability, further refining model performance and supporting more reliable biomass estimation across diverse growing conditions.

The success of biomass estimation is highly dependent on obtaining high-quality data during critical growth stages. The generalization ability of the model under different varieties, planting densities, and environmental conditions still needs to be further verified. Although multi-sensor fusion improves robustness, it also increases data complexity and cost. Moreover, most studies develop dedicated models for a single parameter, failing to utilize the physiological correlations between related traits (for example, dry weight and fresh weight) through a joint modeling framework (Caruana, 1997).

5.4 Disease detection, the case of yellow rust

UAV-based remote sensing offers a powerful tool for the early and non-destructive detection of crop diseases such as yellow rust. By using low-cost multispectral cameras combined with machine learning classifiers like Random Forest (RF), it becomes possible to accurately distinguish infected from healthy plants. Studies have demonstrated that specific vegetation indices—including Ratio Vegetation Index (RVI), Normalized Difference Vegetation Index (NDVI), and Optimized Soil-Adjusted Vegetation Index (OSAVI)—can achieve discrimination accuracy as high as 89.3% (Jinya et al., 2018).

Beyond traditional multispectral methods, deep learning approaches provide even greater capabilities for disease detection. Deep Convolutional Neural Networks (DCNNs) leverage high-dimensional hyperspectral imagery to exploit both spatial patterns and spectral details, enabling precise segmentation and identification of disease areas. These models have achieved high overall accuracy, up to 0.85, outperforming conventional spectral index-based methods and offering a robust solution for automated crop health monitoring (Xin et al., 2019).

The disease detection method based on specific spectral indices is prone to confusion with the spectral responses of nutrient stress (such as nitrogen deficiency) or water stress (Poblete et al., 2017). Its specificity needs to be improved. Although deep learning methods have high accuracy, their decision-making process is difficult to explain, and they usually require a large number of labeled samples for

training, which is difficult to meet in the early stages of disease or when disease outbreaks are infrequent (Berger et al., 2020).

5.5 Estimation of other growth indicators

UAV-based remote sensing methods have been effectively extended to accurately estimate Leaf Area Index (LAI), a key biophysical parameter. Estimation performance is significantly improved by integrating vegetation indices (VIs) with texture features and plant height (PH) data. For instance, the XGBoost model has achieved notably high accuracy with an R^2 value of 0.88 (Mengxi et al., 2023). Additionally, the combination of hyperspectral data and feature selection algorithms such as CARS_SPA has also yielded excellent results, reaching an R^2 of 0.89 (Juanjuan et al., 2021).

Beyond LAI, these techniques have been successfully applied to monitor chlorophyll content and SPAD values, which are critical indicators of plant physiological status. Machine learning algorithms, including Support Vector Machines (SVM) and Long Short-Term Memory (LSTM) networks, have demonstrated strong effectiveness in estimating these parameters using vegetation indices and texture indicators across diverse environmental conditions (Wei et al., 2022; Quan et al., 2023a).

The methodology further demonstrates remarkable versatility through its application to various other agricultural monitoring tasks. These include soil salinity inversion (Guanghui et al., 2020), tiller density estimation (Jinkang et al., 2022), water stress diagnosis (Jingjing et al., 2024), and precise ear segmentation (Juncheng et al., 2020). This broad range of applications underscores the significant potential of UAV-based remote sensing combined with machine learning in advancing precision agriculture practices.

The estimation of these diverse indicators mostly follows a similar "feature extraction - model training" paradigm, which results in a large number of isolated "one problem - one model" researches. They are computationally inefficient and ignores the inherent physiological correlations among different agronomic parameters, failing to achieve performance gains and model simplification through joint learning (Segal et al., 2019).

6. Conclusion and outlook: from limitations to integration path

This comprehensive review systematically examines the evolution of crop phenotyping technologies, with a particular emphasis on the transformative impact of UAV-based remote sensing and machine learning in winter wheat monitoring. Our analysis identifies a clear technological progression and, more importantly, critically assesses the limitations that currently constrain the field. These insights directly inform a strategic path forward for both research and practical application.

6.1 Analysis of the Fundamental Limitations of the Methodology

While the current studies have made progress, they are still facing some key methodological challenges, which constitute the bottlenecks that urgently need to be overcome in this field. First, the insufficiency of current spectral indices presents a fundamental constraint. While widely employed, these indices suffer from a critical lack of specificity. For instance, NDVI effectively captures general "greenness" but fails to distinguish between nitrogen deficiency, water stress, or disease presence. This conflation of responses, coupled with a general lack of standardization and their inability to capture complex, non-linear relationships through higher-order terms or cross-sensor computations, severely limits their diagnostic power for targeted management (Zongpeng et al., 2022; Yu et al., 2025).

Second, the application of machine learning to winter wheat monitoring faces its own set of distinct challenges. A primary constraint is the "ground-truth bottleneck", where the high cost and labor associated with collecting sufficient labeled data (e.g., measured nitrogen content, accurate yield) severely limits model scalability (Cao et al., 2023). Furthermore, models often suffer from limited generalizability across different environments, cultivars, and seasons (Berger et al., 2020), and complex algorithms frequently operate as "black boxes," providing predictions without agronomically meaningful explanations that are vital for field-level decision-making (Zongpeng et al., 2022).

These limitations have given rise to two popular yet suboptimal paradigms in current research. The first is the "one-problem-one-model" approach, which is computationally inefficient and fails to leverage the inherent physiological correlations between related agronomic traits (e.g., fresh and dry biomass), thereby limiting accuracy and robustness (Caruana, 1997). The second is the interpretability gap, where numerous studies establish direct spectral-yield correlations but function as "black boxes," lacking systematic analysis of the physiological drivers, such as

nitrogen content and biomass accumulation, which link spectral signals to the final output (Liao et al., 2023).

6.2 Integrating the forward path: From diagnosing limitations to collaborative solutions

The key challenges like water scarcity and nitrogen application excessive in intensive winter wheat systems are not independent. For example, water deficit directly limits physiological processes, while nitrogen fertilizer overuse under such stress represents an inefficiency. Their effects on final yield are interconnected. This leads to a complex diagnostic problem, which cannot be resolved by monitoring using spectral or thermal information only (Lobell, 2015; Berger et al., 2020). Therefore, the fusion of multispectral and thermal infrared cameras built on UAV platforms can be used to collected this complex interaction information. And the strategic integration of multi-sensor data with advanced machine learning techniques can be used to analyse these challenges. A key conclusion from our study is that single sensor can hardly fully capture the complex physiological processes underlying winter wheat yield formation. For instance, multispectral sensors—delivering chlorophyll and nitrogen-related information via indices such as NDRE—complement thermal infrared sensors, which monitor water stress through indicators like the Crop Water Stress Index (CWSI). Together, they provide synergistic insights into key yield-determining processes, including photosynthetic activity, biomass accumulation, and plant water status. This integrated approach allows the model to disentangle complex stress signals, leading to more robust and physiologically interpretable prediction models (Poblete et al., 2017; Caturegli et al., 2020).

To overcome the challenge of temporal dependency blindness, limited labeled data, and computing efficiency, this study adopts three key machine learning strategies. First, Long Short-Term Memory (LSTM) networks are used to capture crop growth dynamics across different growth stages, enabling temporal modeling beyond static analysis (Yu et al., 2019). Second, semi-supervised learning methods such as self-training help utilize abundant unlabeled UAV data to improve model generalization when ground truth is scarce (Tuia et al., 2016). Finally, multi-task learning allows simultaneous prediction of related traits like dry and fresh biomass, increasing data efficiency and accuracy through shared representations (Caruana, 1997). Combined with multi-sensor fusion, these approaches form an integrated framework for building an interpretable and practical crop monitoring system.

6.3 Synthesis and future perspectives

In conclusion, this review directly determines the experimental and methodological strategies advocated in this article: the use of multi-sensor, multi-time-point drone technology, and analysis through a powerful and easily understandable machine learning model, aiming to go beyond simple correlations and build a diagnostic monitoring system based on physiological principles.

In order to achieve systematic development in this field, future research must focus on several key paths. Firstly, efforts should be concentrated on developing machine learning models based on physical principles, integrating agricultural principles with data-driven algorithms to enhance the interpretability and universality of the models (Yu et al., 2020). Secondly, advancing transfer learning and domain adaptation is crucial for directly addressing issues such as data scarcity and the limited generalizability of models in different environments (Berger et al., 2020). Thirdly, developing integrated multi-task learning systems is essential for efficiently handling multiple monitoring targets simultaneously (Waldner et al., 2019).

Furthermore, an expandable method that combines high-resolution drone data with satellite images is crucial for extending monitoring work from the field to the regional level. Finally, future systems must evolve into a closed-loop decision support platform that can convert multi-source sensor data into actionable management recommendations. This requires closer integration with precision agriculture technologies and the development of user-friendly interfaces for farmers.

In conclusion, the integration of unmanned aerial vehicle (UAV) remote sensing and machine learning has fundamentally changed the way winter wheat monitoring. By directly addressing the limitations of current spectral indices and machine learning applications, and strategically advancing the research directions outlined, this combined technical approach is expected to become an indispensable tool for promoting sustainable precision agriculture and strengthening global food security.

III

Research Methods and Experimental Design

1. Experiment design and data acquisition

1.1 Experimental site and rationale

We conducted a field trial over several years in Xinxiang City, Henan Province, located within China's North China Plain (NCP). This region is a typical representative of the winter wheat production area in the country. The trial site has been used for agricultural experiments for many years. This provides clear and explicit historical background information on soil characteristics, crop performance, and management practices. Although we recently introduced phenotypic analysis technology based on drones, our research is however built upon a solid and reliable historical foundation. The introduction of UAV remote sensing technology represents an improvement in monitoring capabilities on a stable experimental platform, allowing us to capture unprecedented details of the physiological processes behind the agricultural achievements observed over the years.

The experimental design consists of two complementary areas (Field I and Field II), each containing 180 experimental plots, arranged using a randomized complete block design and repeated three times. Despite being an open field, the site provides a sufficiently controllable environment. The flat terrain minimized the uncertainty caused by terrain variations, and the availability of equipment enables us to establish a complex randomized complete block design and set up replicated plots, such as the sprinkler system shown in **Figure 10**, where each sub-switch is controllable. This allows us to create contrasting treatment gradients in water and nitrogen that were fundamental to training our machine learning models.

Figure 10. Experimental field with irrigation facility.

1.2 Treatment structure and temporal scope

During the 2019 - 2020 growing season, this experiment was conducted only in Field I. During this season， the primary variable was the water regime, which was created by applying different irrigation levels to cause varying degrees of water stress. The objective of this winter wheat growing season was to establish a benchmark correlation between the spectral features obtained by the unmanned aerial vehicle and the final yield. Therefore, the focus of field data collection was solely on the yield at harvest time.

To conduct a deeper analysis of the physiological driving factors of yield, this experiment was expanded in terms of scope and scale over the following years. The experiment was carried out simultaneously in both Field I and Field II, with each field area maintaining the same randomized block design structure (a total of 180 plots). The experimental design was also improved, adopting a two-factor system, including various water supply patterns and nitrogen fertilizer application amounts. This multi-factor design created multiple crop growth conditions and physiological states.

1.2.1 Field I: irrigation treatments

This irrigation experiment employed a randomized complete block design and was conducted in three replicates. A large mobile sprinkler irrigation machine (Figure 10) was used to implement different water treatments. The optimal fertilization plan, based on empirical proportions, was uniformly applied throughout the field to isolate the effects of irrigation variations. During the 2019-2020 growing season, winter wheat was subjected to three irrigation levels: conventional irrigation (240 mm), moderate irrigation (190 mm), and light irrigation (145 mm). For each irrigation treatment, 30 varieties were considered and replicated twice in a randomized block. Irrigation operations were carried out at six key growth stages according to the detailed plan scheme listed in **Table 3**.

Table 3. An overview of the water treatment for the 2019-2020 growing season.

Stages	**Irrigation volume**		
	T1	T2	T3
Tillering	35mm	35mm	35mm
Wintering	35mm	35mm	35mm
Reviving	35mm	25mm	20mm
Jointing	50mm	35mm	20mm
Booting	50mm	35mm	20mm

Stages	Irrigation volume		
	T1	T2	T3
Flowering	35mm	25mm	15mm
Total	240mm	190mm	145mm

During the experimental periods of 2021 - 2022 and 2022 - 2023, a total of six irrigation treatments (W1 - W6) were carried out. Each treatment was randomly assigned to 10 experimental plots within each replicate block, resulting in 30 replicate samples for each treatment throughout the entire experiment. Each replicate area contained 60 experimental plots, generating a total of 180 experimental units. Irrigation was conducted according to the detailed plan specified in **Table 4** during the four key growth stages.

Table 4. Irrigation treatments in Field I.

Stages	Irrigation volume					
	W1(100%)	W2(90%)	W3(70%)	W4(50%)	W5(30%)	W6(Rain-fed)
Total	282mm	254mm	198mm	141mm	85mm	0mm
Wintering	75mm	75mm	75mm	75mm	75mm	0mm
Jointing	78mm	67mm	46mm	25mm	15mm	0mm
Booting	51mm	45mm	30mm	16mm	0mm	0mm
Grain filling	78mm	67mm	46mm	25mm	0mm	0mm

1.2.2 Field II: nitrogen fertilization treatments

Field II was designed to study the fertilization effect of nitrogen fertilizer by using a randomized complete block design with three replications. Each replication included 60 experimental plots, resulting in a total of 180 experimental plots in the entire experiment. Six nitrogen fertilizer treatments were set up, and each treatment was randomly assigned to 10 experimental plots within each replication block, ensuring that each treatment had 30 replicate samples in the entire field.

The total fertilizer application amount per experimental plot was proportionally distributed and applied at key growth stages: two-thirds during the tillering stage and one-third during the grain filling stage. The entire field was irrigated according to standard agronomic practices to eliminate the influence of nitrogen fertilizer supply on the results. The specific nitrogen fertilizer application amount and application plan are detailed in **Table 5**.

Table 5. Nitrogen fertilizer treatments in Field II.

Stages	Nitrogen fertilizer application rate					
	330kg/hm^2 （110%） N1	270kg/hm^2 （90%） N2	210kg/hm^2 （70%） N3	150kg/hm^2 （50%） N4	90kg/hm^2 （30%） N5	0kg/hm^2 （0） N6
Jointing	220kg/hm^2	180kg/hm^2	140kg/hm^2	100kg/hm^2	60kg/hm^2	0kg/hm^2
Boosting	110kg/hm^2	90kg/hm^2	70kg/hm^2	50kg/hm^2	30kg/hm^2	0kg/hm^2

1.3 Weather variability in winter wheat growth

Microclimate conditions have a significant impact on the physiological processes of crops, their spectral responses, and the performance of prediction models. During the overwintering period, it is crucial for the survival of winter wheat. To better consider these environmental factors and improve the interpretability of the results, comprehensive meteorological data were collected during the experiment.

To ensure successful overwintering and prevent frost damage, all winter wheat fields were adequately irrigated before entering dormancy in early December. Throughout the overwintering period, the crops naturally experienced various weather conditions. **Table 6** provides a seasonal weather overview for two winter wheat growing seasons, covering the entire period from the start of overwintering to maturity. It includes daily average temperatures, relative humidity, and monthly precipitation data.

Table 6. An overview of the weather within the growing seasons.

Acquisition Stage	Year	Daily mean temperature (℃)	Daily average air humidity (%)	Monthly rainfall (mm)
December of the preceding year	2020	7.88	90.00	10.80
	2022	4.60	61.38	3.70
January	2020	1.67	89.40	37.60
	2022	1.58	87.28	12.60
February	2020	5.48	80.52	17.80
	2022	3.44	69.82	0.00
March	2020	11.84	67.73	4.40
	2022	11.08	76.05	10.80

Acquisition Stage	Year	Daily mean temperature (℃)	Daily average air humidity (%)	Monthly rainfall (mm)
April	2020	15.31	67.11	16.10
	2022	17.16	71.54	9.10
May	2020	23.39	63.50	83.70
	2022	21.43	64.09	109.30

From Table 6, it can be seen that in the two winter wheat experiments conducted in different years, the average daily temperature reached its lowest point in January and its highest point in May. However, the average daily temperature in the same month varied among different years. The average daily humidity did not show a clear relationship with the season or the month, and there were significant differences between the two winter wheat experiments.

In the wheat growth experiment from 2019 to 2020, the highest daily average humidity recorded was 90%, which occurred in December 2019. In contrast, during the wheat experiment in 2021 to 2022, the peak daily average humidity in January was 87.28%.

There were also significant differences in the monthly precipitation between the two winter wheat growth experiments. In the winter wheat experiment from 2019 to 2020, the precipitation was relatively stable. The maximum monthly precipitation in May 2020 was 83.7 millimeters, and the minimum monthly precipitation in March 2020 was 4.4 millimeters. During the winter wheat growth period in 2021 to 2022, the maximum monthly precipitation in May reached 109.3 millimeters, while no precipitation was recorded in February.

1.4 Multi-sensor UAV data acquisition

Integrating multispectral and thermal infrared sensors is a carefully designed strategy aimed at obtaining complementary physiological information. The multispectral data (RedEdge MX (MicaSense Inc., Seattle, WA, USA)) provides insights into photosynthetic capacity and tree crown structure through five bands (blue, green, red, red edge, and near-infrared), while the thermal image (Zenmuse XT2 (DJI, Shenzhen, China)) quantifies water stress through canopy temperature and CWSI calculations. **Figure 11** shows the experimental area images captured by the unmanned aerial vehicle equipped with the RedEdge MX (MicaSense Inc., Seattle, WA, USA) camera (red, green, blue, red edge, and infrared), the RGB digital camera, and the thermal infrared camera.

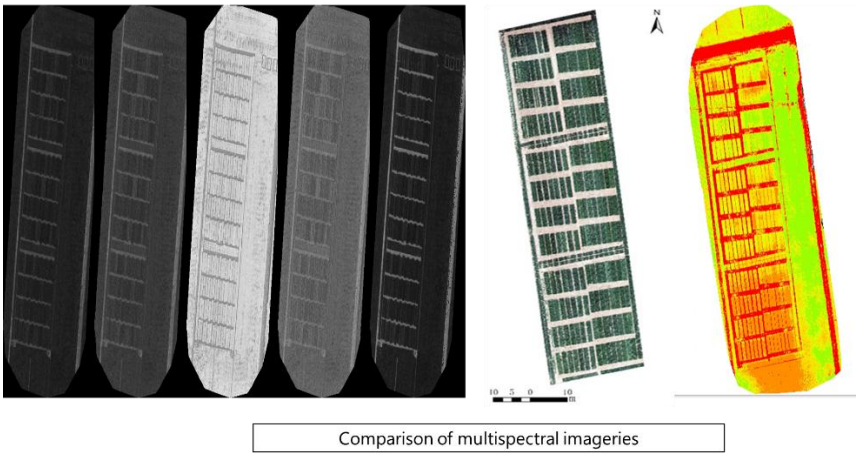

Figure 11. Experimental area images captured by drone carrying sensors.

Unmanned aircraft flight tests were conducted during key stages, including jointing stage, booting stage, heading stage, flowering stage and filling stage. The flights were carried out under clear weather conditions and during the optimal light period (from 10 a.m. to 2 p.m. Beijing time). The Rededge MX (MicaSense Inc., Seattle, WA, USA) multispectral camera and Zenmuse XT2 (DJI, Shenzhen, China) thermal infrared camera mounted on the DJI M210 quadcopter (DJI, Shenzhen, China) were used to collect canopy spectral data for all test areas (**Figure 12**).

Figure 12. M210 quadrotor with multispectral and thermal cameras.

Throughout the entire multi-year period of this study, the unmanned aerial vehicle (UAV) multispectral sensor platform was upgraded from a five-band (blue, green, red, red edge, and near-infrared) system to a four-band (green, red, red edge, and near-infrared) system in the 2022 - 2023 growing season. To maintain consistent input features across all study years and ensure the comparability of the machine learning models, we made a conscious methodical decision to only use the four spectral bands (green, red, red edge, and near-infrared) that are common to both the earlier five-band and the current four-band UAV sensors. This approach applies to all data if the dataset including the data from the 2022 - 2023 season, ensuring that the analysis throughout the study period is based on the same spectral information.

This decision is scientifically justified because the blue band is believed to be more susceptible to atmospheric scattering, and it provides less discriminatory power in vegetation analysis compared to the red-edge band and the near-infrared band, which are the key bands used for estimating chlorophyll and biomass (Song Lin et al., 2023; Guan Hui et al., 2020; Jie et al., 2022; Jie et al., 2023a; Jie et al., 2023b).

In each experimental area (Field I and Field II), a total of 18 ground control points (GCP) were set up. The positions of these points were determined by black and white boards evenly distributed on 180 plots. Winter wheat canopy spectral images were captured using a two-dimensional route planning flight mode, where the camera was set to take images vertically relative to the ground at specified time intervals. The flight route was meticulously planned using the 2D orthophoto images obtained from DJI's GPS ground station. The flight operation achieved a 80% lateral overlap rate and an 85% heading overlap rate, which are crucial for ensuring high-quality image stitching and accurate data collection. The flight was conducted at a height of 40 meters, enabling an appropriate coverage range and details in the captured spectral imagery.

The photogrammetric processing of the acquired drone images was accomplished using the Pix4Dmapper software (Pix4D S.A., Lausanne, Switzerland). After conducting aerial triangulation of the UAV images, the geometric processing was optimized by incorporating the coordinates of the ground control points (GCPs). For multispectral data, radiometric calibration was performed using MicaSense calibration reference panels, which have known reflectance values (MicaSense, Seattle, Washington, USA). These panels were used to convert the raw image digital numbers (DN) to calibrated reflectance values, and measurements were taken immediately before and after each flight.

1.5 Ground truth data

To ensure precise alignment with UAV remote sensing data, ground sampling was carefully synchronized with each drone flight. Within each plot, the five-point sampling method was used (including the four corners and the center point within a 1 m² area), collecting six representative plants per point to form a composite sample. This design effectively captured the variability at the plot level and ensured that the statistical performance used for model training was robust. The sampling work was conducted during key phenological stages (jointing, booting, heading, flowering, and grain filling), to capture the temporal dynamics in crop growth.

During the jointing and booting stages, the nitrogen content of the plants was measured using the standard Kjeldahl nitrogen determination method (Bremerner, 1996). This provided accurate chemical nitrogen content measurement values (%), which were necessary to determine the relationship between spectral characteristics and plant nitrogen content. First, the ground plant samples (about 0.2 grams) were placed in a Kjeldahl digestion tube, and concentrated sulfuric acid and catalysts (such as potassium sulfate and copper sulfate) were added. The samples were heated in a digestion furnace until they were completely digested, converting organic nitrogen into ammonium sulfate. Next, the digested solution was transferred to a Kjeldahl distillation apparatus and an excess amount of sodium hydroxide solution was added to convert ammonium sulfate into ammonia gas. Finally, the ammonium borate solution was titrated with standard hydrochloric acid solution, and the nitrogen content of the sample was calculated based on the consumption of hydrochloric acid. The formula for calculating nitrogen content is as **Eq.1**:

$$Nitrogen\ content\ (\%) = \frac{(V_{sample} - V_{blank}) * C_{HCI} * 14.01}{W_{sample}} * 100 \quad \text{(Eq.1)}$$

Among them, V_{sample} represents the volume of hydrochloric acid consumed by sample titration (mL), V_{blank} represents the volume of hydrochloric acid consumed by blank titration (mL), C_{HCI} is the concentration of hydrochloric acid (mol/L), W_{sample} is the weight of the sample (g), and 14.01 is the molar mass of nitrogen (g/mol).

The fresh weight and dry weight of each sample were immediately measured using a high-precision (0.1 gram) electronic balance. The samples were dried in an oven (at 105°C for 30 minutes, then at 75°C until constant weight) to obtain dry biomass. The

formula for calculating the moisture content is: (fresh weight - dry weight) / fresh weight × 100%. These measurement results directly supported the work of developing a biomass estimation model based on vegetation indices.

During the physiological maturity stage, the entire plot was harvested, bagged, dried, threshed, and weighed. The yield was calculated based on the plot area and standardized to a constant moisture content as a ground reference for the yield prediction model.

All samples were geotagged with high-precision GPS to ensure consistency in spatiotemporal with the drone images. This made pixel-to-sample matching possible, which is crucial for supervised learning algorithms. In the last two growing seasons of the experiment, a total of 2880 ground samples were collected, forming a database with a clear spatial distribution and high precision for training and testing machine learning models related to crop characteristics and yield.

2. Research methods

Based on the research limitations revealed in the aforementioned literature review (insufficient specificity of spectral indices, data annotation bottleneck, model "black box" nature, and the inefficient "one problem, one model" paradigm), this study proposes a systematic methodological framework. This framework aims to construct an interpretable, high-precision, and practical prediction model for winter wheat yield and key physiological parameters through multi-sensor collaborative observation, temporal dynamic feature extraction, efficient data learning, and multi-task joint modeling. This study consists of four logically progressive experiments, designed as shown in **Table 7.**

Table 7. Summary of research method design.

Experiment	Feature engineering	Model building
Yield prediction integrating temporal dynamic characteristics.	Select VIs sensitive to biomass and chlorophyll and CWSI (Jingjing et al., 2024), a dynamic characteristic for characterizing water stress. Enhance the signal-to-noise ratio, and provide clear physiological significance (Liao et al., 2023).	Temporal dynamic feature extraction: using the gating mechanism of LSTM to capture the growth dynamics (Yu et al., 2019). Yield Prediction: RF is selected due to its ability to handle tabular data, strong anti-overfitting capability (Falv et al., 2022).
Semi-supervised cross-year yield prediction for data-scarce scenarios.	The raw reflectance of the multispectral and CWSI during the grain filling period. Raw reflectance retains the most complete spectral information, crucial for identifying the distribution of unlabeled samples (Waldner et al., 2019).	Using self-training algorithm to leverage a large volume of unlabeled data, extending limited ground truth (Tuia et al., 2016). RF is selected for yield estimation.
High-precision Prediction of Plant Nitrogen Content Based on High-dimensional Feature Engineering.	High-dimensional features, including Vis, CWSI, nonlinear relationship features (Gorretta et al., 2020) and Water-nitrogen interaction term (Caturegli et al., 2020).	Different types of machine learning algorithms are adopted to construct prediction models. Feature importance is calculated to verify the effectiveness of high-dimensional engineering.
Joint Prediction of Dry Weight and Fresh Weight Based on Multi-task Learning.	Shared features, including VIs that are sensitive to biomass structure, CWSI, and Water-nitrogen interaction term.	Construct multi-task learning methods, consisting of a shared feature processing layer and two distinct prediction branches responsible for DW and FW prediction, respectively. Thus improving the computational and data utilization efficiency (Cheng et al., 2022).

3. Model validation framework

3.1 Stratified cross-validation procedure

The validation framework integrated several critical components to guarantee robustness and reliability. Firstly, stratification based on treatment was applied to the dataset, categorizing data according to key experimental variables: irrigation levels for Field I and nitrogen fertilization rates for Field II. This approach ensured that each cross-validation fold contained representative samples from all treatment conditions, thereby maintaining the experimental structure throughout both training and validation phases.

Subsequently, an iterative validation process was carried out using the stratified K-fold cross-validation method. The dataset was divided into K approximately equal-sized folds. In each iteration, X folds were retained for validation, while the remaining K - X folds were used for model training. This process was repeated continuously until each fold was used as a validation set exactly once, ensuring a comprehensive and unbiased evaluation.

Finally, this framework employs a systematic model selection and hyperparameter tuning mechanism. Under various model architectures and training parameters, the cross-validation process was repeated. Based on the consistent performance metrics observed across all validation folds (including R^2, root mean squared error (RMSE), and mean absolute error (MAE)), the optimal configuration was selected to provide reliable performance evaluation results.

Figure 13 illustrates the actual application of our validation framework, it was demonstrated through a detailed 5-fold cross-validation example, and the data used was from the winter wheat growing season of 2019 - 2020 in Field I.

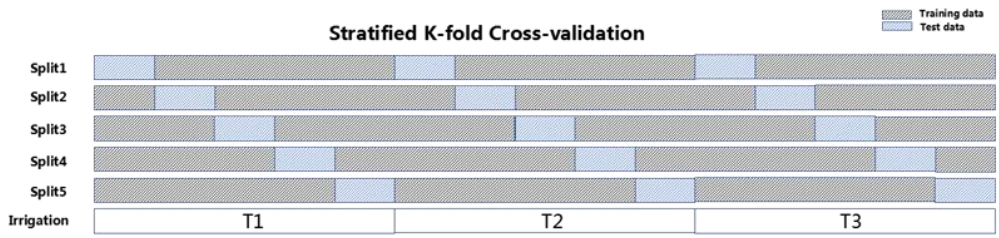

Figure 13. Stratified 5-fold cross-validation for different irrigation treatment in 2019-2020.

During each validation iteration, three key evaluation metrics are calculated: R^2 measures the proportion of variance explained by the model, RMSE quantifies the average size of the prediction error, and MAE provides a robust estimate of the average error size. The final reported performance metrics are the average values of all five validation folds, thereby conducting a comprehensive assessment of the model's universality under different irrigation conditions and genetic backgrounds.

3.2 Validation strategy and performance metrics

To ensure robust evaluation of all predictive models developed in this study, a stratified K-fold cross-validation approach was consistently employed across all analytical chapters. This strategy was specifically designed to address the structured nature of our experimental design while accounting for the limited sample size typical of detailed agronomic studies.

The predictive performance of all models was quantitatively assessed using three complementary statistical metrics: coefficient of determination (R^2), root mean square error (RMSE) and mean absolute error (MAE). The formula for calculating these accuracy parameters are shown in **Eq.2** to **Eq.4**:

$$R^2 = 1 - \frac{\sum_{i=1}^{n}(y_i - \hat{y}_i)^2}{\sum_{i=1}^{n}(y_i - \bar{y})^2} \quad \text{(Eq.2)}$$

$$\text{RMSE} = \sqrt{\frac{1}{n}\sum_{i=1}^{n}(y_i - \hat{y}_i)^2} \quad \text{(Eq.3)}$$

$$\text{MAE} = \frac{1}{n}\sum_{i=1}^{n}|y_i - \hat{y}_i| \quad \text{(Eq.4)}$$

where n denotes the number of samples, y_I and $\hat{y}_I$ denotes the actual and the predicted grain yields of sample i, respectively, $\bar{y}$ is the mean of the measured grain yield.

IV

Temporal yield prediction using an LSTM-RF network

1. Synopsis

This chapter is largely based on the research paper of Shen et al. (2022):

Shen, Y., Mercatoris, B., Cao, Z., Kwan, P., Guo, L., Yao, H., Cheng, Q., 2022. Improving Wheat Yield Prediction Accuracy Using LSTM-RF Framework Based on UAV Thermal Infrared and Multispectral Imagery. *Agriculture* 2022, 12, 892. https://doi.org/10.3390/agriculture12060892.

This chapter addresses research objective 1, as defined in Chapter I, by constructing a dynamic yield prediction model using multi-temporal UAV-based remote sensing information to overcome the limitation of current models that overlook the dynamic growth dependency (Zhao et al., 2016). This chapter introduces a novel hybrid LSTM-Random Forest (LSTM-RF) framework, which leverages the unique advantages of the two powerful algorithms.

The Long Short-Term Memory (LSTM) network is employed to extract complex features from time series of multispectral vegetation indices. It excels at learning the complex, non-linear patterns and long-range dependencies within the seasonal growth data (Yu et al., 2019). The Random Forest (RF) algorithm then utilizes these LSTM-derived temporal features as inputs for the final yield prediction. This choice can provide a robust nonlinear regression model.

This hybrid design has been validated on the dataset of the first year, achieving two main goals. Firstly, it provides an accurate yield prediction model by fully utilizing time information. Secondly, and more importantly, it identifies which specific growth stages and the time patterns learned by it are most predictive of the final yield. This provides actionable agricultural insights and lays the foundation for the in-depth study of physiology in Chapters VI and VII, where these key periods can be examined from the perspectives of nitrogen and biomass dynamics.

2. Materials and data

This experiment was conducted only in field I during the winter wheat growing season of 2019 - 2020. A total of 180 experimental plots were set up, using a randomized complete block design (RCBD), and three replications were carried out. The main variable this season was water regimes, which were created by applying different irrigation levels to cause varying degrees of water stress. The aim this year was to establish a benchmark correlation between the spectral

characteristics obtained by the unmanned aerial vehicle and the final yield, laying the foundation for the proposed temporal yield prediction model in this chapter. Therefore, the focus of field data collection was solely on the grain yield at harvest time.

The basis of this chapter is that the output of winter wheat is not determined at a specific point in time, but is instead determined by the cumulative result of physiological processes occurring during critical growth stages. Especially, water stress during heading can impact ear development, while encountering stress during the grain filling stage will affect the weight of the seeds. Therefore, we used the data from heading stage to grain filling stage as input. The flowchart of the method is shown in **Figure 14**.

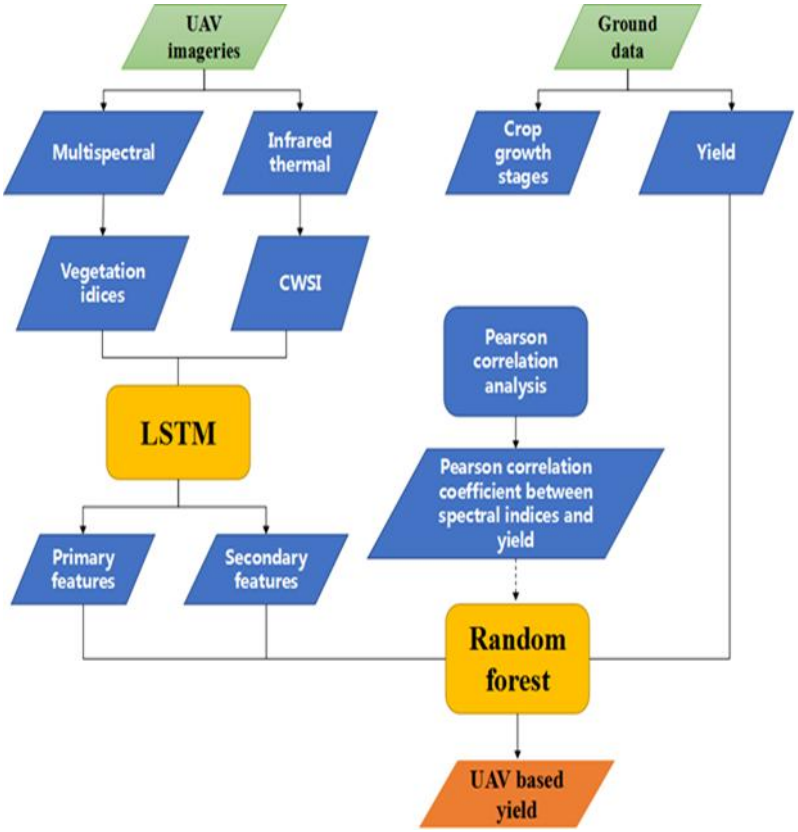

Figure 14. Methodological flowchart for crop yield prediction from the UAV imageries in combination with ground-based data.

2.1 Selection of spectral indices

Spectral indices, derived from canopy reflectance across various wavelengths, have been widely validated in previous literature as reliable indicators for key physiological and biochemical parameters in crops (Berger et al., 2020). The selection of these indices is critical because different VIs show different sensitivities to specific plant traits, and their performance may vary depending on the specific context. This is reflected in numerous formula summaries in previous researches (**Table 1** and **Table 2**). Based on this foundation, in this study, a set of seven vegetation indices was strategically selected for wheat yield estimation (**Table 8**). This selection aims to capture complementary aspects of crop status and align with the theme of multi-sensor fusion.

Table 8. List of 7 vegetation indices which were examined in this study.

Index name	Index acronym	Formula
Normalized difference vegetation index	NDVI	$(R_{NIR} - R_{RED})/(R_{NIR} + R_{RED})$
Modified chlorophyll absorption in reflectance index	MCARI	$\left[\left((R_{RED-EDGE} - R_{RED}) - 0.2\right)(R_{RED-EDGE} - R_{GREEN})\right]9(R_{RED-EDGE} - R_{RED})$
Modified triangular vegetation index 2	MTVI2	$\frac{1.5[1.2(R_{NIR} - R_{GREEN}) - 2.5(R_{RED} - R_{GREEN})]}{\left[(2R_{NIR} + 1)^2 - \left(6R_{NIR} - \frac{5}{R_{RED}}\right) - 0.5\right]}$
Ratio vegetation index 1	RVI1	$\frac{R_{NIR}}{R_{RED}}$
Optimized soil adjusted vegetation index	OSAVI	$1.16(R_{NIR} - R_{RED})/(R_{NIR} + R_{RED} + 0.16)$
Normalized difference plant pigment ratio	PPR	$(R_{GREEN} - R_{BLUE})/(R_{GREEN} + R_{BLUE})$
Crop water stress index	CWSI	$[T_C - (T_{min} - 2)]/[(T_{max} + 5) - (T_{min} - 2)]$

To assess broad vegetation vigor and biomass, the well-established Normalized Difference Vegetation Index (NDVI) and Ratio Vegetation Index (RVI1) were chosen. These indices are basic measures of green biomass and vegetation density, although they may saturate in dense canopies. For evaluating the status of chlorophyll and nitrogen, the Modified Chlorophyll Absorption in Reflectance Index (MCARI) and Modified Triangular Vegetation Index 2 (MTVI2) were adopted. These indices were selected for their enhanced sensitivity to chlorophyll content and leaf area, which are closely related to nitrogen status and photosynthetic capacity. The Optimized Soil Adjusted Vegetation Index (OSAVI) and the Normalized Difference Plant Pigment

Ratio (PPR) were used to study tree canopy structure and pigment distribution. OSAVI improves performance by minimizing the influence of soil background, while PPR provides insights into the composition of the canopy layer pigments. It is crucial to introduce the Crop Water Stress Index (CWSI) to integrate direct measurements of plant physiological status that cannot be obtained solely from optical data. CWSI is generated from thermal infrared images and is used to quantify water stress levels, which is an independent factor determining yield potential. This multi-faceted feature enables the prediction model to utilize the synergistic information from multispectral and thermal sensors, providing a more comprehensive view of growth and stress dynamics, which jointly determine the final yield (Weiss et al., 2020).

3. Method: LSTM-RF

In this part, LSTM-RF estimation model was constructed to predict winter wheat yield. The final structure and parameters of the algorithm have been systematically verified through experiments. Finally, a two-layer long short-term memory network was adopted to extract primary features and secondary features from the input vegetation indices information, then these features were fed into a RF regressor to do winter wheat yield prediction.

3.1 Long short-term memory network

For one long short-term memory cell (**Figure 15**), at a given time t, it has three inputs: the input value of the network at the current time x_t, the output value of the long short-term memory cell of the last time h_(t-1), and the last unit state c_(t-1). It has two outputs: the output value h_t and the state information c_t at the current time.

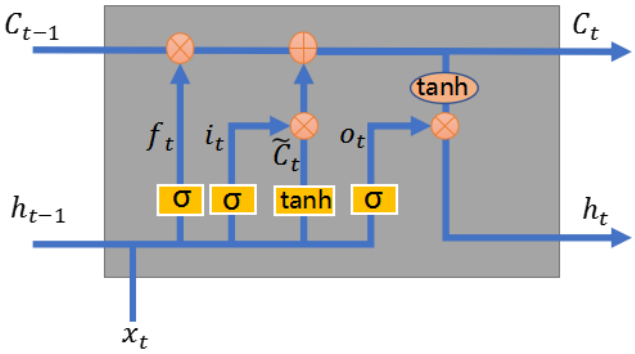

Figure 15. Long short-term memory cell.

LSTM is implemented in three steps (Yu et al., 2019). The first step of LSTM is to determine what information can be passed through the cell state. This decision is controlled by the "Forget Gate" layer through the sigmoid function, which passes or partially passes based on the previous moment's output, as shown by **Eq.5**.

$$f_t = \sigma\left(W_f \cdot [h_{t-1}, x_t] + b_f\right) \quad \text{(Eq.5)}$$

The second step is to generate new information that we need to update. This step consists of two parts, with **Eq.6** representing an "input Gate" layer that uses sigmoid to determine which values to update, and **Eq.7** representing a hyperbolic tangent layer that generates new candidate values and adds them up to get the updated values.

$$i_t = \sigma(W_i \cdot [h_{t-1}, x_t] + b_i) \quad \text{(Eq.6)}$$

$$\tilde{C}_t = \tanh(W_c \cdot [h_{t-1}, x_t] + b_c) \quad \text{(Eq.7)}$$

The two steps above are the process of discarding unwanted information and adding new information as shown in **Eq.8**:

$$C_t = f_t * C_{t-1} + i_t * \tilde{C}_t \quad \text{(Eq.8)}$$

The final step is to determine the output of the model, firstly through the sigmoid layer to get an initial output, as shown in **Eq.9**, and then using hyperbolic tangent layer to scale the values between -1 and 1, and then multiplied pair by pair with the sigmoid output to obtain the output of the model, as shown in **Eq.10**.

$$o_t = \sigma(W_o \cdot [h_{t-1}, x_t] + b_o) \quad \text{(Eq.9)}$$

$$h_t = o_t * tanh(C_t) \quad \text{(Eq.10)}$$

3.2 Random forest regressor

Random forest regressor is insensitive to multiple collinearities, and its results are relatively robust to incomplete or unbalanced data. It can predict well the effects of up to several thousand explanatory variables and is known as one of the best algorithms.

In this paper, the Classification and Regression Tree (CART) decision tree was used as the base learner in the random forest, as shown in **Figure 16**. Next, T rounds of training were carried out on the model through random sampling and random selection of features, and then T weak learners were summed up to obtain the final learner. Self-sampling method was adopted, in other words, sampling with return, and the number

of samples taken in each round of training was equal to the total number of samples. Because of return sampling, some samples may be repeatedly chosen, while others may not be chosen. The selection of features was also by random selection of a fixed number of features to train the model. In this way, the weak learners were not completely independent of each other, yet the correlation was small, which can increase the overall generalization ability of the model.

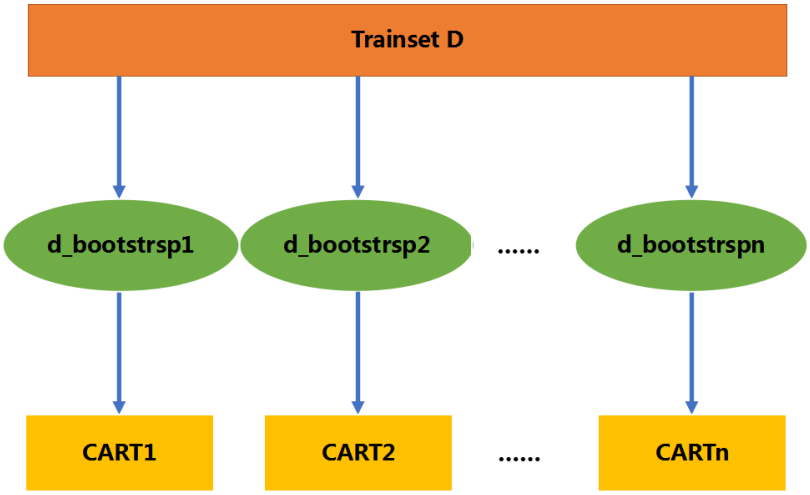

Figure 16. How the random forest regressor works.

Here is a summary of the flow of the random forest algorithm:

Draw a random bootstrap sample of size n (randomly choose n samples from the training set with replacement).

1) Grow a decision tree from the bootstrap sample. Create a training set by randomly sampling the original data with replacement.

2) At each node, randomly select d features and split using the best one (e.g., by MSE).

3) Repeat the steps 1) and 2) k times.

4)The predicted target variable is calculated as the average prediction over all decision trees

3.3 LSTM-RF

In this study, we tried to predict wheat yield with more reliable results through two

processes: extracting the feature of vegetation indices using a two-layer LSTM and predicting wheat yield using the random forest algorithm. **Figure 17** presented a brief description of LSTM-RF used in this paper. A three-layered LSTM-RF neural network model was developed. Its first two layers have three LSTM cells respectively. A dense layer was added to train the LSTM network, once trained the first two LSTM layers would be used to extract features from input variables, and these features would be sent into the random forest regressor to carry out the prediction.

One of the critical issues is to select appropriate input variables. The idea is to choose the combination of multispectral variables that are highly correlated with winter wheat yield. Previous studies have shown that it is better to predict wheat yield by considering the data of multiple growth stages (Reinermann et al., 2020). This paper selected the multispectral data of heading, flowering and grain-filling stages as input variables. In this section, to prove the effectiveness of the proposed method, we measure the objective performance through LSTM algorithm in a comparative experiment. To this end, we compare the performance of wheat yield prediction with LSTM and LSTM-RF.

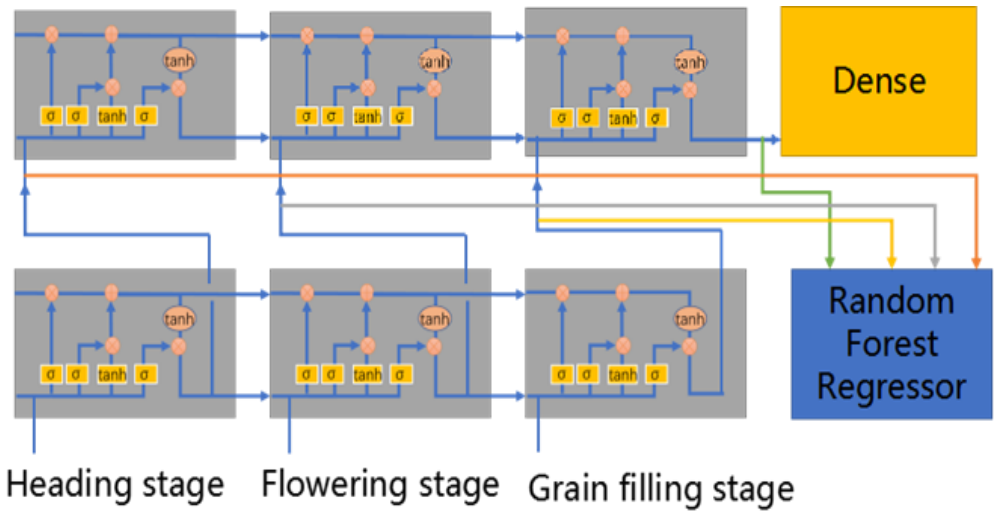

Figure 17. Structure of LSTM-RF.

4. Results

4.1 Statistical description of grain yield

The yield was normally distributed in all treatments and the mean value of yield increased with increasing amount of irrigation (**Figure 18**).

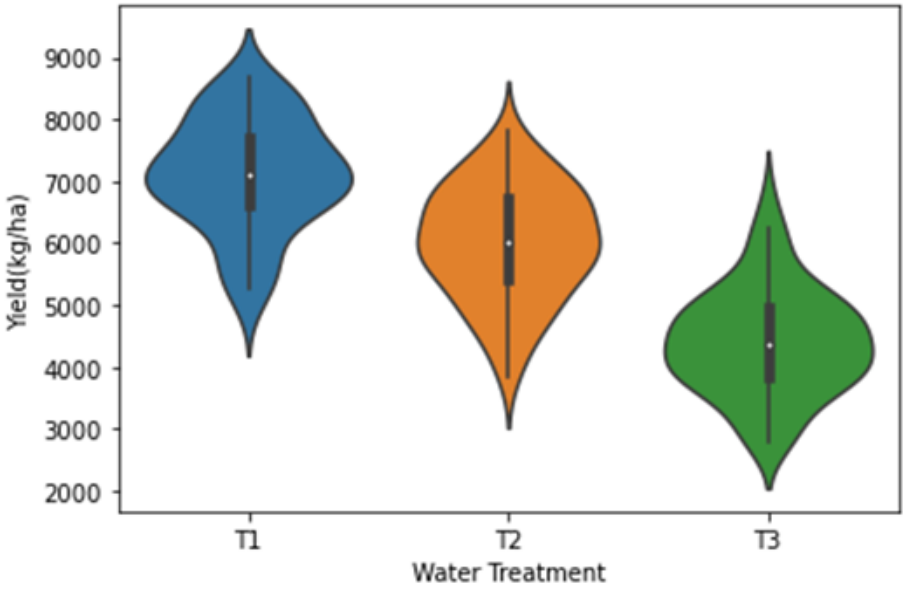

Figure 18. Yield distribution at different irrigation.

4.2 Correlations between vegetative indices and yield

Figure 19 shows the correlation analysis of vegetation indices and yield at three growth stages. At flowering stage and grain filling stage, RVI1 had the highest correlation with yield from r=0.61 to r=0.67, whereas CWSI showed a very strong negative correlation with yield (r=0.67-0.69) at flowering stage and grain filling stage. Strong correlations were estimated between yield and MTVI2, r = 0.60, 0.57, 0.65 at heading stage, flowering stage and grain filling stages, respectively. There were similar relationships between yield and OSAVI (r=0.58, 0.56 and 0.64), NDVI (r=0.60,0.56 and 0.63). PPR was strongly correlated with yield at heading stage, MCARI and yield had a strong correlation at grain filling stage.

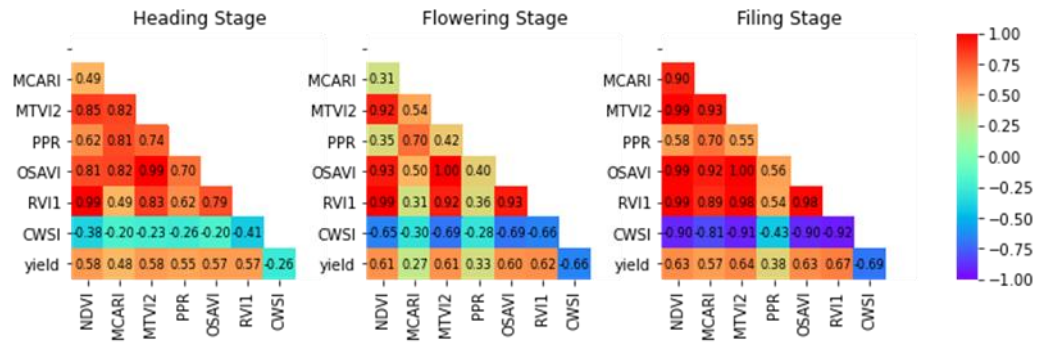

Figure 19. Correlation analysis heat map in the heading stage, flowering stage and grain filling stage respectively.

Figure 20 shows the correlation between the extracted features of LSTM and yield, when vegetation indices in heading, flowering and grain filling stages were sent into LSTM together (Figure 17), four features were obtained. Feature_11 was extracted from the VIs of heading stage (Figure 17), it has a minimum correlation with yield (r=0.49). Feature_12 was extracted from the VIs of flowering stage and it has a higher correlation with yield than feature_11 (r=0.66). Feature_13 was extracted from the VIs of grain filling stage and the correlation between it and yield is higher than feature_12 (r=0.70). Feature_2 was extracted from feature_11, feature_12 and feature_13, it has the highest correlation with yield (r=0.78).

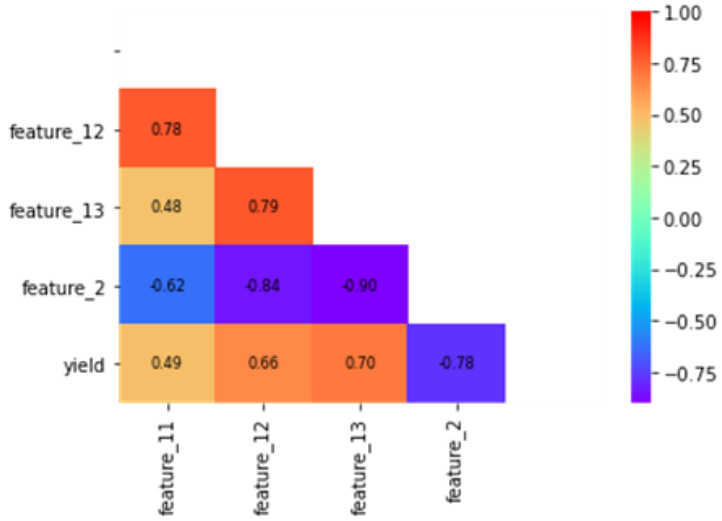

Figure 20. Correlation analysis heat map between the extracted features of LSTM and yield.

4.3 Model performance evaluation

Yield prediction was performed based on vegetation indices at the heading, flowering and grain filling stages (**Table 9**). The model was first trained using LSTM neural network and vegetation indices of three stages, the R^2 of the LSTM model in the training phase and validation phase were 0.60 (RMSE=901.16 kg/ha, MAE=738.58 kg/ha) and 0.61 (RMSE=878.98 kg/ha, MAE=718.99 kg/ha), respectively. By training the above LSTM neural network, three primary features and one advance feature were extracted and used as input features to random forest for yield prediction. Compared with LSTM, the model performance of LSTM-RF had been significantly improved. In the training phase, the R^2, RMSE and MAE of LSTM-RF model were 0.78, 654.56 kg/ha and 515.94kg/ha, respectively. The R^2, RMSE and MAE of LSTM-RF model in model validation phase were 0.78, 684.08 kg/ha and 506.13kg/ha. **Figure 21** shows the relationships between the measured and predicted yield of the LSTM and LSTM-RF models.

Table 9. Results of the estimation of the yield of winter wheat based on features extracted from three stages.

Heading, flowering and grain filling						
Algorithm	Training			Validation		
	R^2	RMSE(kg/ha)	MAE(kg/ha)	R^2	RMSE(kg/ha)	MAE(kg/ha)
LSTM	0.60	901.16	738.58	0.61	878.98	718.99
LSTM-RF	0.78	654.56	515.94	0.78	684.08	506.13

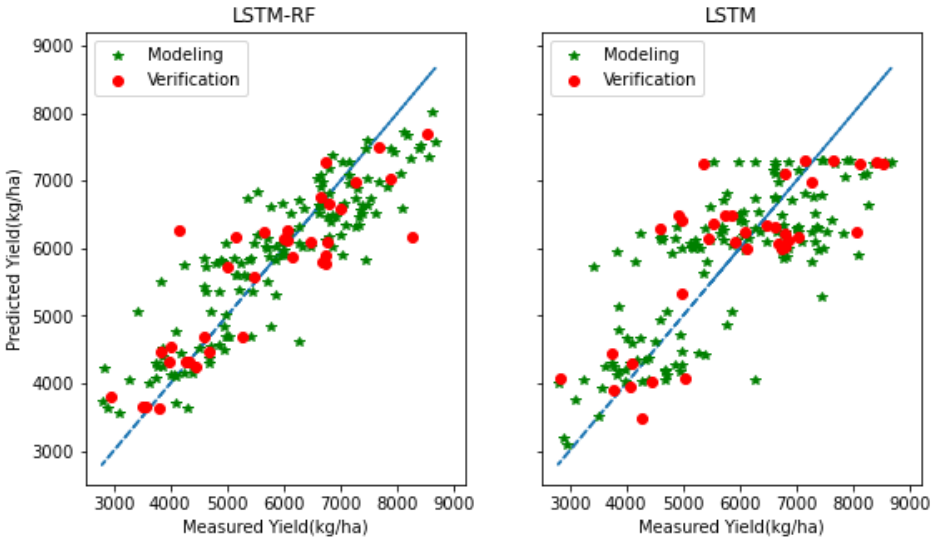

Figure 21. The relationships between the measured and predicted values of -wheat yield based on the LSTM and LSTM-RF models.

5. Discussion

The yield of winter wheat is the cumulative result of complex physiological processes occurring across multiple growth stages. This study explores the temporal nature of yield formation by proposing a hybrid LSTM-Random Forest (LSTM-RF) framework. The main contributions are twofold: (1) it introduces a new method to simulate crop growth dynamics by comprehensively considering the influence of multiple developmental stages on the final yield, and (2) it demonstrates that the feature extraction method based on LSTM provides a more explainable method for handling time-related crop data than other data fusion techniques.

5.1 Physiological interpretation of feature-yield correlations

Vegetation indices derived from multispectral imagery are established proxies for key growth parameters like leaf area index, biomass, and nitrogen content (Zhao et al., 2021; Zhao et al., 2019 and Haider et al., 2019), and consistently show strong associations with crop yield (Jay et al., 2017 and Huiren et al., 2021). Our findings align with this: most VIs exhibited the highest correlation with yield during the grain-filling stage. This is physiologically sound, as the grain-filling period is critical for dry matter translocation from vegetative tissues to the developing grains, directly

determining thousand-grain weight (Yang et al., 2017; Linchao et al., 2022 and Yu et al., 2019).

The Crop Water Stress Index (CWSI), derived from thermal imagery, showed significant yield correlations at both flowering and grain-filling stages. Canopy temperature, as a direct indicator of plant transpiration and water status (Yang et al., 2019), provides complementary information to the spectral VIs. This underscores the value of multi-sensor data fusion, where thermal data captures water stress dynamics that are not directly detectable by optical sensors alone.

While single-stage Vis offer a snapshot of crop status, yield is an integration of season-long growth conditions. Consequently, multi-temporal VIs have been proposed to improve prediction accuracy (Qi et al., 2020). This study advances this concept by using a shallow LSTM network to automatically extract meaningful temporal features from a time-series of seven VIs across three critical growth stages. The LSTM-derived features (**Figure 20**) demonstrated stronger correlations with yield than any single-stage VI. Furthermore, the correlation increased with the number of growth stages included in the feature extraction, and the advanced feature from the second LSTM layer outperformed the primary features from the first layer. This hierarchical improvement confirms the efficacy of LSTM in learning progressive, stage-integrated representations of crop growth, validating our feature extraction methodology.

5.2 Synergistic advantages of the LSTM-RF framework

The integration of high-throughput phenotyping with robust predictive algorithms is crucial for precision agriculture. While machine learning (e.g., Random Forest) and deep learning (e.g., LSTM) are independently successful in yield prediction (Devia et al., 2019; Garcia-Garcia et al., 2021; Shao et al., 2021; Fu et al., 2020; Fu et al., 2022; Wang et al., 2014; Hengl et al., 2018 and Rodriguez-Galiano et al., 2012), our study innovatively combines their strengths.

The LSTM-RF model achieved superior predictive accuracy compared to the standalone LSTM model. We attribute this performance improvement to two key factors. First, the "forgetting gate" mechanism of LSTM itself can regulate the influence of earlier growth stages. For winter wheat, while the grain-filling stage is crucial, the heading stage determines seed setting rate, and the flowering stage is highly sensitive to irrigation management. The RF regressor, trained by the advanced temporal features of LSTM derived from all primary VI features, can more effectively utilize this comprehensive information than the LSTM's final dense layer alone.

Second, the final yield prediction in a standard LSTM is typically performed by the dense layer, which may have limitations in simulating complex nonlinear relationships. Random forest, as an ensemble method, performs well in learning complex nonlinear relationships and usually has higher performance and stronger robustness on tabular data (Hallizyn et al., 2022). Therefore, in our hybrid framework, it becomes a more powerful regressor.

5.3 Limitations and future research directions

This study was based on the first-year data of the Field I dataset under water stress, successfully verifying the feasibility of the LSTM-RF model in yield prediction. However, this model was trained and validated under limited conditions, focusing only on the factor of water pressure. One of the key advantages of our overall research framework lies in its gradual nature. In the following years, the experimental scope was expanded to include both Field I and Field II, while nitrogen treatments were introduced, and plant nitrogen content and biomass data were systematically collected, aiming to directly address this limitation. This enriched dataset provides the necessary foundation for developing and validating more physiologically based intermediate trait models.

6. Conclusions

This study developed a shallow LSTM-RF hybrid framework for winter wheat yield prediction by extracting temporal features from vegetation indices (VIs) during the heading, flowering, and grain-filling stages. The proposed architecture successfully generated integrated temporal features that correlated more strongly with final yield than single-stage VIs. More importantly, this approach establishes a foundation for a comprehensive phenotyping analysis process, indicating that accurate yield prediction can be achieved by directly modeling VIs over time.

It verified the effectiveness of temporal spectral features in predicting winter wheat yield, laying a solid foundation for subsequent research. However, this method heavily relies on a large amount of labeled data (only one year's data). In practical agricultural applications, obtaining sufficient, labeled crop data is costly and often faces the 'small sample' challenge. At the same time, we only used the preset spectral indices and failed to fully explore the deep information of the original spectra. How to utilize less labeled data and fully exploit the potential of the original spectra will be explored in Chapter V.

V

Semi-supervised yield prediction with self-training random forests

1. Synopsis

This chapter is largely based on the research paper of Shen et al. (2024):

Shen, Y., Mercatoris, B., Liu, Q., Yao, H., Li, Z., Chen, Z., Wang, W., 2024 Use Self-Training Random Forest for Predicting Winter Wheat Yield. *Remote Sens.* 2024, 16, 4723.
https://doi.org/10.3390/rs16244723.

In Chapter IV, the LSTM-RF framework trained based on the data from the first year provided reliable preliminary verification results for yield prediction based on time series under water stress. While the practical application of yield prediction in real-world agricultural settings faces a fundamental limitation: the lack of large-scale and accurately labeled yield datasets. This "ground-truth bottleneck" severely restricts the application of supervised machine learning approaches (Cao et al., 2023; Waldner et al., 2019).

The high cost of data annotation process becomes a challenge for many tasks to obtain strong supervisory information such as all real labels (Zhi Hua 2018). To directly address this challenge (which is recognized as a key research gap identified in our conceptual framework), this chapter introduces and validates a self-training random forest (RF) algorithm specifically for winter wheat yield prediction under data scarcity conditions. As a classical semi-supervised learning approach, self-training can use a small labeled dataset to produce pseudo-labels for a much larger unlabeled set, effectively enlarging the training data and overcoming data scarcity (Tuia et al., 2016).

Based on the feature fusion strategy consistently adopted in this paper, our model uses the same strong multispectral and thermal energy features to maintain physiological relevance, while addressing the fundamental limitation of the availability of labeled data.

The contributions of this study are as follows.

(1) Our proposed solution achieves large-scale yield prediction based on ML with a small amount of ground data annotation. It provides a new perspective on the relationship between multispectral reflectance information and winter wheat yield;

(2) Our solution offers a more efficient, time-saving, and labor-saving approach to expanding annotated datasets.

2. Materials and methods

The yield prediction models developed in this chapter are based on the comprehensive dataset collected during the first two years of the experiment, the overall design of which is detailed in Chapter III. Specifically, the models utilize data from two-factor field trials (water regime × nitrogen fertilization level) conducted in both Field I and Field II.

Considering the winter wheat grows for several months, and its yield is easily affected by natural conditions such as weather and diseases, we choose the filling stage before maturity for yield prediction.

Figure 22 illustrates the methodological flowchart for this paper. After data processing, the correlation between multispectral information and winter wheat yield was analyzed. A classical random forest model was then employed to train an initial regressor. Following this, a self-training random forest algorithm was utilized to expand the training set and perform the yield prediction.

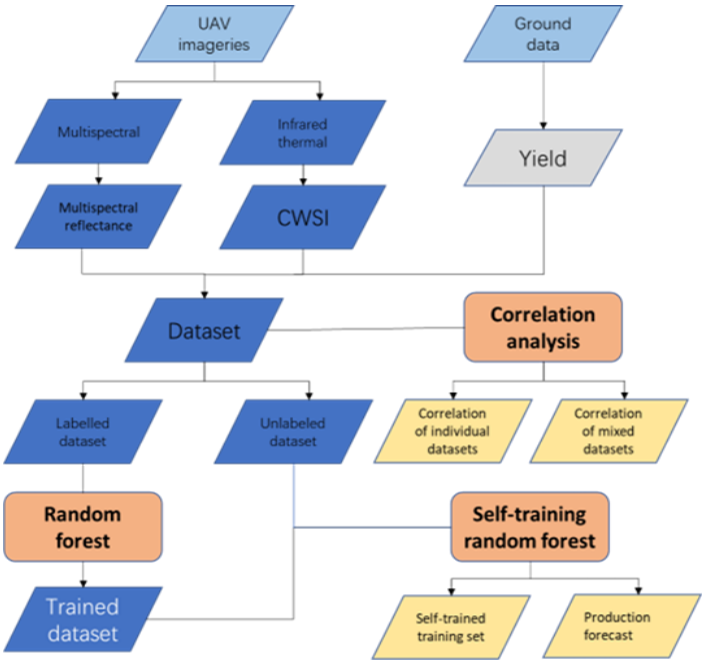

Figure 22. Methodological flowchart for crop yield prediction from the UAV imageries in combination with ground-based data.

The self-training model developed here operates through an iterative process: initially, it is trained on a limited annotated dataset, and then the model selectively labels the most certain prediction results from a larger unlabeled dataset, thereby autonomously expanding its effective training set. This semi-supervised approach has significant advantages over traditional random forest applications in the field of agricultural remote sensing.

2.1 Selection of spectral information

In this research, by using a multispectral camera, the raw reflectance of red light (R_{RED}), green light (R_{GREEN}), blue light (R_{BLUE}), red edge (R_{EDGE}), and near-infrared (R_{NIR}) of wheat during the filling period were collected. To learn more about winter wheat, we utilized a thermal infrared multispectral camera to enhance our collection of multispectral data. This thermal infrared camera captured the temperature characteristics of the winter wheat canopy. Canopy temperature results from complex energy exchanges within agricultural ecosystems and is influenced by various external factors. In this study, we collected the crop water stress index (CWSI), which was used to eliminate sensitivity to surrounding environmental conditions (such as air temperature, humidity, and radiation) and standardize the measured canopy temperature, as the thermal infrared information of winter wheat.

2.2 Pseudo label generation

Self-training belongs to the semi-supervised branch of machine learning algorithms because it trains models using a combination of labeled and unlabeled data. The core idea is to first train a weak regressor with a small amount of annotated data, and then use this weak regressor to predict unlabeled samples. When certain conditions are met, the predicted result is used as the true label of the sample. Then, the model is trained again with the existing annotated data, and the unlabeled samples are annotated and iterated repeatedly, Finally, it ends when the stop condition is reached.

The biggest problem with self-training algorithms is that incorrect pseudo labels introduce too much noise, which can mislead the model's training. Some research (Subhabrata et al., 2020) has found that it is feasible to exploit uncertainty estimation of the underlying neural network to improve self-training mechanism. For each unlabeled data selected, it was passed into NN (neural network) several times. Because dropout was used, they got uncertainty predicted results. Directly averaging the prediction results to obtain the prediction label.

In this study, we moved away from the conventional neural network approach and instead employed a random forest regression model for assigning pseudo labels. The random forest method utilized bootstrapping, which involved sampling with replacement to create new training sets from the original data. Each training set was formed by randomly selecting (n) samples.

For every new training set created, multiple sub-models were trained. The predictions from these individual models were then averaged to generate the pseudo labels. This averaging process effectively exploited the inherent uncertainty within the training data, which enhanced the reliability of the pseudo labels and helped reduce the negative impact of noise in the dataset.

2.3 Multi-scale joint prediction

During the self-training process, samples with high-confidence predictions are more likely to be accurately labeled. However, if these predictions are incorrect, it can lead to mislabeling, which is a challenge since these mislabeled samples are often difficult to predict correctly, distorting the data distribution.

In this paper, after obtaining pseudo-labels using random forest regression, a multi-scale joint prediction approach was employed. Within this framework, trusted pseudo-labels were selectively identified, and data associated with these trusted labels were incorporated into the training set, constituting the self-training process.

Firstly, the entire unlabeled dataset 'e' was uniformly divided into three subsets: 'b', 'c', and 'd'. Specifically, a subset of data 'a' (illustrated in **Figure 23**) was selected, which belongs to the red segment. This dataset 'a' underwent five predictions, based on five distinct training sets constructed by combining the original training set with the pseudo-labeled datasets 'a', 'b', 'c', 'd', and 'e', respectively.

Secondly, pseudo labels were considered trustworthy if the absolute difference between their predicted values and the assigned pseudo labels fell below a predetermined threshold (δ), which was determined through iterative experimentation.

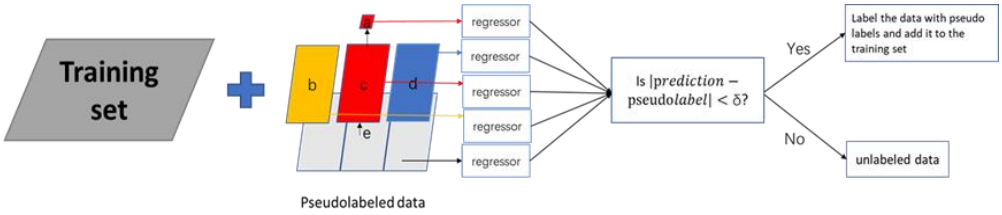

Figure 23. Multi-scale joint prediction.

2.4 Self-training random forest architecture

In this paper, we focused on predicting winter wheat yield and aimed to achieve highly reliable wheat yield forecasts through two processes: (i) training a regressor using a small amount of labeled data and (ii) annotating the data in the unlabeled dataset using a self-training random forest regressor to expand the training set. Two critical issues were identified. The first issue involved selecting an appropriate regression model and a small annotated dataset with comprehensive information to generate trustworthy pseudo labels. Our approach was to use the random forest algorithm to reduce the impact of noise. The second issue was to increase the prediction accuracy of high-confidence samples included in the unlabeled datasets.

Figure 24 illustrated the training process of the self-training random forest algorithm, which involved training the initial random forest model, employing a multi-scale joint prediction method for self-training, labeling unlabeled data, and selecting trustworthy pseudo-labeled data to expand the training set. The specific process was as follows:

- Trained a random forest regressor f_{float}, for winter wheat prediction and calculating pseudo labels for unlabeled samples.
- Then concatenated the training set (X_{train}, y_{train}) with unlabeled samples that had pseudo labels, creating a temporary training set (X_u, y_u). This set was used to select confidence samples (X_{conf}, y_{conf}) to add to the original training set using multi-scale joint prediction method.
- Removed confidence samples from the unlabeled dataset, and repeated the previous step until the stopping criteria were met.
- Finally, made predictions for winter wheat using the newly trained random forest network based on the expanded training set.

Algorithm: Self-training random forest

- Use existing data to train a small dataset with good results.
- Fine-tune a random forest regressor f_{float} of yield prediction on small labeled dataset $(X_{train}, y_{train}) = (X_l, y_l)$, with a coefficient of determination R_l^2.
- **While** stopping criteria not met **do**
  - Use f_{float} to predict y_u of unlabeled dataset X_u
  - **for** (x, y) ∈ (X_u, y_u) **do**
    - Using Multi-scale joint prediction(Take y as a pseudo label and merge it with y_{train}, merge x with X_{train}) to predict $\hat{y}_u$ of X_u
    - Select confidence sample (X_{conf}, y_{conf}); $(X_{conf}, y_{conf}) \in (X_u, y_u)$
  - **end for**
  - Remove selected unlabeled data $X_u \leftarrow X_u - X_{conf}$
  - Combine newly labeled data$(X_{train}, y_{train}) \leftarrow (X_l, y_l) \cup (X_{conf}, y_{conf})$
- **end while**

Figure 24. Pseudo code of self-training random forest.

3. Results

In this section, we analyzed the relationship between the multispectral reflectance information of winter wheat and its yield under different experimental conditions. We verified the efficacy of the self-training random forest in predicting winter wheat yield. To demonstrate the effectiveness of the proposed method, we used 20% of each experimental dataset as the training set, 10% as the test set, and 10% as the validation set to train the initial random forest regressor, while the remaining data was treated as unlabeled data. Finally, we compared the performance of winter wheat yield prediction using the standard random forest (RF) and the self-training random forest.

3.1 Winter wheat yield under different experiments

From **Figure 25**, it was observed that the overall production of winter wheat in 2022 was significantly higher than in 2020. The production under different nitrogen fertilizer treatments in 2022 was slightly greater than that under varying water treatments.

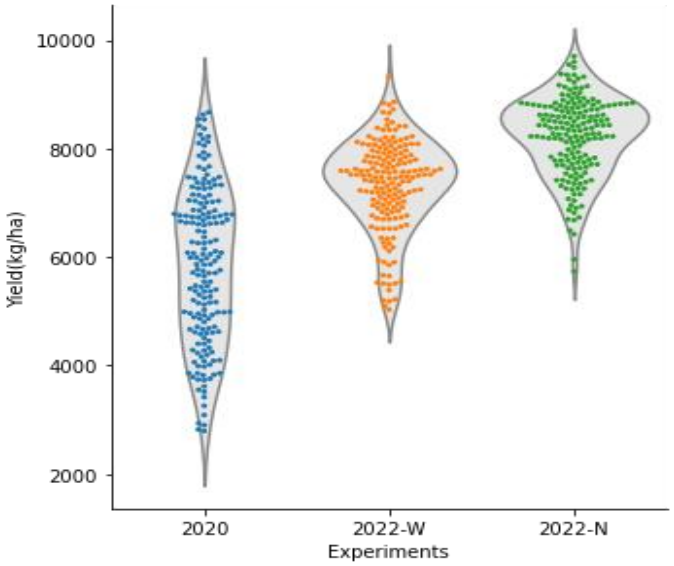

Figure 25. Winter wheat yield distribution under different experiments.

The yield distribution of winter wheat harvested in 2020 was relatively wide, primarily ranging from 4000 kg/ha to 7500 kg/ha. The maximum yield density occurred at approximately 6900 kg/ha, with a small portion of yields exceeding 7500 kg/ha or falling below 4000 kg/ha. In contrast, the yield of winter wheat under different irrigation treatments in 2022 was predominantly concentrated in the range of 6500 kg/ha to 8500 kg/ha, with the highest density observed around 7500 kg/ha. Additionally, there were a few yields in the range of 5000 kg/ha to 6000 kg/ha, while very few exceeded 8000 kg/ha. For the year 2022, the yields of winter wheat under various nitrogen application treatments were mostly found between 7000 kg/ha and 9500 kg/ha, with the maximum yield density occurring around 8800 kg/ha. Though a small portion of yields fell between 6000 kg/ha and 7000 kg/ha, very few yields were recorded below 6000 kg/ha.

In summary, the majority of winter wheat with yields above 7000 kg/ha was concentrated in two experiments conducted in 2022, accounting for most of the experimental data. In contrast, those with yields below 5000 kg/ha were predominantly found in the experiments from 2020, with a relatively small quantity.

The violin plot on the periphery illustrated the overall distribution of winter wheat yield. It can be observed that wider areas of the plot correspond to higher data densities, indicating that there were more data points associated with those yield values. The accompanying scatter plot served to supplement the violin plot, with each point

representing the yield value of an individual experimental plot. This combination of visualizations effectively conveys both the distribution and the variability of winter wheat yields across different experimental conditions.

As can be seen from **Figure 26**, when the irrigation volume is equal to or higher than W3 (198mm), the winter wheat yield of most varieties reaches the optimal level. As the irrigation volume increases, the winter wheat yield of some varieties will increase, but for some other varieties, the winter wheat yield will decrease.

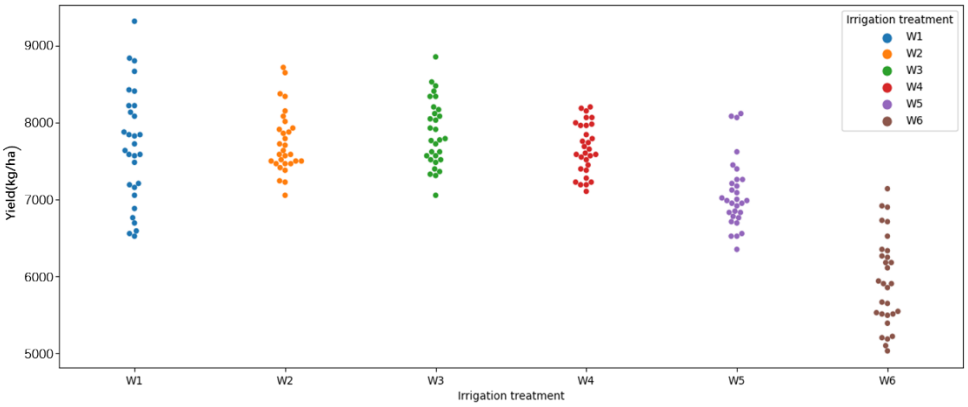

Figure 26. Winter wheat yield distribution under different irrigation treatments in 2022.

3.2 Correlation between multispectral information and winter wheat yield

From **Figure 27**, it is evident that only the Near Infrared (NIR) reflectance displayed a positive correlation with winter wheat yield, while the other five types of multispectral information exhibited negative correlations. This is further illustrated in **Table 10**, which presents the correlation coefficients between various multispectral indices and winter wheat yield.

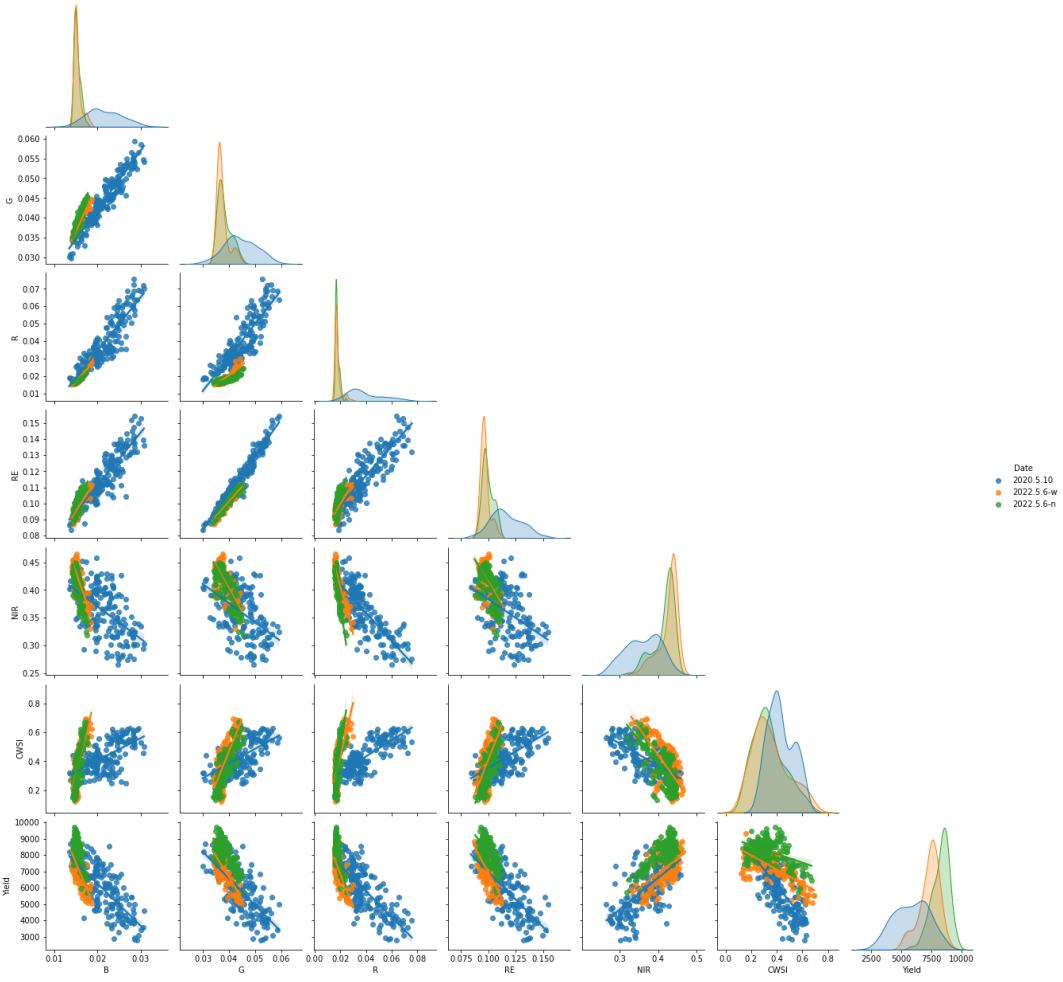

Figure 27. Correlation analysis heat map in filling stage respectively.

Table 10. Correlation index between multispectral indices and winter wheat yield.

Year and treatment	B	G	R	Re	NIR	CWSI
2020.5.10-w	-0.70	-0.70	-0.80	-0.70	0.60	-0.70
2022.5.6-w	-0.70	-0.70	-0.70	-0.70	0.60	-0.70
2022.5.6-n	-0.60	-0.70	-0.70	-0.60	0.70	-0.50
All	-0.80	-0.80	-0.80	-0.80	0.70	-0.60

Analysis of the data under different irrigation amounts revealed that the correlation between red light reflectance and winter wheat yield reached its highest level at r = -0.80, occurring in 2020. Conversely, the correlation involving NIR reflectance was the weakest among the tested indices, with a coefficient of r = 0.6, observed in both 2020 and 2022. Additionally, the reflectance for blue light, green light, red edge, and the water stress index all shared a consistent correlation of r = -0.7, noted in both years.

When examining the effects of varying nitrogen fertilizer applications, the water stress index presented the weakest correlation with winter wheat yield, with a coefficient of r = -0.5. Reflectance measurements for blue light and the red edge yielded a similar correlation of r = -0.6. The correlation coefficients for green light and red reflectance were both r = -0.7, while NIR reflectance exhibited a positive correlation with winter wheat yield at r = 0.7.

Taking into account all wheat samples, it is notable that only the correlation between the Crop Water Stress Index (CWSI) and winter wheat yield did not reach the maximum value observed previously. In contrast, the correlation between NIR reflectance and winter wheat yield remained consistent, retaining its previous maximum value. Interestingly, the correlation between the reflectance of red light, green light, red edge, and winter wheat yield all increased to a value of 0.8, indicating a stronger positive association between these indices and winter wheat yield.

3.3 Findings on the impact of threshold (δ) in pseudo label learning

The choice of the threshold (δ, measured in t/ha) significantly impacts the number and accuracy of trusted pseudo labels. Higher δ values, such as 0.2, allowed for a larger pool of trusted labels (188 in total). However, this came with increased deviations from the true values, with 58 labels exceeding a 10% error, and 130 labels with an error of less than 10%. In contrast, lower δ values (e.g., 0.15 and 0.1) resulted in fewer trusted labels (111 and 50, respectively) and generally smaller errors, with only 8 labels exceeding a 10% error at δ = 0.1.

The number of training rounds also affects the learning process. Fewer rounds led to less trust in the pseudo labels, resulting in smaller deviations from true values. However, increasing the number of rounds, especially at δ = 0.05, resulted in a cumulative increase of trusted labels—from 5 to 112 after 50 rounds. Despite this, the overall errors also increased with 19 labels showing errors greater than 10%, compared to a smaller error rate in fewer rounds.

Through extensive experimentation, a flexible δ strategy was established: for the first three rounds, δ was set to 0.05 minus 0.01 for each round, and afterwards, it was adjusted to 0.015, with a cap of 50 rounds for training. This methodology resulted in 84 trusted pseudo labels, 72 of which had an error of less than 10%, as illustrated in **Figure 28**. The distribution of these labels ranged from 3000 kg/ha to over 9000 kg/ha, pre-dominantly exceeding 7000 kg/ha. Overall, the findings highlight the importance of selecting an appropriate δ value to optimize the accuracy of pseudo labels and the efficiency of the learning process, with higher δ values yielding more but less accurate labels and lower δ values providing fewer but more reliable ones.

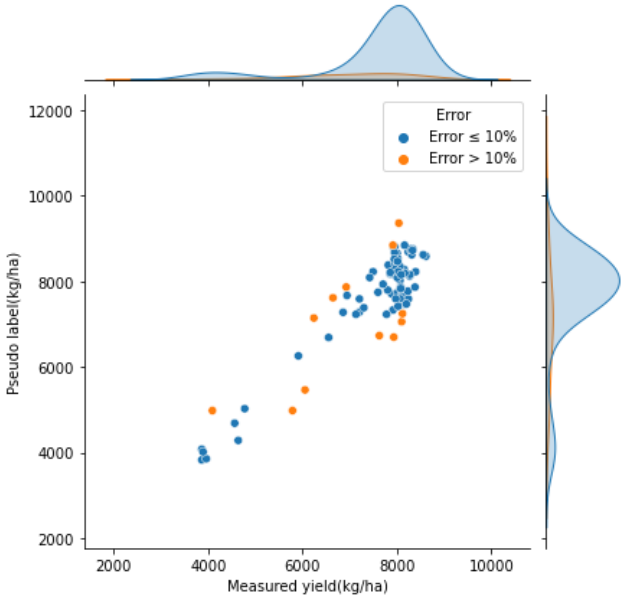

Figure 28. Yield distribution of learned pseudo labels.

3.4 Performance evaluation the yield prediction using multispectral information

By training the random forest (RF) regressor with only 20% of the experimental data (108 data points) for the training set, 10% (54 data points) for the test set, and another 10% (54 data points) for the validation set, we obtained the following results. On the test dataset, we achieved an R^2 of 0.81, RMSE of 681.02 kg/ha, and MAE of 568.97 kg/ha. For the validation dataset, which was never seen during training, we obtained an R^2 of 0.79, RMSE of 736.24 kg/ha, and MAE of 585.85 kg/ha, as shown in **Figure 29**.

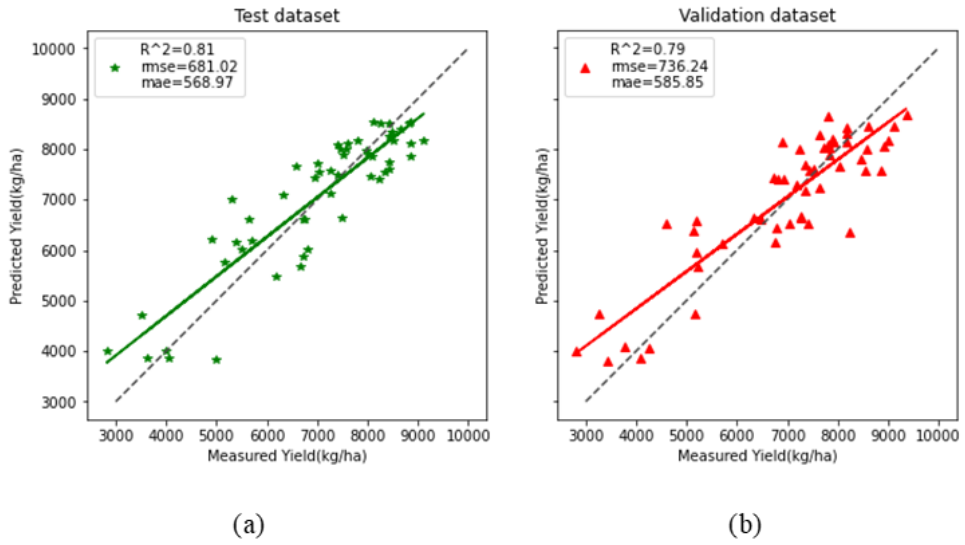

Figure 29. The relationships between the ground-measured and predicted values of winter wheat yield obtained by RF. (a) Description of what is on test dataset; (b) Description of what is on validation dataset.

The testing results indicated that the regressor's performance on the validation dataset, based on the three statistical analysis metrics (R^2, RMSE, MAE), was not as strong as that on the test set.

After self-training, 84 pieces of data added to the training set. Based on the expanded training set, a test with R^2= 0.84, RMSE = 627.94 kg/ha, MAE = 516.94 kg/ha were got on test dataset, a verification with R^2= 0.81, RMSE = 692.96kg/ha, MAE = 550.62kg/ha were got on validation dataset, as showed in **Figure 30**.

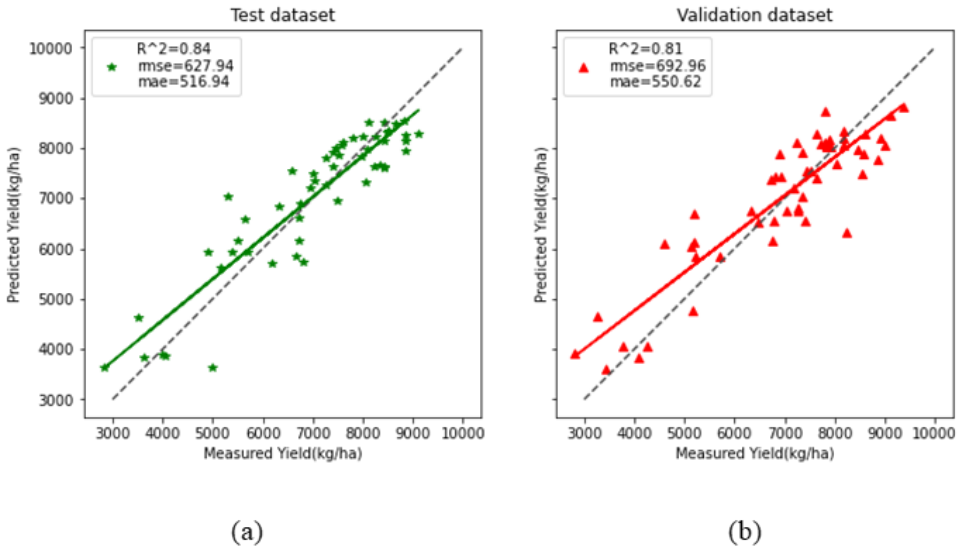

Figure 30. The relationships between the ground-measured and predicted values of winter wheat yield obtained by self-training random forest. (a) Description of what is on test dataset; (b) Description of what is on validation dataset.

In terms of RMSE, compared to the random forest model, the self-training random forest model improved its performance by 7.8% in the test dataset, and 5.6% in the validation dataset. In terms of MAE, compared to the random forest model, the self-training random forest model improved its performance by 9.1% in the test dataset, and 6.0% in the validation dataset.

Whether it was on test dataset, or on validation dataset, the self-training random forest algorithm performed better than the random forest algorithm without a self-training process. Taking into account the three indicators of the coefficient of determination for linear relationship (R^2), RMSE, which is sensitive to outliers in the data, and MAE, which has better robustness against outliers, the self-training random forest model performed better in predicting winter wheat yield than the random forest model.

4. Discussion

4.1 Assessing the relationship between multispectral reflectance and winter wheat yield

Under different external weather conditions, including temperature, humidity and precipitation (shown in Chapter III), different varieties of winter wheat, and different irrigation and fertilization amounts, the correlation between the multispectral reflectance information of winter wheat and its yield remained largely consistent. The more diverse the yield of the data, the clearer the correlation between the multispectral reflectance information of winter wheat and its yield. This indicates that it is feasible to use the multispectral information of winter wheat to predict its yield.

Although there are numerous varieties of winter wheat used to analyze the correlation between their multispectral characteristics and yield, the sampling areas are relatively uniform, all located in the same experimental field, which is somewhat insufficient.

4.2 Challenges and performance factors in self-training random forest for yield prediction

From **Figure 28**, it could be seen that the self-training random forest can effectively label the data, thereby expanding the training dataset. However, further optimization is still needed. As the number of self-training rounds increases, the labeled values tend to spread towards the edges, which may lead to larger errors. The accuracy of the labels annotated by the self-training random forest algorithm improves with the fitting quality of the initial training regressor.

In this experiment, the highest yield proportion of the source dataset falls within the range of 7000 kilograms to 9000 kilograms per hectare. This data segment is where the self-training random forest algorithm learns the most extensively. In the initial random forest training model, there is a significant difference between the predicted yield and the actual yield for values ranging from 5000 kilograms to 7000 kilograms per hectare. The real values of the data learned by the self-training random forest algorithm also show considerable deviations within this range. These indicate that the accuracy of the annotated data obtained through the self-training process depends not only on the distribution of the source data, but also on the selection of the initial small-scale dataset and the training process of the initial random forest model.

This study focused on self-training random forest, while the findings suggest that alternative semi-supervised methods worth of attention. The performance of self-training random forest demonstrated significant dependence on the initial model configuration and data distribution characteristics. Other methods such as co-training or graph-based semi-supervised methods might offer complementary advantages, especially in handling different data structures or noise patterns. Importantly, our

study found that multispectral features are consistently correlated with crop yield under varying conditions, which lays a solid foundation for various semi-supervised learning models. On this basis, subsequent research can identify the optimal semi-supervised method for agricultural yield prediction through comparative experiments.

4.3 Enhancements in winter wheat yield prediction through self-training random forest

A comparison of the results of random forest and self-training random forest, revealed that in terms of data fitting (R^2), prediction accuracy (RMSE), and outlier elimination (MAE), the performance of self-training random forest was superior to that of traditional random forest. This indicates that the self-training random forest algorithm proposed in this paper can improve the accuracy of winter wheat yield prediction when only a small amount of labeled data is used. The main reason for this improvement lies in the self-training process, which generates accurate pseudo-labels for some unlabeled data, effectively expanding the training dataset and improving the accuracy of winter wheat yield prediction.

After expanding the training set through self-training, the output estimation ability of the self-training random forest algorithm was enhanced. The comparison in **Figure 29** and **Figure 30** shows that although the random forest algorithm has significant problems in yield deviation, self-training led to noticeable improvements in predictions at those locations. However, the deviation is still large. This indicates that both the initial random forest training model and the original labeled dataset have a significant impact on the final prediction accuracy of the self-training random forest algorithm.

5. Conclusions

In this research, we analyzed the correlation between multispectral reflectance information and winter wheat yield under various conditions. We proposed a self-training random forest algorithm to annotate the dataset and predict winter wheat yield.

Our test results showed that the correlation between multispectral reflectance information and winter wheat yield was consistent under different weather conditions, irrigation treatments, nitrogen fertilization application amounts, and winter wheat varieties. This consistency suggests that using multispectral reflectance information to predict winter wheat yield is feasible. Moreover, in three experimental datasets, the Pearson correlation between multispectral reflectance and yield was stronger than that

within a single dataset. This finding implies that, within the current land area, an increase in data enhances the relationship between the spectral features of winter wheat and its yield. Additionally, we found that the effectiveness of the initial random forest regression training and the selection of the initial training set have a significant impact on the prediction of winter wheat yield and the data annotation for the self-training random forest. Importantly, the application of the self-training random forest algorithm significantly improved performance, indicating that the algorithm is reliable in predicting winter wheat yield.

These findings emphasize the importance of choosing an appropriate δ value to maximize the accuracy of pseudo-labels and the efficiency of the learning process. A higher δ value generates more labels but also leads to a higher error rate; while a lower δ value generates fewer but more accurate labels, but the learning speed will be slower. The adaptive δ strategy adopted in this study effectively balances these factors, thereby providing a more reliable dataset for further training.

Although we tested over 30 winter wheat varieties under different irrigation and nitrogen fertilizer application conditions, the current algorithm is only applied to small-scale experimental fields and the data is only from Henan Province. To establish the association between multispectral reflectance information (including CWSI) and yield prediction and achieve this goal on a larger scale and in more complex environments, future research needs to accumulate more data under various different conditions and in different regions.

VI

Robust estimation of nitrogen content

1. Synopsis

Based on the temporal yield prediction framework established in Chapter IV and Chapter V, this chapter progresses from modeling final yield to analyzing its fundamental physiological driving factors—addressing research objective 3 of this thesis. While the LSTM-RF hybrid model successfully captured growth dynamics, its reliance on complex temporal features highlights a key issue: what specific physiological mechanisms do these features represent?

Nitrogen content is the primary biochemical determinant of photosynthetic capacity and yield formation. This chapter aims to "open the black box" by developing a powerful and highly accurate plant nitrogen content (PNC) estimator. Prevailing nitrogen management practices, especially in major production regions like China's North China Plain, are often characterized by significant over-application. This not only fails to translate into proportional yield gains but also triggers severe environmental consequences, including soil acidification and water pollution (Chinese Academy of Sciences, 2021; Guo et al., 2010), underscoring an urgent need for precision nitrogen monitoring.

The established approach for estimating PNC from UAV data often involves calculating specific vegetation indices (VIs), such as the normalized difference vegetation index (NDVI) and the normalized difference red edge index (NDRE). These indices, which combine reflectance from discrete bands, have proven valuable for broad assessments of vegetation vigor and nitrogen status (Tucker, 1979). However, they possess inherent limitations. Their formulation is often based on limited band combinations, restricting their ability to capture the full complexity of the spectral response, particularly from sensors with many bands (Driss et al., 2004).

To overcome these limitations, research has evolved in two primary directions. One direction leverages high-resolution hyperspectral imagery and deep learning. Hyperspectral data, with its numerous contiguous bands, provides a rich spectral signature. Deep learning models, particularly convolutional neural networks (CNNs), can automatically extract complex spatial-spectral features from this data, leading to highly accurate prediction models (Tian et al., 2024; Liuchang et al., 2025). However, this approach comes with high costs, computational demands, and data processing complexity that can be prohibitive for routine agricultural use.

This brings us to the second direction, which is the focus of this study: maximizing the value of more accessible and cost-effective multispectral and

thermal data through advanced feature engineering and robust machine learning. While multispectral data has lower spectral resolution, its strategic fusion with thermal information and the construction of high-dimensional feature sets can unlock significant predictive power (Shaohua et al., 2024). Machine learning algorithms—such as random forests and support vector machines—excel at modeling the complex, non-linear relationships between these engineered features and PNC (Huang et al., 2020; Liyuan et al., 2024). They offer a compelling advantage in scenarios with limited data, providing strong performance, computational efficiency, and model interpretability, all of which are practical necessities in agricultural settings.

Therefore, this study proposes a novel framework aimed at bridging the gap between data accessibility and model complexity. We believe that by going beyond conventional VIs through extensive feature engineering—including polynomial expansions, interaction terms between spectral and thermal bands, and statistical transformations—we can construct a feature space with the same information depth as more costly approaches. Through systematically benchmarking a suite of classic but powerful machine learning models on this high-dimensional feature set, this study aims to develop a robust, accurate, and practically feasible method for monitoring the nitrogen content of winter wheat, thereby providing a key tool for precise nitrogen fertilizer management and becoming a crucial component of the comprehensive yield prediction process. It also evaluates several machine learning algorithms to determine the most effective method for estimating plant nitrogen concentration (PNC) during key growth stages (grain filling and jointing). Additionally, this study also identified key nitrogen content thresholds, converting spectral-based diagnostics into practical agricultural recommendations to achieve precise field management.

2. Materials and methods

2.1 Experimental data for nitrogen modeling

The plant nitrogen content (PNC) estimation models developed in this chapter are based on the comprehensive dataset collected during the second and third years of the progressive three-year experiment. Specifically, this chapter utilizes the data from two-factor field experiments conducted simultaneously in Field I and Field II (water conditions × nitrogen fertilizer application rate), with plant nitrogen content at jointing and booting stages as the target variable. This experimental design was

carefully selected to generate a wide range of nitrogen content gradients within the crop canopy, which is crucial for developing and validating reliable PNC estimation models. The inclusion of both water and nitrogen stress factors ensures that the model is trained under complex and realistic field conditions, thereby enhancing its generalizability beyond single stress scenarios.

2.2 Constructing high-dimensional composite features

In the study of predicting nitrogen content in winter wheat using multispectral data, a single spectral band or vegetation index often fails to fully reflect the nitrogen nutrition status of crops. In order to improve the accuracy and robustness of the prediction model, this study introduces the concept of high-dimensional combined features. High dimensional combination features refer to the combination of multiple spectral bands, vegetation indices, and environmental variables through mathematical transformations or statistical methods to generate new feature variables. These features can more comprehensively capture the spectral information of winter wheat canopy and its complex relationship with nitrogen content, thereby improving the predictive ability of the model. In this study, in order to construct high-dimensional combined features to improve the accuracy of the winter wheat nitrogen content prediction model, we adopted various feature engineering methods, including band ratio and difference features, polynomial feature extension, thermal infrared correlation features, and statistical features.

2.2.1 Band ratio and difference features

By calculating the ratio and difference between multispectral bands, vegetation indices and characteristic variables sensitive to nitrogen content are generated, including normalized vegetation index (NDVI), normalized red edge index (NDRE), normalized green vegetation index (GNDVI), and red edge to red band ratio (red_re_ratio). The formulas are shown in **Table 11**.

Table 11. Vegetation indices and characteristic variables sensitive to nitrogen content.

Name	Formula
NDVI	$\frac{R_{NIR} - R_r}{R_{NIR} + R_r}$
NDRE	$\frac{R_{NIR} - R_{re}}{R_{NIR} + R_{re}}$
GNDVI	$\frac{R_{NIR} - R_g}{R_{NIR} + R_g}$
Red_re_ratio	$\frac{R_{re}}{R_r}$

2.2.2 Polynomial feature extension

To capture the nonlinear relationships and interactions between spectral bands, we perform polynomial extensions on the red (Red), green (Green), near-infrared (NIR), and red edge bands. Stack the original spectral band data into a matrix spectral feature. Use second-order polynomial extensions (Polynomial Features) to generate the square terms of the original band and their pairwise interaction terms (such as Red × Green, Red × NIR, etc.). The final generated polynomial feature matrix poly feature, including 'red', 'green', 'nir', 're', 'red^2', 'red*green', 'red*nir', 'red*re', 'green^2', 'green*nir', 'green*re', 'nir^2', 'nir*re' and 're^2', a total of 14 features, significantly expands the dimensionality of the feature space and better describes the complex relationship between spectral information and nitrogen content.

2.2.3 Thermal infrared correlation features

Combining thermal infrared data and multispectral data to generate features related to canopy temperature: Combine the thermal infrared band (Thermal) with the thermal infrared difference (Thermal Diff). Calculate the interaction terms between thermal infrared and vegetation indices (such as Thermal × NDVI, Thermal × NDRE) to reflect the impact of temperature on vegetation growth and nitrogen nutrition. The final generated thermal infrared feature matrix thermal features provide additional environmental information for the model.

2.2.4 Statistical features

Generate descriptive features through statistical analysis of spectral band data: calculate the mean (mean_Spectral) and standard deviation (STD_Spectral) of

spectral bands to characterize the overall level and variability of spectral reflectance. These statistical features can enhance the model's ability to capture the distribution characteristics of spectral data.

2.3 Model building

This study used eight typical machine learning algorithms, including Ridge Regression (RR), Support Vector Regression (SVR), K-Nearest Neighbors (KNN) regression, RF, AdaBoost regression, Gradient Boosting Regression (GBR), Light GBM regression and ANN, to construct a winter wheat nitrogen content prediction model.

RR is a linear regression based on the Ordinary Least Squares (OLS) method, by adding an L2 regularization term (the sum of the squares of the coefficients) to address the issue of multicollinearity in linear regression. SVR uses radial basis function (RBF) as the kernel function to fit data by maximizing the interval, which can handle nonlinear relationships and has robustness to outliers. KNN Regression is a non-parametric regression method based on distance metrics, the predicted value is the average of the target values of the K nearest neighbor samples. RF is an ensemble learning algorithm based on multiple decision trees, reduce variance through Bagging (with replacement sampling), and output the average prediction of each tree. It can handle nonlinear relationships and is robust to outliers and noise. AdaBoost regression is a boosting method, based on decision trees as the base learner, which iteratively adjusts sample weights to gradually optimize the model. It can improve the performance of weak learners and is suitable for processing high-dimensional data. GBR is also a boosting framework, unlike adaboost regressor, it does not directly adjust the sample weights but gradually fits the residuals through gradient descent to construct multiple regression trees. Light GBM regression is an optimized implementation based on gradient boosting, using histogram algorithm (discretize the continuous features into histograms) for acceleration, and splitting nodes according to the Leaf-wise strategy. ANN is a complex combination of multiple layers of neurons, with weights optimized through backpropagation to fit functions. It supports end-to-end learning without the need for feature engineering.

In order to evaluate the predictive performance of the model, the validation process adhered to the unified framework outlined in Chapter III, employing stratified 10-fold cross-validation, with each iteration reserving 3 for validation and the remaining 7 for model training.

3. Results

3.1 Nitrogen content in jointing and booting stage

Figure 31 illustrates the different nitrogen content in winter wheat between jointing stage and booting stage under contrasting irrigation and fertilizer treatment. For winter wheat nitrogen content at jointing stage, nitrogen content during the early jointing stage (March 31, 2023) in nitrogen-fertilized plots (2023N) exhibited substantial variability, ranging from 10 mg g^{-1} to 43 mg g^{-1}. Comparatively, late jointing stage measurements (April 11, 2022) across both watering (2022W) and nitrogen-fertilized (2022N) treatments showed reduced variation, with values spanning 10 mg g^{-1} to 35 mg g^{-1}.

At booting stage, nitrogen content displayed consistent temporal patterns, with water-different plots (2022W) and nitrogen-fertilized plots (2023N) both constrained to 10–30 mg g^{-1}. Notably, the 2022 nitrogen-fertilized treatment (2022N) demonstrated a distribution range 5–27 mg g^{-1}.

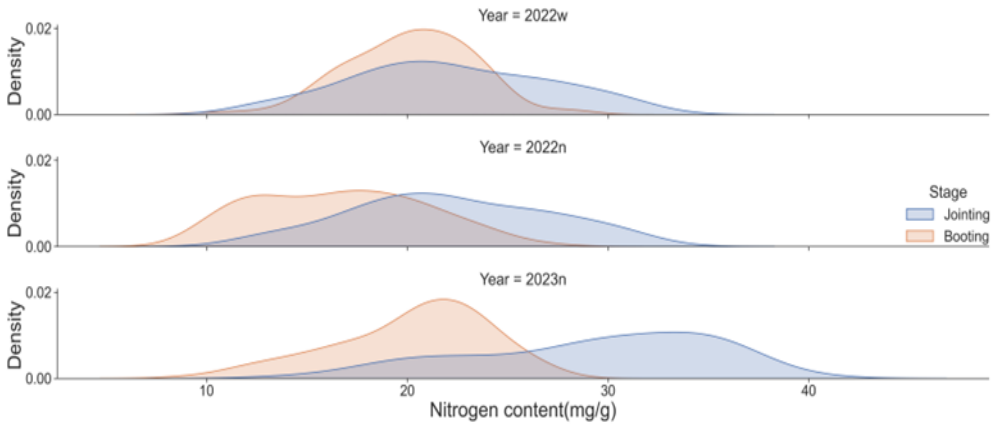

Figure 31. KDE plots of nitrogen content by different treatment and growth stages.

During the jointing stage, the winter wheat is in a rapid period of vegetative growth, the dynamic changes in nitrogen absorption and distribution are significant, resulting in a wide range of nitrogen content. In booting stage, the winter wheat shifts to reproductive growth, and nitrogen metabolism becomes stable. The range of nitrogen content is relatively narrow.

3.2 Nitrogen content prediction using VIs and multispectral reflectance

The relationships between winter wheat nitrogen content and eight spectral predictors, including four Vis (NDVI, NDRE, GNDVI and red_re_ratio) and four multispectral reflectance (red, green, NIR and redege), were established using the eight ML algorithms. The results showed that LightGBM produced the highest accuracy in jointing stage, with an R^2 of 0.85 and 0.82, RMSE of 2.49mg/g and 2.86mg/g, and MAE of 1.95mg/g and 2.36mg/g at the training set and testing set, respectively (**Table 12**). Followed closely by AdaBoost Regressor and RF regressor.

Table 12. Performance of eight ML methods for winter wheat nitrogen content prediction using Vis and multispectral reflectance at jointing stage.

Method	Training set			Testing set		
	R^2	RMSE	MAE	R^2	RMSE	MAE
Ridge	0.76	3.18	2.42	0.74	3.42	2.64
SVR	0.77	3.13	2.00	0.77	3.23	2.36
KNN	0.73	3.37	2.67	0.71	3.61	2.89
RF	0.82	2.76	2.11	0.81	2.94	2.40
AdaBoost	0.83	2.67	2.02	0.81	2.93	2.35
GBR	0.83	2.70	2.10	0.80	2.96	2.35
Light GBM	0.85	2.49	1.95	0.82	2.86	2.36
ANN	0.70	3.46	2.68	0.67	3.49	2.73

In booting stage, RF regressor performed best, with an R^2 of 0.72 and 0.71, RMSE of 2.13mg/g and 2.34mg/g, and MAE of 1.66mg/g and 1.77mg/g at the training set and testing set, respectively (**Table 13**).

Table 13. Performance of eight ML methods for winter wheat nitrogen content prediction using VIS and multispectral reflectance at booting stage.

Method	Training set			Testing set		
	R^2	RMSE	MAE	R^2	RMSE	MAE
Ridge	0.65	2.40	1.90	0.63	2.62	1.90
SVR	0.64	2.44	1.83	0.63	2.64	2.00
KNN	0.65	2.39	1.84	0.65	2.55	1.94
RF	0.72	2.13	1.66	0.71	2.34	1.77
AdaBoost	0.71	2.19	1.73	0.69	2.41	1.87
GBR	0.72	2.15	1.66	0.69	2.42	1.81
Light GBM	0.68	2.30	1.80	0.66	2.51	1.91
ANN	0.51	2.81	2.21	0.50	2.50	1.91

As shown in **Table 12**, during the jointing stage, the plants are in a rapid nutritional growth period, and the dynamic changes of nitrogen absorption and distribution are significant, resulting in a wide range of nitrogen content. Although the model can capture the main trend (with a high R^2), due to the large variability of the actual values, the absolute error (RMSE, MAE) is correspondingly high. The data distribution range is wide, and the model may capture nonlinear relationships or extreme values. The high R^2 reflects a good trend fitting, but the large range of data leads to error accumulation (such as high values being underestimated or low values being overestimated).

At the booting stage, the plants shift to reproductive growth, and nitrogen metabolism tends to be stable, with a narrower range of nitrogen content. Although the model's explanatory power is weak (with a low R^2), the differences in actual values are small, and the absolute error is naturally low. The data are concentrated in a small range, and the predicted values by the model are close to the actual mean. The low R^2 indicates that it cannot explain subtle variations, but the absolute error is reduced due to the small numerical differences.

3.3 Nitrogen content prediction using high-dimensional composite features

We employed eight machine learning algorithms to model the relationships between winter wheat nitrogen content and high-dimensional composite features, including 4 Vis, 14 polynomial feature, 4 thermal features, mean spectral and spectral standard deviation.

The results showed that AdaBoost produced the highest accuracy in jointing stage, with an R^2 of 0.86 and 0.84, RMSE of 2.49 mg/g and 2.55mg/g, and MAE of 1.95mg/g and 1.98mg/g at the training set and testing set, respectively (**Table 14**). Followed closely by Light GBM Regressor and RF regressor.

Table 14. Performance of eight ML methods for winter wheat nitrogen content prediction using high-dimensional composite features at jointing stage.

Method	Training set			Testing set		
	R^2	RMSE	MAE	R^2	RMSE	MAE
Ridge	0.78	3.07	2.29	0.77	3.05	2.26
SVR	0.79	3.01	1.89	0.77	3.09	2.36
KNN	0.76	3.21	2.51	0.73	3.34	2.36
RF	0.85	2.56	1.99	0.84	2.59	2.05
AdaBoost	0.86	2.49	1.95	0.84	2.55	1.98
GBR	0.85	2.56	1.99	0.84	2.56	2.05
Light GBM	0.85	2.56	2.01	0.84	2.53	2.06
ANN	0.74	3.36	2.60	0.73	3.20	2.47

During the booting stage (**Table 15**), both AdaBoost and random forest (RF) regressors demonstrated strong predictive performance, although with distinct advantages in different metrics. AdaBoost achieved superior accuracy, reflected in a higher R^2 value, indicating better overall model fit, as well as a lower RMSE, reflecting reduced error magnitude. In contrast, RF exhibited greater robustness to outliers, resulting in the lowest mean absolute error (MAE) among the models compared.

Table 15. Performance of eight ML methods for winter wheat nitrogen content prediction using high-dimensional composite features at booting stage.

Method	Training set			Testing set		
	R^2	RMSE	MAE	R^2	RMSE	MAE
Ridge	0.68	2.27	1.82	0.65	2.66	1.93
SVR	0.70	2.20	1.45	0.70	2.46	1.86
KNN	0.69	2.24	1.77	0.67	2.58	2.01
RF	0.77	1.92	1.51	0.75	2.22	1.64
AdaBoost	0.78	1.87	1.52	0.76	2.21	1.65
GBR	0.76	1.97	1.55	0.76	2.21	1.68
Light GBM	0.75	1.99	1.58	0.75	2.26	1.74
ANN	0.65	2.36	1.85	0.64	2.16	1.71

The robustness of the models was further confirmed by the low variability in performance across cross-validation folds. For the composite feature models during

the booting stage, the RMSE showed standard deviations of 0.08–0.12 mg/g, while MAE variations ranged from 0.06 to 0.09 mg/g. This low inter-fold variability underscores the consistent performance of our approach across different data subsets.

Compared to nitrogen content prediction models based on vegetation indices (VIs) and multispectral reflectance, the high-dimensional composite feature approach demonstrated superior accuracy across both jointing and booting stages, with particularly pronounced improvements during the booting stage. The composite feature model achieved an 8% increase in R^2 (from 0.71 to 0.76) and an 8% reduction in RMSE (from 2.34 to 2.21 mg/g), alongside a 9.4% decrease in MAE (from 1.81 to 1.64 mg/g), highlighting its enhanced capability to capture subtle metabolic variations during reproductive growth phases.

The comparative analysis revealed consistent superiority of tree-based ensemble methods (Random Forest, AdaBoost, Gradient Boosting, and LightGBM) in predicting winter wheat nitrogen content across both jointing and booting stages, outperforming linear/instance-based models (Ridge, SVR, KNN). Notably, AdaBoost achieved the highest precision at jointing stage (R^2=0.86), while Random Forest and Adaboost performed excelled at booting stage. Artificial neural networks (ANN) demonstrated the poorest performance, with R^2 values 12-18% lower than ensemble counterparts, due to overparameterization and spectral noise amplification.

Compared **Table 12** and **Table 14**, it could be seen that incorporating high-dimensional spectral combination features enhanced the predictive capability for nitrogen content compared to relying solely on conventional vegetation indices (VIs) at jointing stage. As **Figure 32** shows, the prominence of interaction terms like nir*re and nonlinear components such as nir^2 in the top 10 important features suggests that spectral combinations capture complex, non-linear relationships between spectral bands and nitrogen dynamics that traditional VIs alone cannot fully characterize. Features like mean_spectral and std_spectral further complement this by encoding overall spectral response patterns and variability, which may reflect physiological status or stress signals beyond the scope of predefined VIs. This underscores the value of leveraging raw spectral data or derived combinatorial features to uncover latent interactions and improve model robustness.

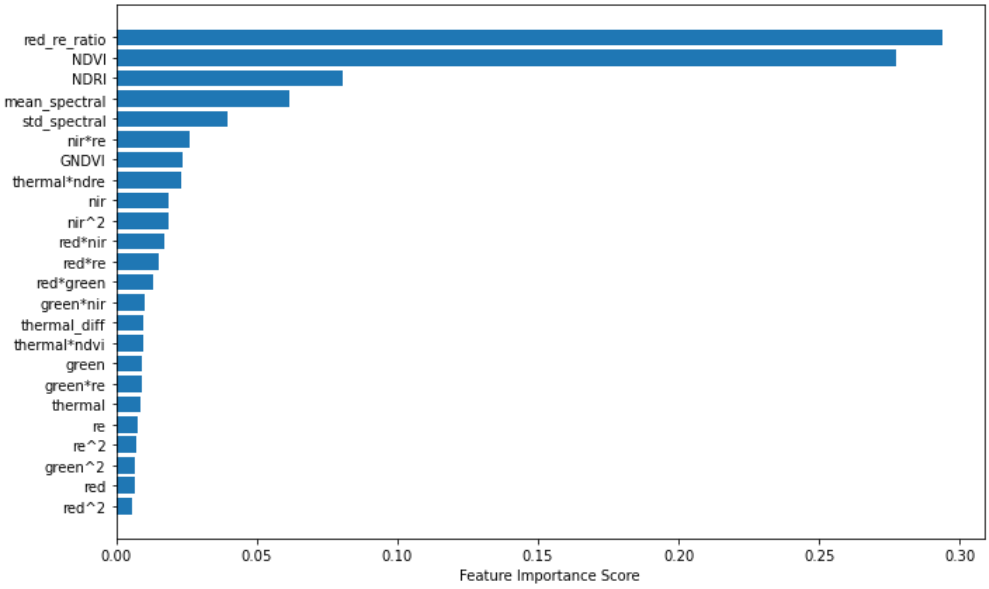

Figure 32. The importance value of each input parameter from the RF regressor for nitrogen content prediction at the jointing stage.

Compared **Table 13** and **Table 15**, it indicates that incorporating high-dimensional spectral combination features significantly enhanced the predictive capability for nitrogen content compared to relying solely on conventional vegetation indices (VIs) at booting stage. As shown in **Figure 33**, it demonstrates high-dimensional spectral combination features continued to outperform conventional vegetation indices (VIs) in predicting nitrogen content during the booting stage, as evidenced by the dominance of thermal*ndre, red², and nir*re in the top-ranked features. The inclusion of thermal*ndre highlights the critical role of thermal-band interactions with spectral indices in capturing temperature-mediated nitrogen dynamics, which traditional Vis often overlook. Additionally, std_spectral ranking third suggests that spectral variability—potentially linked to heterogeneous canopy structures or stress responses—provides complementary diagnostic power. The persistence of nonlinear terms like red² and cross-band products such as nir*re further reinforces that nitrogen regulation during booting involves multifaceted spectral interactions that linear or single-index approaches fail to fully resolve.

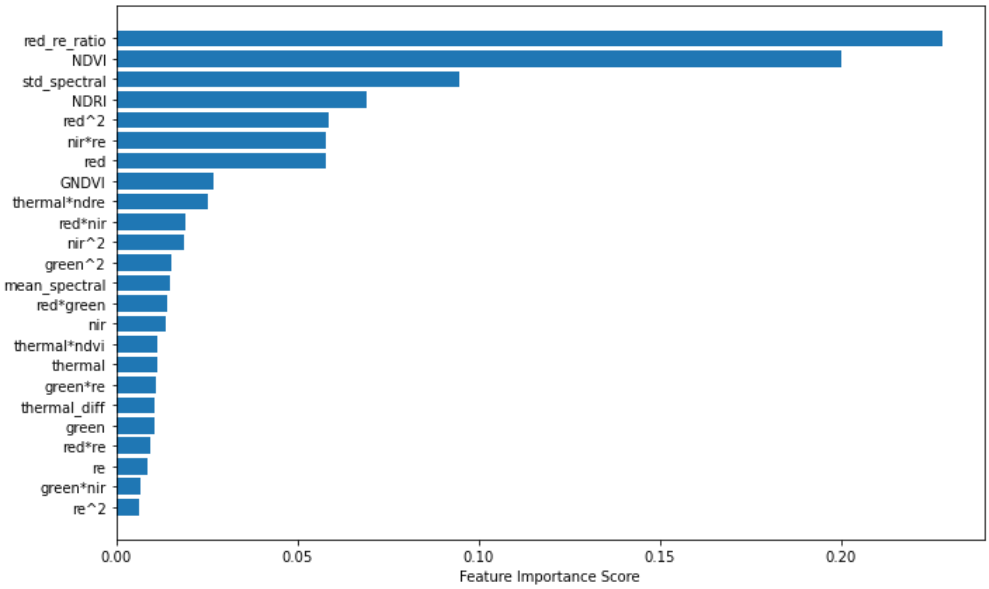

Figure 33. The importance value of each input parameter from the RF regressor for nitrogen content prediction at the jointing stage.

It is worth noting that, in the plant nitrogen content prediction, red-edge radiation (red_re_ration) and the normalized difference vegetation index (NDVI) consistently rank as the top two indicators, irrespective of whether the plant is in the jointing stage or the booting stage. These two metrics have proven to be highly reliable for estimating nitrogen levels across different growth phases due to their sensitivity to variations in leaf reflectance and vegetation health.

During the jointing stage, a critical period when plants begin to form reproductive structures, red_re_ratio and NDVI maintain their prominence as the most effective predictors of nitrogen content. Following closely behind, the nitrogen difference ratio index (NDRI) ranks third in this specific phase. The NDRI's ability to detect subtle changes in nitrogen concentration makes it a valuable supplementary tool for precision agriculture applications during this time.

Similarly, in the booting stage, where plants transition into producing flowers and seeds, red_re_ratio and NDVI continue to lead as the primary indicators for nitrogen prediction. In this phase, NDRI shifts slightly to occupy the fourth position among the predictive indices. This shift may be attributed to differences in canopy structure and light absorption patterns as plants mature.

The consistent performance of these indices underscores their importance in agricultural monitoring systems. By leveraging these tools, farmers and researchers can make informed decisions regarding fertilizer application rates, thereby optimizing crop yield while minimizing environmental impact. Furthermore, understanding the relative rankings of these indices at various stages of plant development allows for more targeted and efficient resource management strategies.

3.4 The relationship between nitrogen content and yield

During early jointing (2023 nitrogen application treatments), yields stabilized when plant N exceeded 25 mg/g, while in late jointing (2022 irrigation and nitrogen treatments), a lower threshold of 15 mg/g was observed, below which yields declined with reduced N (**Figure 34**).

Figure 34. The relationship between yield and plant nitrogen content at the jointing stage under water treatment in 2022, and nitrogen fertilizer treatment in 2022 and 2023. Note: the red and blue lines are the fitted curves of the linear plateau model and quadra.

At the booting stage (**Figure 35**), yields plateaued at N levels above 15 mg/g, with significant reductions below this threshold.

Figure 35. The relationship between yield and plant nitrogen content at the booting stage under water treatment in 2022, and nitrogen fertilizer treatment in 2022 and 2023. Note: the red and blue lines are the fitted curves of the linear plateau model and quadra.

The analysis reveals critical thresholds for winter wheat yield response to plant nitrogen (N) content across growth stages (**Figure 34**, **Figure 35**). These findings suggest that optimal N thresholds vary by growth stage: higher N sufficiency is required during early vegetative growth (jointing), while reproductive stages (booting) prioritize sustaining moderate N levels (~15 mg/g). Exceeding these thresholds provides no yield benefit, emphasizing the need for stage-specific N management to avoid over-application while preventing deficits. This supports precision agriculture strategies that dynamically adjust N inputs based on real-time plant N diagnostics and phenological progression.

4. Discussion

This study successfully moved from the temporal yield prediction established in Chapter IV and V to a mechanistic understanding of one of the key physiological driving factors - the plant nitrogen content. By leveraging the experimental design expanded in the second and third years (which introduced nitrogen gradients and synchronous multi-sensor data collection), we have moved beyond the "black box" model of direct spectral yield correlations. Our research results indicate that by combining multispectral and thermal data using advanced feature engineering and

machine learning techniques, a robust estimation of the plant nitrogen content can be achieved, thereby "opening the box" to reveal the key nitrogen dynamic changes.

4.1 Dynamics of nitrogen content and implications for sensing

The observed differences in plant nitrogen content (PNC) between the jointing and booting stages (as shown in **Figure 31**) are in line with established crop physiological principles. The wide range of PNC during the jointing stage reflects rapid vegetative growth and active nitrogen absorption and transport phases, providing dynamic and diverse targets for remote sensing. In contrast, the narrower range during the booting stage indicates stable nitrogen metabolism as the plant is transitioning to the reproductive growth stage. These physiological changes have a direct impact on the performance of the prediction model. The high R^2 but relatively large absolute error during the jointing stage indicates that the model effectively captures the main trends in the wide distribution of data, while the lower R^2 but smaller absolute error during the booting stage suggests that although the overall trend is less obvious, the predicted values are closer to the actual values within the compressed range.

4.2 The value of high-dimensional feature engineering

One of the core findings of this chapter is that models using high-dimensional composite features consistently outperform those relying solely on conventional variable indicators and raw reflectance. The performance improvement is particularly evident in the booting stage (with an 8% increase in R^2 value and a 9.4% reduction in MAE), highlighting the critical limitations of predefined VIs: their inherent simplicity often fails to capture the complex, nonlinear interactions between canopy biochemistry and spectral responses.

The feature importance analysis (**Figure 32**, **Figure 33**) provides a mechanistic explanation for this improvement. The significance of interaction terms (such as nir*re), polynomial terms (such as red^2), and fused features (such as thermal*ndre) indicates that the relationship between canopy reflectance and nitrogen content is not linear or additive. Features like std_spectral further contribute by encoding the heterogeneity of the canopy, which may be related to the distribution of nitrogen. This suggests that our feature engineering strategy successfully creates an informative feature space that can describe the physiological state of the crop more comprehensively than standardized indicators.

4.3 Algorithm performance and practical considerations

The consistent outstanding performance of tree-based ensemble methods (such as Random Forest, AdaBoost, and Light GBM) compared to linear models and artificial neural networks highlights their suitability for this task. These methods inherently possess the ability to model complex nonlinear relationships and handle heterogeneous data, making them highly suitable for our high-dimensional feature set. The poor performance of ANN is likely attributable to overparameterization given the dataset size, reinforcing the practical advantage of ensemble methods in agricultural remote sensing applications where large, labeled datasets are often a constraint.

4.4 Linking nitrogen status to final yield

By combining the PNC estimates with the yield data, this chapter establishes a crucial link between the intermediate physiological characteristics and the final agronomic outcomes. The nitrogen thresholds for different growth stages were determined (**Figure 34**, **Figure 35**) - approximately 25 mg/g at early jointing and 15 mg/g at booting - which is not merely a simple prediction but also provides actionable management information. These thresholds define the sufficient levels beyond which additional nitrogen application no longer promotes yield. This discovery directly addresses the issue of excessive nitrogen application mentioned in the introduction and provides a quantitative basis for precise nitrogen fertilizer management, enabling farmers to make informed decisions during the growing period to optimize input efficiency.

5. Conclusions

This chapter successfully dissects one of the key physiological components relied upon in the yield prediction conducted in Chapter IV and V. By integrating multispectral and thermal data from unmanned aerial vehicles and using tree-based ensemble machine learning models (particularly AdaBoost and RF), high-precision estimation of winter wheat nitrogen content can be achieved, and it performs most robustly during critical growth stages. Feature engineering is crucial. Moving beyond traditional vegetation indices and introducing high-dimensional composite features - such as band interactions, polynomial terms, and thermal-spectral fusion - can significantly improve the accuracy and interpretability of the model, thereby capturing the complex, nonlinear features of the nitrogen spectrum relationship.

The physiological pathway of yield is quantifiable. The nitrogen content thresholds determined at the jointing stage (approximately 25 mg/g) and the late booting stage (approximately 15 mg/g) establish a key, data-based connection between spectral diagnosis and yield potential. This enables the PNC estimates based on UAVs and ML methods to be transformed into precise agricultural prescriptions, thereby reducing the risks associated with insufficient yield and excessive application harmful to the environment.

In summary, this chapter effectively "opens" the "black box" of yield formation in the aspect of nitrogen dynamics. The framework developed here not only predicts an intermediate feature, it also provides a physiological-based precise management tool.

VII

Multi-task learning for joint biomass estimation

1. Synopsis

Building upon the physiological foundation established in the previous chapter, which focused on nitrogen content as a key driver of yield, this chapter further explores another critical component of the yield equation: biomass accumulation. The nitrogen content status reflects the biochemical potential of growth, while biomass represents its physical manifestation, directly linking the growth of the crop to the final grain yield.

Accurate and non-destructive monitoring of above-ground biomass (AGB) can help optimizing resource management, and understanding crop responses to environmental stress. It is fundamental for winter wheat yield prediction. AGB is the physical manifestation of crop growth, can directly link vegetative development to grain production. Specifically, dry weight (DW) quantifies the accumulation of photosynthetic organic matter and shows a strong positive correlation with final grain yield, while fresh weight (FW) characterizes real-time plant water content and transport efficiency (Lobell et al., 2015; Ge et al., 2012). Their ratio offers a direct proxy for water use efficiency, providing a scientific basis for precision irrigation.

However, traditional destructive sampling methods are inefficient and incompatible with the needs of current precision agriculture. Remote sensing, particularly from unmanned aerial vehicles (UAVs), has emerged as the useful tool for field-scale, non-destructive monitoring. UAV-based multispectral data can effectively capture structural and pigment-related information of plant. By quantifying water stress through indices like the CWSI, thermal imagery could provide a critical complementary signal, which correlates with stomatal conductance and water use dynamics (Gonzalez-Dugo et al., 2006). The fusion of multispectral vegetation indices and thermal data has been identified to significantly improve the accuracy of biomass estimation models (Fernandez et al., 2020).

Despite these advances, a remaining methodological limitation is the prevalent "one-problem-one-model" paradigm. Many approaches typically develop separate, isolated models for predicting DW and FW. This is inefficient and fails to leverage the intrinsic physiological correlation between these parameters, potentially limiting model robustness and explanatory power (Caruana, 1997).

Building upon the physiological monitoring foundation established in preceding chapters, this chapter directly addresses this limitation by introducing comprehensive multi-task learning (MTL) methods for the joint prediction of winter wheat dry weight and fresh weight. We hypothesize that by sharing feature

representations during model training, the joint estimation of these intrinsically related traits can improve data efficiency, while maintain prediction accuracy.

Our methodology advances beyond conventional single-task modeling in two key aspects: (1) the construction of a comprehensive, physiologically-informed feature set integrating spectral reflectance, vegetation indices, thermally-derived CWSI, and their interaction terms; and (2) the explicit incorporation of phenological stage as a key biological variable.

By constructing this integrated analytical framework for key growth stages—from jointing to filling—this chapter aims to provide a reliable, efficient tool for growth monitoring. More importantly, it seeks to bridge spectral responses with crop functional dynamics, thereby contributing a critical component to a comprehensive, physiology-informed yield prediction system for winter wheat. The complete analytical framework, illustrated in **Figure 36.**

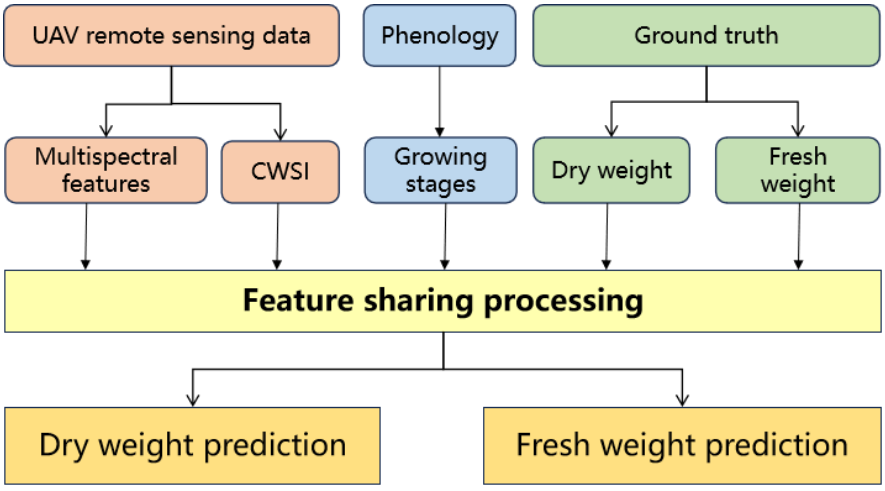

Figure 36. Methodological flowchart of the joint prediction of DW and FW.

2. Materials and methods

The biomass estimation experiment collected winter wheat information during 2021-2022 and 2022-2023 winter wheat growing seasons of the progressive field experiment. This ensures methodological consistency across the physiological analysis within this thesis. The analysis utilizes data from separate trials conducted

in Field I and Field II. Field I involved water regime treatments, while Field II focused on nitrogen fertilization treatments.

The stratification for cross-validation was conducted based on the experimental treatments. The dataset was divided into 10 folds of approximately equal size, with stratification ensuring that each fold maintained proportional representation of all treatment combinations. During each validation iteration, 7 folds (70% of data) were used for model training while the remaining 3 folds (30%) were reserved for validation.

2.1 Spectral features construction

Based on extensive empirical validation and practical application in agricultural remote sensing, the following vegetation indices (VIs) have been systematically selected as effective predictors for winter wheat biomass estimation (as shown in **Table 16**).

Table 16. Vegetation index in winter wheat biomass estimation.

Name	Formula	Advantage
NDVI	$(R_{NIR} - R_r)/(R_{NIR} + R_r)$	Strong correlation with green biomass and canopy density during early to mid-growth stages.
NDRE	$\frac{R_{NIR} - R_{re}}{R_{NIR} + R_{re}}$	Enhanced sensitivity to chlorophyll content and nitrogen status, particularly in mid-to-late growth stages.
GNDVI	$\frac{R_{NIR} - R_g}{R_{NIR} + R_g}$	Compared with the traditional NDVI, GNDVI is more sensitive to green vegetation and can more accurately assess the vegetation coverage and growth status.
CIR	$\frac{R_{NIR}}{R_r}$	Complementary to NDVI and NDRE, especially in multi-sensor data fusion.

To address the combined influence of thermal and multispectral data on winter wheat biomass prediction, interaction terms VHI (NDVI × CWSI) is generated as a part of input features. This term captures synergistic relationships between spectral reflectance and crop water stress dynamics, which are critical for robust biomass estimation.

Based on the above analysis, the final input feature set used for predicting the biomass of winter wheat, integrating data from multiple sources to optimize the accuracy and interpretability of the model was organized, as shown in **Table 17**.

Table 17. Input feature set for winter wheat biomass prediction.

Types	Name	Physical meaning
Reflectivity	R_r, R_g, R_{re}, R_{NIR}	Reflectance of each multispectral band
Environmental factor	CWSI	Degree of water stress
Vegetation index	NDVI, NDRE, GNDVI, CIR	Reflecting biomass, chlorophyll content, and canopy structure
Interaction features	VHI (NDVI×CWSI)	The relationship between water stress and spectral response

2.2 Multitask regression model

Multi-output random forest is a multi-objective prediction method based on ensemble learning. Its core principle lies in constructing independent decision tree models for each target variable, while adopting a shared mechanism in the feature selection stage to enhance computational efficiency and maintain feature consistency. At the implementation level, the base learners are typically extended to a multi-output form by using the multi output regressor wrapper, enabling the model to handle multiple related targets simultaneously. This method not only inherits the inherent robustness and anti-overfitting characteristics of RF, but also supports the analysis of feature importance, which is very helpful for understanding the contribution of different features to multi-objective predictions.

The multi-output light GBM achieve collaborative optimization among multiple target variables by constructing independent gradient boosting tree sequences for each target variable, while sharing the splitting criteria during the feature splitting process. The significant advantage of this method lies in its powerful ability to model nonlinear relationships, which can automatically identify important features and perform dynamic feature selection, significantly enhancing the model's expressiveness. By leveraging the iterative optimization feature of the gradient

boosting framework, this model maintains high prediction accuracy while effectively handling high-dimensional data and missing value issues, and is particularly suitable for complex large-scale multi-output regression tasks.

The multi-output neural network adopts an architecture combining shared hidden layers with task-specific output layers. Through the deep network structure, it simultaneously learns the shared features of multiple targets. Its core advantage lies in the end-to-end learning ability. The model can automatically extract discriminative feature representations from the original data without the need for manual feature engineering. The inherent strong representation learning ability of deep neural networks enables it to capture complex nonlinear correlations between targets, while the independent design of the output layer ensures the flexibility of each target prediction. This architecture is particularly suitable for handling high-dimensional and complexly correlated multi-target prediction problems.

2.3 Stratified sampling for dataset division

To ensure the representativeness of both the training and testing datasets, stratified sampling was employed based on dry weight (DW) as a key stratification variable. This approach was particularly suitable, since DW not only represents a primary prediction target but also strongly correlates with fresh weight (FW), with a pearson correlation coefficient of 0.85 ($p < 0.001$), as demonstrated in **Figure 37**. This high correlation ensures that stratification based on DW effectively captures the distribution characteristics of FW simultaneously.

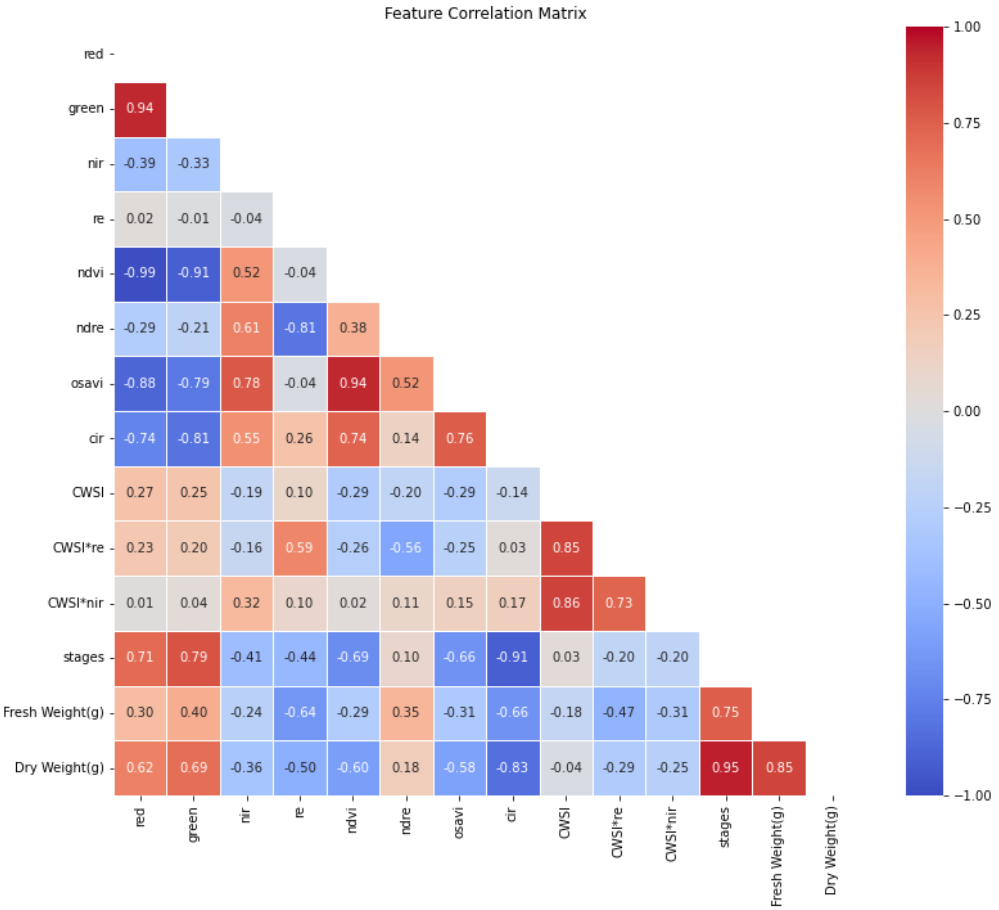

Figure 37. Pearson correlation between features, and between features and dry-fresh weight.

The continuous dry weight values were first converted into ordered categorical variables, followed by proportional allocation of samples from each stratum to maintain the original distribution patterns. The dataset was ultimately divided into training and testing sets at a 7:3 ratio. As shown in **Figure 38**, this stratified sampling approach successfully ensured proportional representation of various dry and fresh weight ranges in both training and testing sets.

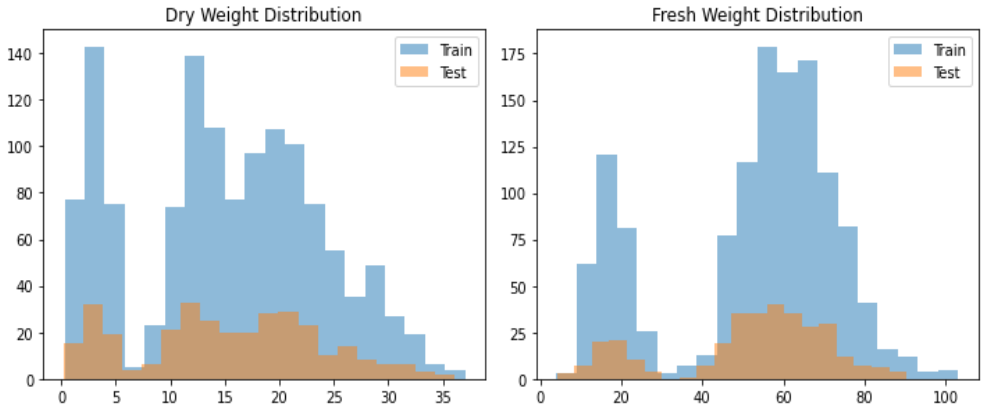

Figure 38. Stratified sampling according to dry weight distribution.

3. Results

3.1 Changes in dry and fresh weights of winter wheat

The changes in dry and fresh weights of winter wheat during different growth stages are significantly influenced by its physiological processes and the environment. In this study, the jointing stage (when stem growth is rapid), the booting stage (when photosynthetic products accumulate in large quantities), the heading and flowering stage (when the wheat spike develops completely and photosynthetic products are transferred to the spike), and the grain filling stage, which is when grains are filling and dry matter accumulates rapidly, were chosen.

From **Figure 39**, it can be seen that the changes in dry and fresh weights of winter wheat also follow this pattern. From the jointing stage to the grain filling stage, the dry weight of winter wheat accumulates in an upward trend, with little change in speed. The fresh weight increases most rapidly from the jointing stage to the booting stage. From the booting stage to the heading and flowering stage, the fresh weight changes little and increases the least. From the heading and flowering stage to the grain filling stage, the speed of the fresh weight increases again.

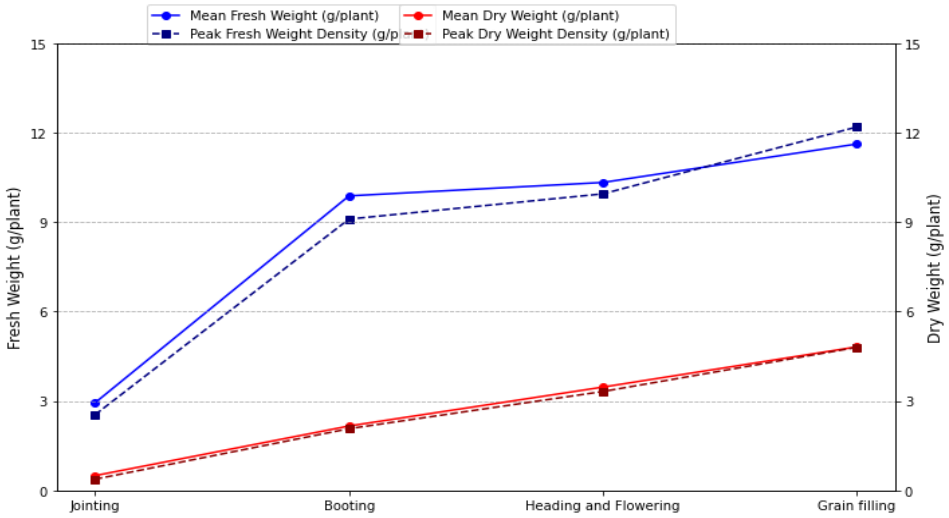

Figure 39. Dry and fresh weights of winter wheat in different stages.

Of course, the changes in the dry and fresh weights of winter wheat not only vary with its own growth and development stages, but also are related to the wheat variety and environmental factors. For instance, the growth rates of high-stem wheat and low-stem wheat may be different. Whether there is water stress, temperature changes, or the length of daylight can all potentially affect the accumulation of the dry and fresh weights of winter wheat. Here, we aim to use unmanned aerial vehicle (UAV) remote sensing and machine learning to predict the dry and fresh weights of winter wheat with relatively high accuracy in complex situations, solely based on the canopy spectral information. The method of using UAV remote sensing to study winter wheat may thus have the value and significance of being promoted.

The changes in dry and fresh weights of winter wheat at different growth stages directly reflect the dynamic evolution law of the water content of the plants. The water content can be calculated through the following **Eq.11**:

$$\text{Water Content (\%)} = (1-(\text{Dry weight}) / (\text{Fresh weight})) \times 100\% \qquad \text{(Eq.11)}$$

As can be seen from **Figure 40**, the water content of winter wheat plants decreases from the jointing stage to the grain filling stage. Among them, the decrease is the slowest from the jointing stage to the booting stage, and the fastest from the booting stage to the heading and flowering stage. However, there are points beyond the scope

of the box plot in each stage, both above and below. This indicates that for each stage, the water content of some winter wheat plants varies significantly compared to the majority. This might be related to the winter wheat variety, or to differences in irrigation or fertilization. It could be caused by nutritional reasons, resulting in part of winter wheat plants entering the next growth stage either too early or too late.

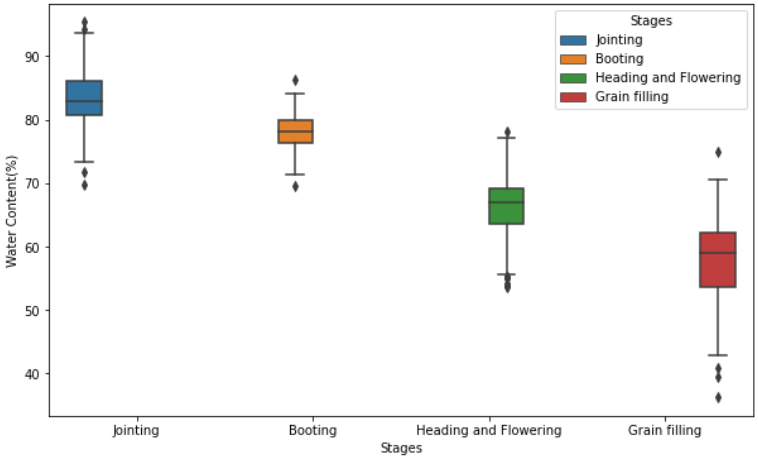

Figure 40. Water content during different stages.

3.2 Combined prediction of dry and fresh weight

In this study, we implemented a comparative analysis of three machine learning frameworks, including deep learning method, for the joint prediction of dry and fresh biomass weight in winter wheat. The predictive models were trained under three distinct input configurations. The first utilized spectral features of the winter wheat canopy, including both multispectral and thermal infrared features. The second input removed the thermal infrared features (CWSI). While the third incorporated the winter wheat growth stages on the basis of the previous inputs.

In order to compare with the joint prediction approach, this chapter also adopted individual random forest models to predict the dry weight and fresh weight of winter wheat separately.

3.2.1 Both multispectral and thermal infrared features as input

The comprehensive evaluation results using multispectral and thermal infrared features of winter wheat canopy as input—including model performance metrics (R^2, RMSE, MAE) and computational efficiency indicators (training time, prediction time)—are systematically presented in **Table 18**.

Table 18. The comprehensive evaluation results using multispectral and thermal infrared features of winter wheat canopy as input.

Model	Target	R^2	RMSE (g)	MAE (g)	Train_Time (s)		Pred_Time (s)	
Single_RF	Dry weight	0.9324	1.9042	1.3766	0.6227	1.2022	0.0148	0.0277
	Fresh weight	0.9072	6.2925	4.5555	0.5795		0.0129	
Multi_RF	Dry weight	0.9324	1.9042	1.3766	1.1726		0.0195	
	Fresh weight	0.9072	6.2925	4.5555				
Multi_LightGBM	Dry weight	0.9227	2.0374	1.4895	0.5452		0.0000	
	Fresh weight	0.8941	6.7344	4.8674				
Multi_DNN	Dry weight	0.8861	2.4679	1.8404	10.4896		1.2555	
	Fresh weight	0.8648	7.5491	5.7974				

Based on the results, it could be seen that random forest models (both single and multi-output) demonstrated the highest predictive accuracy for both dry and fresh weight estimation, achieving identical R^2 values of 0.9324 and 0.9072 respectively. The multi-output RF showed moderately decreased training time (1.17s vs 1.20s) and prediction time (0.02 vs 0.03).

Multi-output Light GBM presented a balanced performance with competitive accuracy (R^2: 0.9227 dry, 0.8941 fresh) and significantly faster training time (0.55s) compared to other models, while achieving near-instantaneous prediction speed.

Multi-output DNN exhibited the lowest accuracy metrics among the compared models (R^2: 0.8861 dry, 0.8648 fresh) while requiring substantially longer training time (10.49s) and higher prediction time (1.26s).

The multi-output models demonstrate remarkable computational efficiency while maintaining nearly identical predictive accuracy compared to their single-output counterparts. The efficiency gains primarily stem from three key mechanisms: shared feature computation that eliminates redundant preprocessing and transformation operations; optimized batch processing that enables simultaneous loss calculation for both targets with unified gradient updates; and enhanced memory access efficiency that reduces parameter redundancy and improves data batch processing.

Notably, the multi-output RF achieved identical R^2 values of 0.9324 (dry weight) and 0.9072 (fresh weight) while reducing training time by approximately 20% and prediction time by 33% compared to running separate single-output models. This efficiency improvement is particularly valuable for practical applications where both computational resources and prediction accuracy are critical considerations. The architectural optimizations allow the multi-output models to leverage shared representations and computational pathways, effectively maintaining prediction performance while significantly reducing the overall computational burden and time requirements.

3.2.2 Only multispectral features as input

The evaluation results using solely the multispectral features of the winter wheat canopy as input—including model performance metrics (R^2, RMSE, and MAE)—are systematically presented in **Table 19**.

Table 19. The comprehensive evaluation results using multispectral features.

Model	Target	R^2	RMSE (g)	MAE (g)
Single_RF	Dry weight	0.9310	1.9234	1.3820
	Fresh weight	0.9035	6.4137	4.5703
Multi_RF	Dry weight	0.9310	1.9234	1.3820
	Fresh weight	0.9035	6.4137	4.5703
Multi_Light GBM	Dry weight	0.9210	2.0591	1.4928
	Fresh weight	0.8866	6.9549	4.9467
Multi_DNN	Dry weight	0.8727	2.5983	1.9316
	Fresh weight	0.8517	7.9232	6.1141

The exclusion of the CWSI feature demonstrated a differential impact across prediction targets and algorithms. The performance reduction was more pronounced for fresh weight prediction compared to dry weight, indicating that CWSI contains particularly valuable information for moisture-related biomass estimation.

Especially, the negative impact of CWSI removal was most significant for the DNN model, which exhibited the largest performance degradation among all algorithms. This suggests that DNN architectures are better able to leverage the subtle patterns in thermal infrared data captured by CWSI, making them more susceptible to performance loss when this feature is excluded.

The multi-output RF and Light GBM models showed more robust performance despite CWSI removal, maintaining relatively stable prediction accuracy across both target variables.

In Conclusion, CWSI provides particularly valuable information for fresh weight prediction, and its contribution is most critical for deep learning approaches, while tree-based models demonstrate greater robustness to its exclusion, as shown in **Figure 41.**

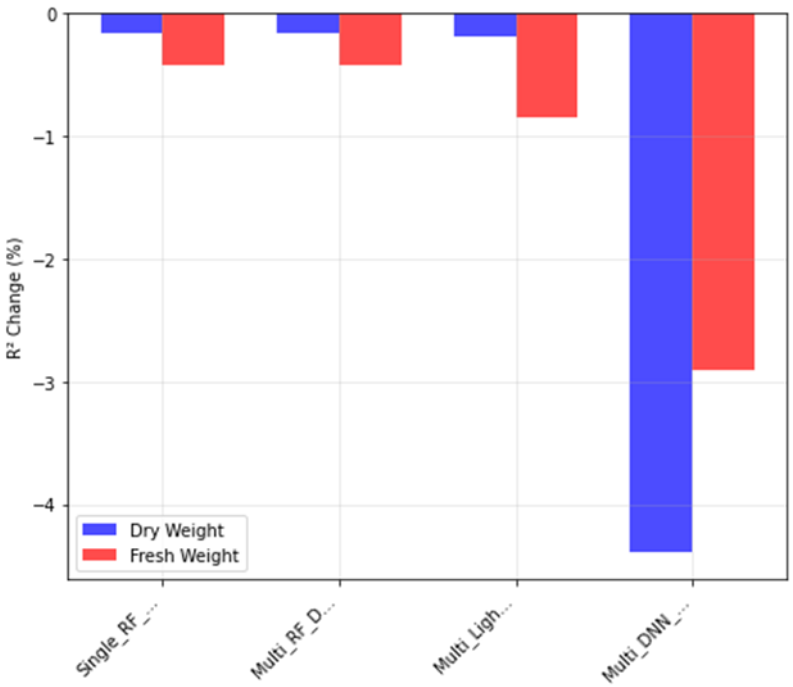

Figure 41. The effect of removing the CWSI on DW and FW prediction.

3.2.3 The canopy spectral features and phenology of the winter wheat as input

The evaluation results using the spectral features (multispectral and themal features) and growth stages of the winter wheat canopy as input—including model performance metrics (R^2, RMSE, and MAE)—are systematically presented in **Table 20**.

Table 20. The comprehensive evaluation results using spectral features and phenology.

Model	Target	R^2	RMSE (g)	MAE (g)
Single_RF	Dry weight	0.9397	1.8004	1.3070
	Fresh weight	0.9176	5.9288	4.3413
Multi_RF	Dry weight	0.9397	1.8004	1.3070
	Fresh weight	0.9176	5.9288	4.3413
Multi_Light GBM	Dry weight	0.9364	1.8504	1.3426
	Fresh weight	0.9092	6.2281	4.5315
Multi_DNN	Dry weight	0.9029	2.2791	1.6976
	Fresh weight	0.8915	6.8135	5.2549

Based on the comprehensive analysis incorporating multispectral features, thermal infrared data, and winter wheat growing stages, the evaluation reveals significant insights into winter wheat biomass prediction.

The inclusion of phenological features demonstrates a clear enhancement in predictive performance across all models compared to previous results using only spectral and thermal infrared features. Multi-output RF maintains its superior performance with identical R^2 values of 0.9397 for dry weight and 0.9176 for fresh weight prediction, showing perfect consistency between single and multi-task configurations. These results represent an improvement over previous models without phenological features, where R^2 values were approximately 0.9310 for dry weight and 0.9035 for fresh weight.

Multi-output Light GBM shows particularly notable improvement with phenological incorporation, achieving R^2 values of 0.9364 for dry weight and 0.9092 for fresh weight - representing approximately 1.5% and 2.5% improvement respectively over previous results without phenological features. This performance places Light GBM much closer to Random Forest in predictive accuracy while maintaining its computational efficiency advantages.

The DNN model benefits most significantly from phenological information, with dry weight R^2 improving from approximately 0.8727 to 0.9029 (3.4% improvement) and fresh weight from 0.8517 to 0.8915 (4.7% improvement). This substantial enhancement suggests that DNN architectures are particularly effective at leveraging the temporal patterns encoded in phenological features.

The comprehensive analysis confirms that phenological features provide valuable temporal context that complements spectral and thermal information, particularly for capturing growth-stage-specific patterns in biomass accumulation. The consistent improvement across all algorithms, especially for fresh weight prediction, indicates that phenological stages contain critical information about plant water content and vegetative development patterns.

The specific improvements and performance differences are detailed in **Figure 42**. The incorporation of phenological features resulted in an approximately 2-5% improvement in R^2 across various model architectures. Notably, fresh weight prediction demonstrated greater benefits from phenological information compared to dry weight estimation. Among all models, DNN exhibited the most substantial relative improvement following the integration of phenological features. The multi-task learning framework maintained its computational efficiency advantages while

simultaneously achieving enhanced predictive accuracy. The optimal feature configuration combines spectral, thermal infrared, and phenological features for comprehensive biomass assessment.

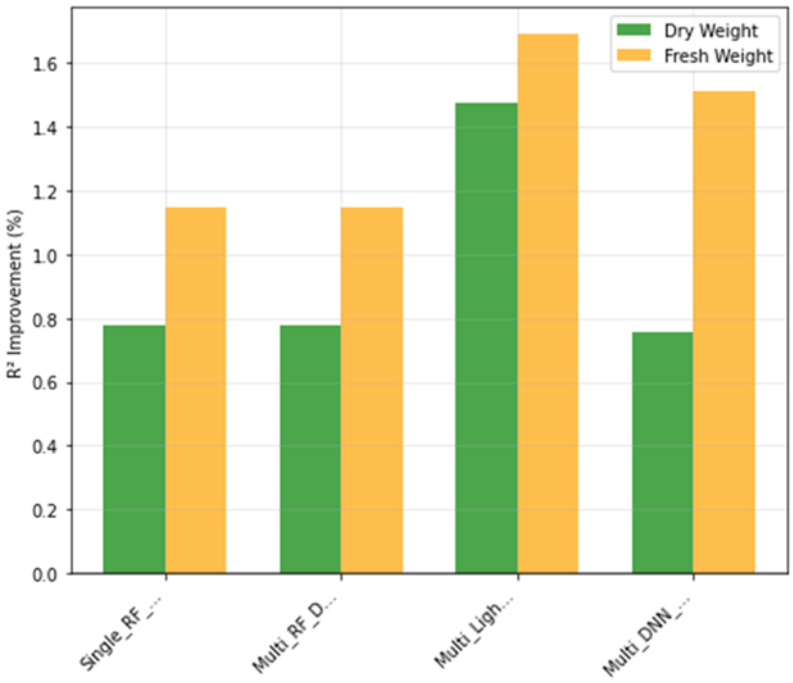

Figure 42. The effect of phenology addition on DW and FW prediction.

3.3 The relationship between biomass and yield

The yield formation of winter wheat is the dynamic outcome of biomass accumulation during various growth and development stages, water regulation, and the distribution of photosynthetic products. **Figure 43** shows the relationship between dry weight, fresh weight, water content and yield during the four growth stages of winter wheat. As can be seen from the figure, the Pearson's correlation between the water content and fresh weight of winter wheat plants and yield is the strongest during the grain filling period, followed by the jointing period. This is consistent with the empirical understanding that the grain filling period is the stage with the highest water utilization efficiency for winter wheat, and water shortage leads to a decrease in grain weight; while the jointing period is the critical water requirement period for winter wheat, and water shortage results in shorter internodes.

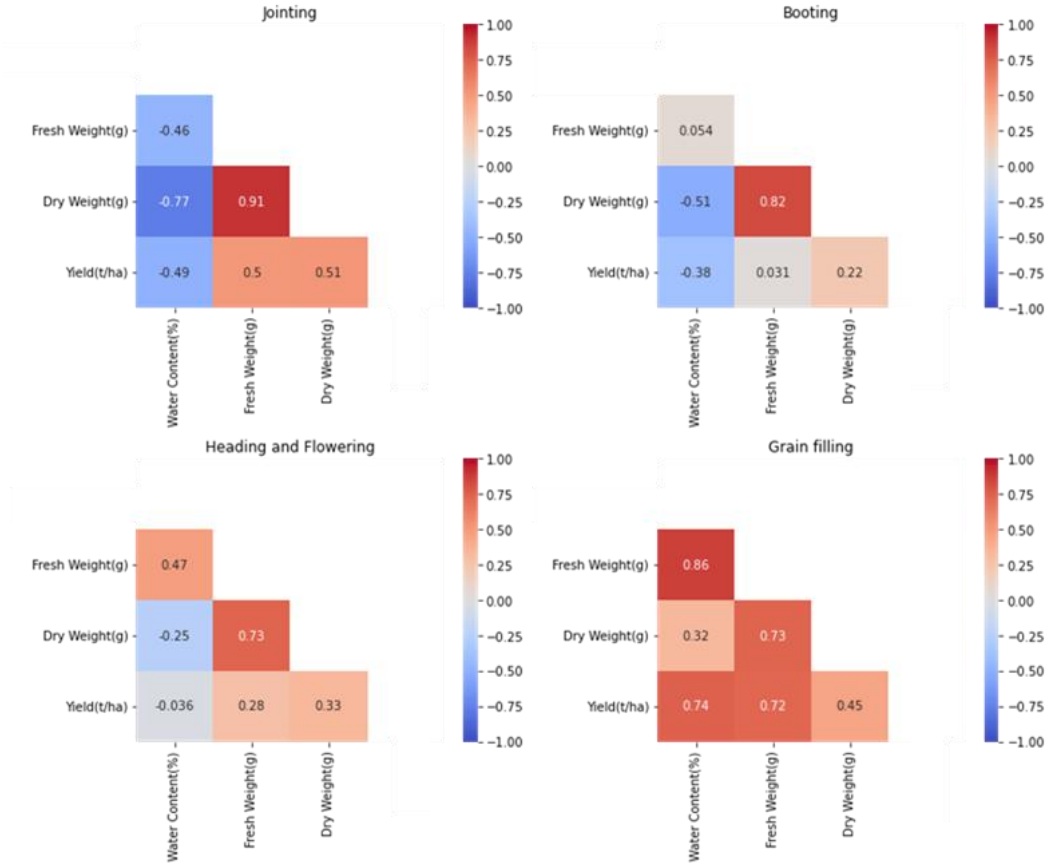

Figure 43. The relationship between dry/fresh weight and yield during different stages.

Figure 44 further details the grain filling stage relationships. When fresh weight < 80 g/6 plants, yield increases linearly with biomass accumulation, When fresh weight ⩾ 80 g/6 plants, yield plateaus due to source-sink balance limits (photosynthate transport capacity saturated).

When the water content of winter wheat plant is below 66%, yield rises with hydration (optimal turgor pressure for nutrient transport). But when water content is above 66%, there won't be further gain (excessive water dilutes assimilates or promotes disease).

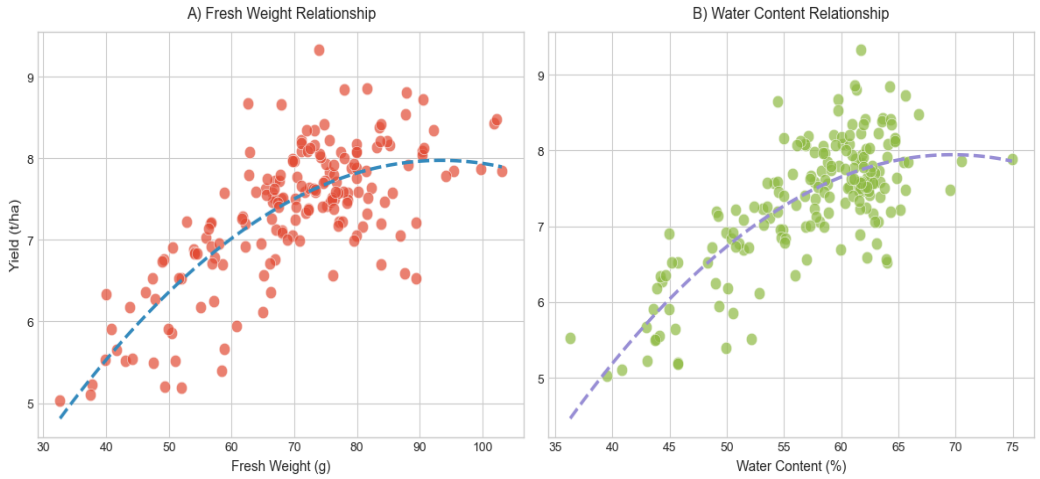

Figure 44. Relationships between biomass and yield in grain filling stage.

4. Discussion

This study reveals the important potential of the multi-output machine learning based on UAV remote sensing for the accurate and efficient prediction of winter wheat biomass (dry and fresh weight). Our results illuminate several key aspects of this approach.

4.1 The advantage of multi-task learning for biomass prediction

The most important advantage of multi-output machine learning (including deep learning) observed in this study is enhanced computational efficiency without decreasing predictive accuracy. The multi-output random forest method got identical R^2 values (0.9324 for dry weight, 0.9072 for fresh weight) to the separate single-output model, while reducing training time by about 20% and prediction time by nearly 33%. This efficiency stems from shared feature computation, which results in reducing parameter redundancy. Since dry and fresh weight are intrinsically linked physiological traits as shown in **Figure 37**, multi-output machine learning methods allow the models to learn their shared underlying patterns from the canopy spectral features simultaneously. This makes multi-output machine learning frameworks particularly valuable for practical agricultural applications, because it requires rapid, concurrent estimation of multiple biomass parameters.

4.2 The role of phenology in improving prediction accuracy

The incorporation of phenological (winter wheat growth stages) information consistently improved the prediction accuracy of both dry and fresh weight in all models. For instance, multi-DNN's R^2 for fresh weight increased from 0.8517 to 0.8915 (4.7% improvement) with the addition of phenology. This improvement is because biomass accumulation and water content are stage-specific, which governed by the physiological processes. For example, from jointing to booting, the fresh weight accumulation rapidly and during heading and flowering, the dry matter transfer to the spike rapidly, these all create distinct spectral and biophysical patterns. By providing this temporal context, phenology allows the models to better interpret the canopy spectral signals, leading to more accurate and generalized predictions that explain the dynamic evolution of the crop.

4.3 The contribution of thermal features to fresh weight estimation

Thermal features, specifically the crop water stress index (CWSI), played a particularly role for winter wheat fresh weight estimation. The removal of CWSI led to a more obvious decrease for fresh weight prediction accurate compared to dry weight. This is physiologically logical, because plant water content influence fresh weight directly. CWSI, as an indicator of plant water stress and canopy temperature, directly correlates with the plant's water content. The results that multi_DNN was most affected by its removal suggests that DNNs are particularly skilled in leveraging the subtle patterns in thermal information, while tree-based models like multi_RF and multi_Light GBM showed greater robustness, possibly due to their ability to compensate with other multispectral information.

4.4 Main sources of error in the models

Although the high accuracy achieved, several potential sources of error exist. First, perhaps due to factors, like genetic differences (variety), micro-variations in soil properties, or uneven irrigation and fertilization, were not fully captured by the model, resulting in the presence of outliers in water content (**Figure 40**), which indicates significant variability among individual plants. Second, while phenology was included, the models may not fully explain the complex interactions between environmental stressors (e.g., fleeting water or heat stress) and spectral responses at a fine temporal scale. Finally, the plateau in yield at high biomass levels (**Figure 43/44**) suggests that the relationship between biomass and final yield is not linear, indicating the complexity is much higher than that pure biomass prediction models can address.

4.5 Adaptability of the framework to other crops

The proposed framework is highly adaptable to other crops. The core methodology, which utilizes UAV-based multispectral and thermal sensors for canopy data collection and leverages machine learning (specifically multi-task learning) for prediction, is crop agnostic. The key to successful adaptation would lie in retraining the models with crop specific data that contains the target crop's unique phenological stages, structure characteristics, and the specific relationships between its canopy spectral feature, biomass accumulation, and water content. For instance, the critical growth stages and the importance of certain spectral indices would differ for rice or corn, but the underlying computational framework remains valid and promising.

5. Conclusions

This study successfully developed and validated a robust framework for predicting winter wheat dry and fresh biomass using UAV remote sensing and multi-task machine learning. It can be seen that multi-task learning emerged as the superior paradigm for simultaneous dry weight and fresh weight prediction. Compared to single-output modeling, this framework significantly enhanced computational efficiency without compromising predictive accuracy.

The combination of multispectral data, thermal infrared imagery (CWSI), and phenological information, yielded the most accurate and robust biomass predictions. This multi-source fusion enabled the model to capture complex interactions among photosynthesis, water status, and stage-specific physiological processes.

Different types models' performance differed across algorithms. Tree-based ensembles, especially random forest, demonstrated superior overall performance and robustness. Light GBM provided an optimal trade-off between speed and accuracy, whereas deep neural networks, though initially less accurate, exhibited the most substantial improvement when enhanced with additional features such as thermal and phenological information.

Quantifiable relationships were identified among biomass, water content, and yield. Strong correlations were confirmed—especially during jointing and grain-filling stages—and a nonlinear threshold effect was observed: beyond certain values of biomass or moisture, yield plateaued, underscoring the importance of source–sink balance and optimal water conditions.

The framework proved highly transferable. The methodology is not limited to winter wheat, it might be adapted to analyze other crops in the future, like corn and rice, as an efficient, reliable, and non-destructive tool, supporting high-throughput phenotyping and precision agriculture.

VIII

General conclusions and discussions

1. Synthesis of key findings and reconciliation with research objectives

This study has successfully addressed the three interconnected research objectives outlined in Chapter I by systematically applying advanced computational methods to interpret the spectral characteristics of the winter wheat canopy. The findings, presented across the empirical chapters, reflect a hierarchical and comprehensive understanding of yield formation—progressing from establishing direct spectral-yield correlations to decoding the underlying physiological traits that affect the final agronomic outcome.

The first objective focused on developing a dynamic yield prediction framework. This was conclusively met through the LSTM-RF hybrid model introduced in Chapter IV, which effectively captured the temporal dynamics of yield formation. The key finding was that integrating information across multiple growth stages is fundamentally more powerful than using single-stage snapshots. This was evidenced by the hierarchical features extracted by the LSTM, where the correlation with yield strengthened progressively—from r=0.49 for a feature based solely on the heading stage to r=0.78 for the advanced feature that synthesized information from heading, flowering, and grain-filling stages. This demonstrates the critical importance of capturing growth dynamics for reliable yield forecasting.

The second objective sought to overcome the practical constraint of limited labeled data by creating a data-efficient framework. The self-training RF model developed in Chapter V provided an effective solution to this "ground-truth bottleneck." A pivotal finding was the importance of an adaptive threshold (δ) strategy for selecting high-confidence pseudo-labels, which balanced quantity and accuracy to expand the training set with 84 reliable data points. This semi-supervised approach demonstrated remarkable efficiency, maintaining a competitive prediction performance (validation R^2=0.81, RMSE=692.96 kg/ha, MAE=550.62 kg/ha) while utilizing only 40% of the original manually labeled data, thereby offering a scalable and cost-effective solution for practical applications.

The final objective was to "open the black box" of yield prediction by precisely estimating key physiological parameters. This mechanistic understanding was delivered in Chapters VI and VII. In Chapter VI, a robust link was established between spectral data and plant nitrogen content (PNC). A central finding was the superior performance of models using high-dimensional composite features over conventional

vegetation indices (VIs), with AdaBoost achieving a testing R^2 of 0.84 (RMSE=2.55 mg/g) for PNC at the jointing stage. This highlights the value of capturing complex, non-linear spectral interactions. Furthermore, the analysis revealed critical, stage-specific nitrogen thresholds (~25 mg/g at early jointing and ~15 mg/g at booting), providing actionable insights for precision nitrogen management. In Chapter VII, the multi-task learning framework demonstrated high efficiency for simultaneous biomass prediction. The Multi-output random forest model achieved high accuracy for dry and fresh weight (R^2=0.9397 and 0.9176, respectively) while reducing computational time by 33% compared to separate single-output models. This chapter also quantified the relationship between biomass and yield, identifying plateau thresholds (e.g., yield stabilization at a fresh weight of ~80 g/6 plants and plant water content of ~66% during grain filling) that underscore the importance of source-sink balance.

In conclusion, this research has logically progressed from predicting what the yield will be, to solving the practical problem of data scarcity, and finally to explaining why through the lens of fundamental plant physiology. The findings collectively establish a robust, efficient, and interpretable framework for agricultural remote sensing that bridges the gap between complex data and actionable agronomic insights.

2. Implications for precision agriculture

This research introduced significant methodological innovations that enhance the efficiency and interpretability of crop monitoring. By strategically integrating multispectral and thermal data, we demonstrated that a carefully processed multi-sensor fusion can capture critical physiological information necessary for robust phenotypic prediction. While hyperspectral imaging undoubtedly offers higher spectral resolution and may achieve marginally superior accuracy in some specific applications (e.g., Jinkang et al., 2022 reported hyperspectral data yielding more accurate results with mean relative error = 5.46% than multispectral data = 7.71% for tiller density estimation), our approach focuses on extracting maximum value from more accessible and operationally simpler sensor suites. The performance gap for key agronomic parameters like yield and nitrogen content is often minimal when using optimized feature engineering with multispectral and thermal data, as evidenced by our high R^2 values (0.78-0.93), making it a highly cost-effective and practical alternative for widespread deployment, particularly in resource-constrained

agricultural systems (Juncheng et al., 2023b demonstrated the potential of low-cost UAV RGB imagery for field-scale yield prediction).

From a computational perspective, the multi-task learning framework effectively addressed operational limitations for real-time applications by improving computational efficiency by 20% to 33% while maintaining prediction accuracy. Moreover, the LSTM-based temporal feature extraction provides a novel method to capture the complex interrelationships between growth stages, advancing beyond the static analysis offered by traditional vegetation indices.

In terms of practical application, this research offers actionable strategies for field management. The identified biomass and hydration thresholds, such as a fresh weight of ≥80 grams per six plants and a plant water content of ≤66% during grain filling, provide clear, data-driven triggers for precision irrigation, enabling more efficient utilization of water resources. For nutrient management, models utilizing polynomial-expanded spectral features demonstrated the capability to accurately monitor nitrogen content as early as the booting stage (R^2=0.76, RMSE=2.21 mg/g), thereby supporting timely variable-rate fertilization decisions. Furthermore, the validated semi-supervised learning methods significantly reduced the dependency on large, expensively acquired labeled datasets, enhancing the potential for scalable and practical implementation across diverse agricultural systems.

3. Limitations and generalizability

While the models developed in this study demonstrated high predictive accuracy under our experimental conditions, their spatiotemporal generalizability must be rigorously evaluated against known challenges in the domain. A primary consideration is geographical transferability. Our models, calibrated in the semi-arid region of northern China, may exhibit spectral bias when applied to regions with distinct climatic and atmospheric conditions, such as humid or tropical zones. This aligns with the methodology of Yang et al. (2023) who utilized multi-temporal and multi-feature vegetation indices across different environments. Our field experiments were indeed limited by the size of the site, which is inevitable in controlled studies. However, the core contribution of this research is not to provide a directly replicable "experimental template", but to construct and validate an expandable technical framework. This framework addresses the issue of insufficient data through semi-supervised learning, captures key physiological processes through multi-sensor fusion, and understands the growth patterns of crops through time-series modeling. These methods are universal. To apply it to a larger scale, the key next step is to conduct limited and precise calibrations in the target area, based on this framework, to quickly

build localized models instead of repeating all the detailed experiments. Therefore, the scalability of this research lies in the efficiency and adaptability of its methods.

Furthermore, while our study incorporated multi-year data, the interannual variability captured may not fully represent the long-term impacts of climate change and increasing frequency of extreme weather events. Many agricultural remote sensing studies, including our own, face the constraint of limited temporal depth (Zongpeng et al., 2023b incorporated multiple growth stages but acknowledged temporal limitations). Extending validation over a longer timeline is crucial to assess model robustness against these evolving environmental pressures.

Regarding cultivar specificity, our framework must be tested across a broader range of wheat varieties, particularly those with divergent canopy architectures and phenological traits (e.g., erectophile vs. planophile leaves). While previous research has highlighted the sensitivity of vegetation indices to canopy structure (Xiaofeng et al., 2021 explored spectral indices for different phenotypic traits), our study, like others that leverage a diverse but specific set of varieties, has not fully decoupled this effect. Future research should explicitly investigate the model's performance across genetically distinct pools to ensure broad applicability.

On a technical level, several limitations common to optical remote sensing approaches persist. Similar to the findings of Jingjing et al. (2024) in water stress diagnosis, our canopy-centric methodology has inherent limitations in detecting sub-surface stresses, such as root diseases or early-stage water deficits deep in the soil profile. Moreover, while we processed data to minimize noise, model performance remains susceptible to environmental variables like atmospheric conditions, sensor view angles, and soil background effects—a well-documented challenge in the field that we, like many others (e.g., Fan et al., 2022 in multi-source data fusion), have not fully resolved.

Finally, while we emphasized the cost-effectiveness of our multi-sensor fusion compared to hyperspectral imaging, a more explicit quantification of the investment required for hardware (UAVs, multispectral/thermal sensors) and computational resources is needed. This is particularly critical for assessing scalability in smallholder systems, where the cost-benefit analysis must be considered, a point underscored by the practical implementation challenges noted in Juncheng et al. (2023b) regarding field-scale applications.

4. Future research directions

Based on our research findings and the limitations discussed in the previous section, we propose several strategic directions for future research. These recommendations are positioned within the current state of the art in agricultural remote sensing and aim to address both persistent challenges and emerging opportunities.

4.1 Advancing methodological sophistication

Future work should focus on developing models with a stronger physiological basis and greater general applicability. By combining real-time weather data from local weather stations with climate models, it is possible to dynamically place remote sensing signals in specific contexts, going beyond the static segments of this study, to improve dynamic predictions of stress events such as drought or frost. Additionally, to directly address the issue of spatial universality limitations, developing robust transfer learning and domain adaptation frameworks is a key step in the next steps, which will be based on the initial progress in this field (Yang et al., 2023; Zong Peng et al., 2023b). A key part of this methodological advancement is to systematically compare our LSTM-RF framework with transformer for time series and CNN for hyperspectral data. Benchmarking our LSTM-RF framework against these, will help clarify the trade-off between model complexity and performance, thereby ensuring the selection of the most powerful tool for specific agricultural tasks. Finally, in addition to relying solely on remote sensing data, fusing these multimodal data streams - which is a recognized approach to building a more comprehensive digital agriculture system (Zhu Chencheng et al., 2023a; Fan et al., 2022) - is crucial for comprehensively understanding the factors influencing crop growth performance.

4.2 Bridging to practical application and edge computing

Converting predictions into timely intervention measures requires attention to technology deployment and the establishment of trust. A clear trend is the shift towards edge computing to achieve real-time analysis (Zhu Chencheng et al., 2023b), which should be utilized to facilitate immediate on-site decisions. This ultimate manifestation is the development of closed-loop systems, in which artificial intelligence models will automatically generate prescription maps for automatic variable-rate fertilization, thus seamlessly connecting the prediction model with the application equipment, as envisioned in earlier studies on automatic decision support systems (Jie et al., 2023b). At the same time, to overcome the "black box" impression and cultivate farmers' trust, promoting explainable artificial intelligence is crucial. We must go beyond the importance of global feature significance and adopt technologies

that can provide intuitive and causal explanations for specific recommendations, directly addressing the challenge of creating truly farmer-centered applications (Song Lin et al., 2023).

4.3 Ecosystem-Driven Scalability and Adoption

To make these technologies have a wide-ranging impact, they must be verified and adjusted outside of the experimental environment. The next crucial step is to test the transferability of our framework on other major grains (such as corn and rice), which is considered a necessary step for evaluating the universality of the phenotypic prediction model (Juanjuan et al., 2022; Jinkang et al., 2022). To establish a connection between the technology and end-users, future development must be designed with farmers at the center, which may lead to the emergence of mobile applications that provide guiding alerts in an intuitive format, as demonstrated in actual diagnostic studies (Jingjing et al., 2024). Finally, to overcome the problem of data scarcity and ensure the continuous improvement of the model, establishing a collaborative data ecosystem is a promising approach. This can be achieved through a platform that collects labeled data from farmers via mobile applications, thus forming a virtuous cycle consistent with a more open and inclusive vision of digital agriculture, as discussed in the context of the scalable monitoring framework (Zongpeng et al., 2022).

4.4 Ethical and environmental considerations

Integrating unmanned aerial vehicles (UAVs) and artificial intelligence (AI) technologies into the agricultural sector holds great potential, but it also requires rigorous ethical and environmental reviews beyond technical performance. This study highlights several key considerations that should guide the responsible application of these tools.

High-resolution UAV images raise important issues regarding data sovereignty and privacy. The detailed spectral and spatial information collected from farmland represents valuable intellectual property, thus requiring a clear governance framework to protect farmers' rights and prevent the misuse of their data.

From an environmental perspective, although UAV-based systems can improve resource utilization efficiency, their comprehensive ecological impact must be acknowledged. This includes greenhouse gas emissions and energy consumption generated by the manufacturing, operation, and handling of UAV fleets and computing infrastructure. Conducting a comprehensive life cycle assessment is

crucial for quantifying whether the net sustainability benefits (such as reduced water and fertilizer use) outweigh the technological footprint.

Social economic equity is another key issue. The significant initial investment in hardware and technical expertise may exacerbate existing disparities, creating a "digital divide" that could marginalize small-scale farmers. Therefore, promotion strategies should prioritize inclusive models - such as cooperative ownership or service-based platforms - to ensure widespread equitable access.

Furthermore, excessive reliance on algorithmic recommendations may lead to the loss of traditional farmers' knowledge. It is important to position digital technology as a tool for assisting decision-making, rather than replacing farmers' expertise and intuition.

Addressing these multifaceted challenges requires interdisciplinary collaboration, covering technology, ethics, policy, and the agricultural sector, to ensure the development of digital agriculture is morally grounded and socially responsible.

IX

References

Adedeji, O., Sun, Y., Li, S., Guo, W., 2025. Effects of Spatial Resolution on Assessing Cotton Water Stress Using Unmanned Aerial System Imagery. *Remote Sens.,* 2025, 17, 4018. DOI:10.3390/rs17244018.

Alessandro, M., Joby, M., Prince, C., Sathishkumar S., Robert M., 2024. Are unmanned aerial vehicle-based hyperspectral imaging and machine learning advancing crop science? *Trends in Plant Science*, February 2024, Vol. 29, No. 2. DOI: 10.1016/j.tplants.2023.09.001.

Alexis, P., Melissa, W., Chang L. and Yang C., 2022. Evaluation of Random Forests (RF) for Regional and Local-Scale Wheat Yield Prediction in Southeast Australia. *Sensors,* 2022, 22, 717. DOI:10.3390/s22030717.

Alirezazadeh, P., Schirrmann, M., Stolzenburg, F., 2024. A comparative analysis of deep learning methods for weed classification of high-resolution UAV images. *Plant Dis Prot,* 131, 227–236. DOI:10.1007/s41348-023-00814-9.

Anatoly, A.G., Andre´s, V., Vero´nica, C., Donald, C. R., Timothy, J. A., 2005. Remote estimation of canopy chlorophyll content in crops. *Geophysical Research Letters, OL.,* 32, L08403, 1448. DOI:10.1029/2005GL022688.

Anna, C., Salah, S., Brett, W., 2018. Machine learning approaches for crop yield prediction and nitrogen status estimation in precision agriculture: A review. *Computers and Electronics in Agriculture,* 151 (2018) 61–69. DOI:10.1016/j.compag.2018.05.012.

Atzberger, C., 2013. Advances in remote sensing of agriculture: Context description, existing operational monitoring systems and major information needs. *Remote Sensing,* 5(2), 949-981. DOI:10.3390/rs5020949.

Baoyuan, Z., Wenbiao, W., Jingping, Z., Menglei, D., Qian, S., Xuguang, S., Zhen, C., Xiaohe, G., 2024. A spectral index for estimating grain filling rate of winter wheat using UAV-based hyperspectral images, *Computers and Electronics in Agriculture,* Volume 223, 2024, 109059, ISSN 0168-1699, DOI:10.1016.2024.109059.

Bei, Z., Yingwen, C., Hao, L., Yuxiao, W., Sumeng, Y., Ning, Y., Xuqian, B., Jialiang, H., Pingliang, X., Zhitao, Z., Junying, C., 2024. Monitoring soil moisture content in the root zone of winter wheat with multi-angle multispectral imagery, *International Journal of Remote Sensing,* 45:14, 4692-4709, DOI:10.1080/01431161.2024.2367173.

Beltrame, L., Salzinger, J., Koppensteiner, L.J., Fanta-Jende, P., 2024. TriNet: Exploring More Affordable and Generalisable Remote Phenotyping with Explainable Deep Models. *Drones,* 2024, 8, 407. DOI:10.3390/drones8080407.

Berger, K., Atzberger, C., Danner, M., D'Urso, G., Mauser, W., Vuolo, F., & Hank,

T., 2020. Evaluation of the PROSAIL Model Capabilities for Future Hyperspectral Model Environments: A Review Study. *Remote Sensing,* 12(3), 442. DOI:10.3390/rs12030442.

Bouras, E. H., Thapa, S., Olsson, P. O., Albertsson, J., Eklundh, L., 2023. Assimilation of Sentinel-2 data into a Crop Growth Model for High-resolution Crop Yield Mapping. *Global Environmental Change / Remote Sensing for Sustainable Agriculture III Oral,* id. GC44E-04.

Cao, Q., Miao, Y., Shen, J., Yu, W., Yuan, F., Cheng, S., Liu, Y., 2023. Improving in-season estimation of rice yield potential and responsiveness to topdressing nitrogen application with Crop Circle active crop canopy sensor. *Precision Agriculture,* 24(2), 755-779. DOI:10.1007/s11119-022-09973-5.

Carolina, S. P., Jose´, L. C., David, B., Kazuko Y.S., and Matthew P. R., 2012. Phenotyping transgenic wheat for drought resistance. *Journal of Experimental Botany,* Vol. 63, No. 5, pp. 1799–1808, 2012. DOI:10.1093/jxb/err385.

Caruana, R., 1997. *Multitask learning. Machine Learning,* 28(1), 41–75. DOI:10.1023/A:1007379606734.

Caturegli, L., Corniglia, M., Gaetani, M., Grossi, N., Magni, S., Migliazzi, M., Volterrani, M., 2020. Unmanned aerial vehicle to estimate nitrogen status of turfgrasses. *PLoS ONE,* 15(2), e0228268. DOI:10.1371/journal.pone.0228268.

Changsai, Z., Yuan, Y., Lijuan, W., Xuewei, Z., Shuo, C., Zaixing, S., Shuxia, Z., Yong, X., 2024. Estimation of the Bio-Parameters ofWinter Wheat by Combining Feature Selection with Machine Learning Using Multi-Temporal Unmanned Aerial Vehicle Multispectral Images. *Remote Sens.,* 2024, 16, 469. DOI:10.3390/rs16030469.

Chaofa, B., Hongtao, S., Suqin, W., Kefei, Z., Meng, W., Yindi, Z., Yaqin, S., Huifu, Z., Xuewei, Z. and Shuo, C., 2022. Prediction of Field-Scale Wheat Yield Using Machine Learning Method and Multi-Spectral UAV Data. *Remote Sens.,* 2022, 14, 1474. DOI:10.3390/rs14061474.

Cheng, Z., Gu, X., Du, Y. et al., 2024. Multi-modal fusion and multi-task deep learning for monitoring the growth of film-mulched winter wheat. *Precision Agric,* 25, 1933–1957 (2024). DOI:10.1007/s11119-024-10147-8.

Chengxin, J., Chen, C., Rui, L., Yuanyuan, Z., Xiaochun, Z., Ruilin, S., Tao, L., Chengming, S., 2023. Remote sensing monitoring of wheat leaf rust based on UAV multispectral imagery and the BPNN method. *Food Energy Secur.,* 2023; 12: e477.DOI:10.1002/fes3.477.

Chinese Academy of Sciences. 2021. National Report on Soil Health and Fertilizer Utilization. *Beijing: CAS Press.*

Chiu, M.S., Wang, J., Evaluation of Machine Learning Regression Techniques for Estimating Winter Wheat Biomass Using Biophysical, Biochemical, and UAV Multispectral Data. *Drones,* 2024, 8, 287. DOI:10.3390/ drones8070287.

Dong, P.;Wang, M., Li, K., Qiao, H., Zhao, Y., Bacao, F., Shi, L., Guo,W., Si, H., 2024. Research on the Identification of Wheat Fusarium Head Blight Based on

Multispectral. Remote Sensing from UAVs. *Drones,* 2024, 8, 445. DOI:10.3390/drones8090445.

Dongho, L., Hyeonjin, K. and Jonghwa, P., 2021. UAV, a Farm Map, and Machine Learning Technology Convergence Classification Method of a Corn Cultivation Area. *Agronomy,* 2021, 11, 1554. DOI:10.3390/agronomy11081554.

Driss, H., John, R. M., Elizabeth, P., Pablo, J. Z., Ian, B. S., 2004. Hyperspectral vegetation indices and novel algorithms for predicting green LAI of crop canopies: Modeling and validation in the context of precision agriculture. *Remote Sensing of Environment,* 90(3), 337-352. DOI:10.1016/j.rse.2003.12.013.

Fan, D., Changchun, L., Weiguang, Z., Shuaipeng, F., Qian, C. and Zhen, C., 2022. Estimation of Nitrogen Content in Winter Wheat Based on Multi-Source Data Fusion and Machine Learning. *Agriculture,* 2022, 12, 1752. DOI:10.3390/agriculture12111752.

Falv, W., Mao, Y., Longfei, M., Tong, Z., Weilong, Q., Wei, L., Yinghua, Z., Zhencai, S., Zhimin, W., Fei, L. and Kang, Y., 2022. Estimation of Above-Ground Biomass of Winter Wheat Based on Consumer-Grade Multi-Spectral UAV. *Remote Sens.,* 2022, 14, 1251. DOI:10.3390/rs14051251.

FAO., 2021. *Smallholder Farmers and Market Constraints.* Rome: UN Food and Agriculture Organization.

FAO., 2022. *Agricultural production statistics 2000–2020*. Available at: cb9180en.pdf (fao.org)

FAO., 2023. *The State of Food Security and Nutrition in the World 2023.* Rome: Food and Agriculture Organization.

Farrah, M. M., Khairudin, N., Zed, Z., Mohamad, A. T., Asniyani, N. H. A., Muhamad, F. C. H., Siti, N. M. Z., Derraz, R. and Mohd, R. I., 2021. UAV- and Random-Forest-AdaBoost (RFA)-Based Estimation of Rice Plant Traits. *Agronomy*, 2021, 11, 915. DOI:10.3390/agronomy11050915.

Fatemeh, K., Amin, T., Aria, A., Pasquale, D., Luca, D. V., Francesco, P., 2024. Performance Assessment of Machine Learning Algorithms for Yellow Rust Wheat Disease Classification with UAV RGB Images. *IEEE International Workshop on Metrology for Agriculture and Forestry (MetroAgriFor),* Padua, Italy, 2024, pp. 450-455, DOI: 10.1109/MetroAgriFor63043.2024.10948768.

Feng,W.; Lan, Y., Zhao, H., Tang, Z., Peng,W., Che, H., Zhu, J., 2024. Identification of High-Photosynthetic-Efficiency Wheat Varieties Based on Multi-Source Remote Sensing from UAVs. *Agronomy,* 2024, 14, 2389. DOI:10.3390/agronomy14102389.

Fernandez, J. E., Alcon, F., Diaz-Espejo, A., Hernandez-Santana, V., Cuevas, M. V., 2020. Water use indicators and economic analysis for on-farm irrigation decision: A case study of a super high density olive tree orchard. *Agricultural Water Management,* 176, 119-130. DOI:10.1016/j.agwat.2020.106074.

Frederik, C., Nathalie, W., Dirk, I. and Stijn, D., 2017. Unlocking the potential of plant phenotyping data through integration and data-driven approaches. *Current Opinion in Systems Biology,* 2017, 4:58–63. DOI:10.1016/j.coisb.2017.07.002.

Ge, T., Sui, F., Bai, L. Chengli T., Ningbo S., 2012. Effects of water stress on growth, biomass partitioning, and water-use efficiency in summer maize (Zea mays L.) throughout the growth cycle. *Acta Physiol Plant*, 34, 1043–1053 (2012). DOI:10.1007/s11738-011-0901-y.

Geurts, P., Ernst, D. & Wehenkel, L., 2006. Extremely randomized trees. *Mach Learn,* 63, 3–42 (2006). DOI:10.1007/s10994-006-6226-1.

Ghizlane, A., Jamal, E. D., Imane, S., Samir, B. and Ettarid, M., 2021. Mapping Wheat Dry Matter and Nitrogen Content Dynamics and Estimation of Wheat Yield Using UAV Multispectral Imagery Machine Learning and a Variety-Based Approach: Case Study of Morocco. *AgriEngineering*, 2021, 3, 29–49. DOI:10.3390/agriengineering3010003.

Gitelson, A. A., Andrés V., Timothy J. A., Donald C. R., Galina K., Bryan L., 2003. Remote estimation of leaf area index and green leaf biomass in maize canopies. *Geophysical Research Letters,* 30(5), 1248. DOI:10.1029/2002GL016450.

González-Dugo, M.P., Moran, M.S., Mateos, L., Bryant, R., 2006. Canopy temperature variability as an indicator of crop water stress severity. *Irrig Sci,* 24, 233–240. DOI:10.1007/s00271-005-0022-8 .

GOV China, 2021. The 14th *Five Year Plan for Promoting Modernization of Agriculture and Rural Areas.* Available at: https://www.gov.cn/zhengce/content/2022-02/11/content_5673082.htm.

Gowhar, M., Shruti, K., Abhijeet, A., 2022. Pankaj Kumar, Suraj Kumar Singh, Majid Farooq, Brian Alan Johnson, Akshay Rai and Netrananda Sahu. Assessing the Yield of Wheat Using Satellite Remote Sensing-Based Machine Learning Algorithms and Simulation Modeling. *Remote Sens.,* 2022, 14, 3005. DOI:10.3390/RS14133005.

Guanghui, Q., Gengxing, Z. and Xue, X., 2020. Soil Salinity Inversion of Winter Wheat Areas Based on Satellite-Unmanned Aerial Vehicle-Ground Collaborative System in Coastal of the Yellow River Delta. *Sensors,* 2020, 20(22), 6521. DOI:10.3390/s20226521.

Guo, J. H.,.Liu, X. J, Zhang, Y., Shen, J. L., Han, W. X., Zhang, W. F., Christie, P., Goulding, K. W. T., Vitousek, P. M., and Zhang, F. S., 2010. Significant Acidification in Major Chinese Croplands. *Science,* 327,1008-1010(2010). DOI:10.1126/science.1182570.

Guo, Y., Chen, S., Li, X., Cunha, M., Jayavelu, S., Cammarano, D., Fu, Y., 2021. Integrated phenology and climate in rice yields prediction using machine learning methods. *Field Crops Research,* 264, 108075. DOI:10.1016/j.ecolind.2020.106935.

Guo, Y., He, J., Zhang, H., Shi, Z., Wei, P., Jing, Y., Yang, X., Zhang, Y., Wang, L.; Zheng, G., 2024. Improvement of Winter Wheat Aboveground Biomass

Estimation Using Digital Surface Model Information Extracted from Unmanned-Aerial-Vehicle-Based Multispectral Images. *Agriculture,* 2024, 14, 378. DOI:10.3390/agriculture14030378.

Guohui, D., Liyan, S., Jie, D., Robert, J., Shuchen, Liu., Mujahid, A., Li, S., Mingxing, W., Jin, X., Greg, D., Dong, J., Xiu-e, W., and Ji, Z., 2023. The Dissection of Nitrogen Response Traits Using Drone Phenotyping and Dynamic Phenotypic Analysis to Explore N Responsiveness and Associated Genetic Loci in Wheat. *Plant Phenomics,* 22 Dec 2023, Vol 5, Article ID: 0128. DOI:10.34133/plantphenomics.0128.

Hai, H., Jianxi, H., Quanlong, F., Junming, L., Xuecao, L., Xinlei, W. and Quandi, N., 2022. Developing a Dual-Stream Deep-Learning Neural Network Model for Improving County-Level Winter Wheat Yield Estimates in China. *Remote Sens.,* 2022, 14(20), 5280. DOI:10.3390/rs14205280.

Hansen, P. M., Jørgensen, J. R., & Thomsen, A. (2002). Predicting grain yield and protein content in winter wheat and spring barley using repeated canopy reflectance measurements and partial least squares regression. *The Journal of Agricultural Science,* 139(3), 307-318. DOI:10.1017/S0021859602002320.

Hari, S. N., João, V. S., Chiter, M. P., Timothy, J. K., Dipaka, R. S., Suresh, K. K., Hanuman, S. Jat., Harminder, S. S., Parbodh, C. S., Mangi, L. J., Tek, B. S., 2022. Interpretable machine learning methods to explain on-farm yield variability of high productivity wheat in Northwest India. *Field Crops Research,* Volume 287, 2022, 108640, ISSN 0378-4290. DOI:10.1016/j.fcr.2022.108640.

Huang, F., Gao, S., Yao, X., 2020. Estimation of winter wheat leaf nitrogen concentration using machine learning algorithm and multi-color space. *Journal of Nanjing Agricultural University,* 2020, 43(2): 364-371. DOI:10.7685/jnau.201903073.

Jianjun, W., Qi, Z., Jiali, S., Chang, L., Tingxuan, Z., Junjie, D., Yunyu, X., Lingtian, Z., Weiling, W., Guisheng, Z., Changwei, T. and Zhongyang, H., 2021. UAV- and Machine Learning-Based Retrieval of Wheat SPAD Values at the Overwintering Stage for Variety Screening. *Remote Sens.,* 2021, 13(24), 5166; DOI:10.3390/rs13245166.

Jibo, Y., Guijun, Y., Changchun, L., Yang, L., Jian, W., Wei, G., Xinming, M., Qinglin, N., Hongbo, Q., Haikuan, F., 2024. Analyzing winter-wheat biochemical traits using hyperspectral remote sensing and deep learning. *Computers and Electronics in Agriculture,* Volume 222, 2024, 109026, ISSN 0168-1699. DOI:10.1016/j.compag.2024.109026.

Jie, J., Peter, M.A., Chunsheng C., Qiang C., Yongchao T., Yan Z., Xiaojun L., Weixing C., 2023a. Combining UAV and Sentinel-2 satellite multi-spectral images to diagnose crop growth and N status in winter wheat at the county scale. *Field Crops Research,* 294 (2023) 108860. DOI:10.1016/j.fcr.2023.108860.

Jie, J., Peter, M.A., Jiayi Z., Ruhua L., Youyan Z., Qiang C., Yongchao T., Yan Z., Weixing C., Xiaojun L., 2022. Combining fixed-wing UAV multispectral

imagery and machine learning to diagnose winter wheat nitrogen status at the farm scale. *European Journal of Agronomy,* 138 (2022) 126537. DOI:10.1016/j.eja.2022.126537.

Jie, J., Yanlian, W., Qing, L., Yan, L., Qiang, C., Yongchao, T., Yan, Z., Weixing, C., Xiaojun, L., 2023b. Developing an efficiency and energy-saving nitrogen management strategy for winter wheat based on the UAV multispectral imagery and machine learning algorithm. *Precision Agric.,* 24, 2019–2043 (2023). DOI:10.1007/s11119-023-10028-6.

Jin, X., Liu, S., Baret, F., Hemerlé, M., & Comar, A., 2021. Estimates of plant density using UAV RGB imagery for high-throughput phenotyping in wheat breeding. *Remote Sensing of Environment,* 2017, 198:105-114. DOI:10.1016/j.rse.2017.06.007.

Jing, Y., Shiwen, Z., Yanhai, Z., Ruixin, H. and Abubakar, S. L., 2023. Construction of aWinter Wheat Comprehensive Growth Monitoring Index Based on a Fuzzy Degree Comprehensive Evaluation Model of Multispectral UAV Data. *Sensors,* 2023; 23(19):8089. DOI:10.3390/s23198089.

Jingjing, W., Yu, L., Wentao, W., Suyi, L., Haohui, Z., Xin, H., Yunling, W., Haijun, Y., Wouter, H. M., 2024. A robust model for diagnosing water stress of winter wheat by combining UAV multispectral and thermal remote sensing. *Agricultural Water Management,* 291 (2024) 108616. DOI:10.1016/j.agwat.2023.108616.

Jingqi, Z., Huiren, T., Pengxin, W., Kevin, T., Shuyu, Z., Hongmei, L., 2022. Improving wheat yield estimates using data augmentation models and remotely sensed biophysical indices within deep neural net-works in the Guanzhong Plain, PR China. *Computers and Electronics in Agriculture,* 192 (2022) 106616. DOI:10.1016/j.compag.2021.106616.

Jinkang, H., Bing, Z., Dailiang, P., Ruyi, Y., Yao, L., Chenchao, X., Cunjun, L., Tao, D., Moren, F., Huichun, Y., Wenjiang, H., Binbin, L., Mengmeng, W., Enhui, C. and Songlin, Y., 2022. Estimation of wheat tiller density using remote sensing data and machine learning methods. *Front. Plant Sci.,* 13:1075856. DOI:10.3389/fpls.2022.1075856.

Jinya, S., Cunjia, L., Matthew, C., Xiaoping, H., Conghao, W., Xiangming, X., Qingdong, L., Lei, G., Wen-Hua, C., 2018. Wheat yellow rust monitoring by learning from multispectral UAV aerial imagery. *Computers and Electronics in Agriculture,* 155 (2018) 157–166. DOI:10.1016/j.compag.2018.10.017.

Jinya, S., Dewei, Y., Baofeng, S., Zhiwen, M., Cunjia, L., Xiaoping, H., Xiangming, X., Lei, G., and Wen-Hua, C., 2021. Fellow, IEEE. Aerial Visual Perception in Smart Farming: Field Study of Wheat Yellow Rust Monitoring. *IEEE TRANSACTIONS ON INDUSTRIAL INFORMATICS,* VOL. 17, NO. 3, MARCH 2021. DOI: 10.1109/TII.2020.2979237.

Jiˇrí, M., Vojtˇech, L., Igor, H., Vladimír, S. and Jakub, E., 2022. Comparison of Proximal and Remote Sensing for the Diagnosis of Crop Status in Site-Specific Crop Management. *Sensors,* 2022, 22(1), 19. DOI:10.3390/s22010019.

Jody, Y., Jinfei, W., Brigitte, L. and Yang, S., 2022. Nitrogen Estimation for Wheat Using UAV-Based and Satellite Multispectral Imagery, Topographic Metrics, Leaf Area Index, Plant Height, Soil Moisture, and Machine Learning Methods. *Nitrogen,* 2022, 3(1), 1-25. DOI:10.3390/nitrogen3010001.

Jose, A. F. G., Peter, L., Irene, B. S., Veerle, D., Geert, H., Isabel, R. R., Jose, L. A. and Shawn, C. K., 2020. Automatic wheat ear counting using machine learning based on RGB UAV imagery. *The Plant Journal,* (2020) 103, 1603–1613. DOI:10.1111/tpj.14799.

Juanjuan, Z., Tao, C., Lei, S., Weiwei, W., Zhen, N., Wei, G. and Xinming, M., 2022. Combining spectral and texture features of UAV hyperspectral images for leaf nitrogen content monitoring in winter wheat. *INTERNATIONAL JOURNAL OF REMOTE SENSING,* 2022, VOL. 43, NO. 7, 2335–2356. DOI:10.3389/fpls.2023.1272049.

Juanjuan, Z., Tao, C., Wei, G., Xin, X., Hongbo, Q., Yimin, X. and Xinming, M., 2021. Leaf area index estimation model for UAV image hyperspectral data based on wavelength variable selection and machine learning methods. *Plant Methods,* 17, 49 (2021). DOI:10.1186/s13007-021-00750-5.

Juncheng, M., Binhui, L., Lin, J., Zhicheng, Z., Yongfeng, W., Weihua, J.., 2023a. Field-scale yield prediction of winter wheat under different irrigation regimes based on dynamic fusion of multimodal UAV imagery. *International Journal of Applied Earth Observation and Geoinformation,* 118 (2023) 103292. DOI:10.1016/j.jag.2023.103292.

Juncheng, M., Yunxia, L., Keming, D., Feixiang, Z., Lingxian, Z., Zhihong, G., Weihua, J., 2020. Segmenting ears of winter wheat at flowering stage using digital images and deep learning. *Computers and Electronics in Agriculture,* 168 (2020) 105159. DOI:10.1016/j.compag.2019.105159.

Juncheng, M., Yongfeng, W., Binhui, L., Wenying, Z., Bianyin, W., Zhaoyang, C., Guangcai, W., and Anqiang, G., 2023b. Wheat Yield Prediction Using Unmanned Aerial Vehicle RGB-Imagery-Based Convolutional Neural Network and Limited Training Samples. *Remote Sens.,* 2023, 15(23), 5444; DOI:10.3390/rs15235444.

Kamilaris, A., & Prenafeta-Boldú, F. X. (2018). Deep learning in agriculture: A survey. *Computers and Electronics in Agriculture,* 147, 70-90. DOI:10.1016/j.compag.2018.02.016.

Kaur, S., Kakani, V. G., Carver, B., Jarquin, D., & Singh, A. (2024). Hyperspectral imaging combined with machine learning for high-throughput phenotyping in winter wheat. *The Plant Phenome Journal,* 7, e20111. DOI:10.1002/ppj2.20111.

Kaushal, S., Gill, H.S., Billah, M.M., Khan, S.N., Halder, J., Bernardo, A., Amand, P.S., Bai, G., Glover, K., Maimaitijiang, M., Sehgal, S.K., 2024. Enhancing the potential of phenomic and genomic prediction in winter wheat breeding using high-throughput phenotyping and deep learning. *Front. Plant Sci.,* 15:1410249. DOI: 10.3389/fpls.2024.1410249.

Kenichi, T., Noa, I. and Xiao, M., 2021. Prediction of plant-level tomato biomass and yield using machine learning with unmanned aerial vehicle imagery. Tatsumi et al. *Plant Methods,* (2021) 17:77. DOI:10.1186/s13007-021-00761-2.

Kianoosh, H., Hamed, G., Saleh, T., Victoria. N., Jonathan, C., Jamey, J., 2023. Application of UAS-Based Remote Sensing in Estimating Winter Wheat. *Phenotypic Traits and Yield During the Growing Season,* PFG (2023) 91:77–90. DOI: 10.1007/s41064-022-00229-5.

Li, X., Su, X., Li, J., Anwar, S., Zhu, X., Ma, Q., Wang,W., Liu, J., 2024a. Coupling Image-Fusion Techniques with Machine Learning to Enhance Dynamic Monitoring of Nitrogen Content in Winter Wheat from UAV Multi-Source. *Agriculture,* 2024, 14, 1797. DOI:10.3390/agriculture14101797.

Li, Z., Cheng, Q., Chen, L., Zhang, B., Guo, S., Zhou, X., Chen, Z., 2024b. Predicting Winter Wheat Yield with Dual-Year Spectral Fusion, Bayesian Wisdom, and Cross-Environmental Validation. *Remote Sens.,* 2024, 16, 2098. DOI:10.3390/rs16122098.

Liao, Z. Q., DAI, Y. L., Wang, H., Quirine, M. K,, Lu, J. S.,, Zhang, F. C., Li, Z.J., Fan J. L., 2023. A double-layer model for improving the estimation of wheat canopy nitrogen content from unmanned aerial vehicle multispectral imagery. *Journal of Integrative Agriculture,* 2023, 22(7): 2248–2270. DOI:10.1016/j.jia.2023.02.022.

Linglin, Z., Guozhang, P., Ran, M., Jianguo, M., Weibo, L., Binyuan, X., Zhengang, L. and Rui, S., 2021. Wheat Yield Prediction Based on Unmanned Aerial Vehicles-Collected Red–Green–Blue Imagery. *Remote Sens.,* 2021, 13(15), 2937. DOI:10.3390/rs13152937.

Liuchang X., Xinyuan S., Ketao W., Tong Z., Chenghao L., Junqi N., Xiaochen J., Jianqin H., Hailin F., 2025. Enhancing canopy nitrogen estimation in Torreya Grandis based on advanced SLIC-EVI and HMT-seCNN methods using hyperspectral UAV data. *Computers and Electronics in Agriculture,* Volume 231, April 2025, 109977. DOI:10.1016/j.compag.2025.109977.

Liu, Y., He, Y., Liu, F., Xu, L., Feng, X., Tsng, Y., Wang, Z., 2023. Application and market of agricultural sensor technology in China: current status and future perspectives. *Journal of Zhejiang University,* (Agric. & Life Sci.). 49（3）：293 ~304，2023. DOI:10.3785/j.issn.1008-9209.2022.04.062.

Liyuan, Z., Xiaoying, S., Yaxiao, N., Huihui, Z., Aichen, W., Yaohui, Z., Xingye, Z., Liping, C., Qingzhen, Z., 2024. Estimating Winter Wheat Plant Nitrogen Content by Combining Spectral and Texture Features Based on a Low-Cost UAV RGB System throughout the Growing Season. *Agriculture,* 2024, 14(3), 456; DOI:10.3390/agriculture14030456.

Lobell, D. B., 2015. The use of satellite data for crop yield gap analysis. *Field Crops Research,* 143, 56-64.

Lobell, D. B., Thau, D., Seifert, C., Engle, E., Little, B., 2015. A scalable satellite-based crop yield mapper. *Remote Sensing of Environment,* 164, 324-333. DOI:10.1016/j.rse.2015.04.021.

Lucas, C., Jordan, M., Yiannis, A., Jia, G., Mostafa, R. G., Md, A. B., 2022. Using UAV-based hyperspectral imaging and functional regression to assist in predicting grain yield and related traits in wheat under heat-related stress environments for the purpose of stable yielding genotypes. *Precision Agriculture,* (2022) 23:622–642. DOI:10.1007/s11119-021-09852-5.

Lukas, P., Anja, H., Ludwig, R., Johannes, S. S. and Patrick, O. N., 2022. UAV-Based Estimation of Grain Yield for Plant Breeding: Applied Strategies for Optimizing the Use of Sensors, Vegetation Indices, Growth Stages, and Machine Learning Algorithms. *Remote Sens.,* 2022, 14, 6345. DOI:10.3390/rs14246345.

Ma, X., Chen, P., & Jin, X., 2022. Predicting Wheat Leaf Nitrogen Content by Combining Deep Multitask Learning and a Mechanistic Model Using UAV Hyperspectral Images. *Remote Sensing,* 14(24), 6334. DOI:10.3390/rs14246334.

MOA (Ministry of Agriculture). (2020). *China Agricultural Development Report.* http://www.moa.gov.cn.

Mengxi, Z., Yu, L., Maodong, F., Cunjun, L., Zixiang, Z., Haoran, M., Enguang, X. and Yanmin, R., 2023. Combining spectral and texture feature of UAV image with plant height to improve LAI estimation of winter wheat at jointing stage. *Front. Plant Sci.,* 14:1272049. DOI:10.3389/fpls.2023.1272049.

Michael, M., Mariana, B., Mirco, B., Monica, P., Alfred, S., Andy, N., 2022. Field-level crop yield estimation with PRISMA and Sentinel-2. *ISPRS Journal of Photogrammetry and Remote Sensing,* 187 (2022) 191–210. DOI:10.1016/j.isprsjprs.2022.03.008.

Michael, S., Niels, L., Antje, G., Andreas, G. and Karl-Heinz, D., 2021. Early Detection of Stripe Rust in Winter Wheat Using Deep Residual Neural Networks. *Frontiers in Plant Science,* 2021, 12, 469689. DOI:10.3389/fpls.2021.469689.

Ministry of Agriculture and Rural Affairs. (2023). *China Agricultural Statistical Yearbook 2022.* Beijing: China Agriculture Press.

Ministry of Agriculture and Rural Affairs of the People's Republic of China, 2023. *Guiding Opinions on National Wheat Autumn and Winter Planting in 2023.* Available at: https://www.moa.gov.cn/gk/nszd_1/2023/202309/t20230922_6436990.htm.

National Bureau of Statistics. (2022). *China Statistical Yearbook 2021.* Beijing: China Statistics Press.

NDRC (National Development and Reform Commission). (2021). *National Agricultural Cost-Benefit Data.* https://www.ndrc.gov.cn/.

Nduku, L., Munghemezulu, C., Mashaba-Munghemezulu, Z., Masiza, W., Ratshiedana, P.E., Kalumba, A.M., Chirima, J.G., 2024. Field-Scale Winter Wheat Growth Prediction Applying Machine Learning Methods with Unmanned Aerial Vehicle Imagery and Soil Properties. *Land,* 2024, 13, 299. DOI:10.3390/land13030299.

Ning, L., Yapeng, W., Hengbiao, Z., Xia, Y., Yan, Z., Weixing, C., Tao, C., 2022. An assessment of multi-view spectral information from UAV-based color-infrared images for improved estimation of nitrogen nutrition status in winter wheat. *Precision Agriculture,* (2022) 23:1653–1674. DOI: 10.1007/s11119-022-09901-7.

Ning L., Wenhui W., Qiaofeng Z., Dong L., Xia Y., Yongchao T., Yan Z., Weixing C, Fred B., Shouyang L. Tao C., 2019. Estimation of Nitrogen Nutrition Status in Winter Wheat From Unmanned Aerial Vehicle Based Multi-Angular Multispectral Imagery. *Front. Plant Sci.,* 10:1601. DOI:10.3389/fpls.2019.01601.

Pocas, I., Cunha, M., Pereira, L. S., & Allen, R. G., 2014. Satellite-based evapotranspiration of a super-intensive olive orchard: Application of METRIC algorithms. *Biosystems Engineering,* 01 Dec 2014, 128:69-81. DOI:10.1016/j.biosystemseng.2014.06.019.

Poblete, T., Ortega-Farías, S., Moreno, M. A., & Bardeen, M., 2017. Artificial neural network to predict vine water status spatial variability using multispectral information obtained from an unmanned aerial vehicle (UAV). *Sensors,* 17(11), 2488. DOI:10.3390/s17112488

Qi, W., Xiaokai, C., Huayi, M., Huiling, M., Shiyu, J. and Qingrui, C., 2023. UAV Hyperspectral Data Combined with Machine Learning for Winter Wheat Canopy SPAD Values Estimation. *Remote Sens.,* 2023, 15(19), 4658; DOI:10.3390/rs15194658.

Quan, Y., Yuting, Z., Weilong, L., Jianjun, W., Weiling, W., Irshad, A., Guisheng, Z. and Zhongyang, H.., 2023a. Better Inversion of Wheat Canopy SPAD Values before Heading Stage Using Spectral and Texture Indices Based on UAV Multispectral Imagery. *Remote Sens.,* 2023, 15(20), 4935. DOI:10.3390/rs15204935.

Quan, Y., Yuting, Z., Weilong, L., Jianjun, W., Weiling, W., Irshad, A., Guisheng, Z. and Zhongyang, H., 2023b. Estimation of Winter Wheat SPAD Values Based on UAV Multispectral Remote Sensing. *Remote Sens.,* 2023, 15(14), 3595. DOI:10.3390/rs15143595.

Rabi, N. Sahoo, R. G. R., Shalini, G., Rajeev, R., Mahesh, C. M., Abir, D., Joydeep, M., Rajkumar, D., Abhishek, M., Anchal, D., Subhash, B., Pravin, K. U., Kapila, S., Sudhir, K., Mahesh, K., Viswanathan, C., Manoj, K., 2024. Drone remote sensing of wheat N using hyperspectral sensor and machine learning. *Precision Agriculture,* (2024) 25:704–728. DOI: 10.1007/s11119-023-10089-7.

Rajendra, P.S., Ram, L.R., Sudhir, K.S., 2020. Applications of Remote Sensing in Precision Agriculture: A Review. *Remote Sens.,* 2020, 12(19), 3136. DOI:10.3390/rs12193136.

Ramoelo, A., Skidmore, A. K., Cho, M. A., Mathieu, R., Heitkönig, I. M. A., Dudeni-Tlhone, N., & Schlerf, M., 2012. Regional estimation of savanna grass nitrogen using the red-edge band of the spaceborne RapidEye sensor. *International Journal of Applied Earth Observation and Geoinformation,* 19(1), 151-162. DOI:10.1016/j.jag.2012.05.009.

Rebecca, J. T., Daniel, K.Y. T., Anowarul, I. B., Smi, U., Richard, M. T., 2020. A phenotyping strategy for evaluating the high-temperature tolerance of wheat. *Field Crops Research,* 255 (2020) 107905. DOI:10.1016/j.fcr.2020.107905.

Revill, A., Myrgiotis, V., Florence, A., Hoad, S., Rees, R., MacArthur, A., & Williams, M., 2021. Combining Process Modelling and LAI Observations to Diagnose Winter Wheat Nitrogen Status and Forecast Yield. *Agronomy,* 11(2), 314. DOI:10.3390/agronomy11020314

Rodriguez-Galiano, V. F., Ghimire, B., Rogan, J., Chica-Olmo, M., & Rigol-Sanchez, J. P., 2012. An assessment of the effectiveness of a random forest classifier for land-cover classification. *ISPRS Journal of Photogrammetry and Remote Sensing,* 67, 93-104. DOI:10.1016/j.isprsjprs.2011.11.002.

Ruhua, L., Pei, Z., Zhaopeng, F., Jie, J., Jiancheng, W., Qiang, C., Yongchao, T., Yan, Z., Weixing, C., Xiaojun, L., 2023. Improving the spatial and temporal estimation of ecosystem respiration using multi-source data and machine learning methods in a rainfed winter wheat cropland. *Science of the Total Environment,* 871 (2023) 161967. DOI:10.1016/j.scitotenv.2023.161967.

Ryoya, T., Tsutomu, M., Takashi, S.T. T., 2023. Winter wheat yield prediction using convolutional neural networks and UAV-based multispectral imagery. *Field Crops Research,* 291 (2023) 108786. DOI:10.1016/j.fcr.2022.108786.

Sehijpreet, K., Vijaya, G. K., Brett, C., Diego, J., Aditya, S., Hyperspectral imaging combined with machine learning for high-throughput phenotyping in winter wheat. *The Plant Phenome Journal.* DOI: 10.1002/ppj2.20111.

Seishi, N., 2022. High-throughput field crop phenotyping: current status and challenges. *Breeding Science,* 72: 3–18 (2022). DOI:10.1270/jsbbs.21069.

Shao, H. B., Chu, L. Y., Jaleel, C. A., & Zhao, C. X. (2009). Water-deficit stress-induced anatomical changes in higher plants. *Comptes Rendus Biologies,* 331(3), 215-225. DOI:10.1016/j.crvi.2008.11.003.

Shaohua, Z., Jianzhao, D., Xinghui, Q., Yuezhi, G., Li, H., Linru, L., Tiancai, G., Wei, F., 2024a. Combining spectrum, thermal, and texture features using machine learning algorithms for wheat nitrogen nutrient index estimation and model transferability analysis. *Computers and Electronics in Agriculture,* Volume 222, July 2024, 109022. DOI:10.1016/j.compag.2024.109022.

Shaohua, Z., Li, H., Jian-Zhao, D., Shao-Long, Z., Tian-Cong, Y., U. R. S. Schulthess, Tian-Cai, G., Chen-Yang, W., Wei, F., 2024b. Aboveground wheat biomass estimation from a low-altitude UAV platform based on multimodal remote sensing data fusion with the introduction of terrain factors. *Precision Agriculture,* (2024) 25:119–145. DOI:10.1007/s11119-023-10062-4.

Shaozhong K., Xinmei H., Taisheng D., Ling T., Xiaoling S., Hongna L., Xiaolin L., Zailin H., Sien L., Risheng D., 2017. Improving agricultural water productivity to ensure food security in China under changing environment: From research to

practice. *Agricultural Water Management,* Volume 179, 2017, Pages 5-17, ISSN 0378-3774. DOI:10.1016/j.agwat.2016.05.007.

Shilei, L., Fangjie, L., Maofang, G., Zhaoliang, L., Pei, L., Sibo, D. and Jianqiang, R., 2021. A New Method for Winter Wheat Mapping Based on Spectral Reconstruction Technology. *Remote Sens.,* 2021, 13(9), 1810. DOI:10.3390/rs13091810.

Shu, M., Wang, Z., Guo, W., Qiao, H., Fu, Y., Guo, Y., Wang, L., Ma, Y., Gu, X., 2024. Effects of Variety and Growth Stage on UAV Multispectral Estimation of Plant Nitrogen Content of Winter Wheat. *Agriculture,* 2024, 14, 1775. DOI:10.3390/agriculture14101775.

Shuaipeng, F., Muhammad, A. H., Yonggui, X., Xin, S., Zhen, C., Qian, C., Fuyi, D., Riqiang, C., Yuntao, M., 2023. UAV based multi sensor data fusion and machine learning algorithm for yield prediction in wheat. *Precision Agriculture,* (2023) 24:187–212. DOI:10.1007/s11119-022-09938-8.

Shuaipeng, F., Muhammad, A. H., Yuntao, M., Meiyan, S., Qian, C., Zongpeng, L., Zhen, C. and Yonggui, X., 2021. Entropy Weight Ensemble Framework for Yield Prediction of Winter Wheat Under Different Water Stress Treatments Using Unmanned Aerial Vehicle-Based Multispectral and Thermal Data. *Front Plant Sci.,* 2021 Dec 20:12:730181. DOI:10.3389/fpls.2021.730181.

Shutao L., Weiwei S., Leyuan F., Yushi C., Pedram G., Jón A.B., 2019. Deep learning for hyperspectral image classification: An overview. *IEEE Transactions on Geoscience and Remote Sensing,* 59(9), 7410-7431. DOI:10.1109/TGRS.2019.2907932.

Shweta, P., Patel, N. R. and Ajit, G., 2023. Machine Learning-Driven Remote Sensing Applications for Agriculture in India—A Systematic Review. *Agronomy,* 2023, 13(9), 2302. DOI:10.3390/agronomy13092302.

Siqi, Y., Ling, H., Haobo, W., Huazhong, R., Hongbo, Q., Peijun, L. and Wenjie, F., 2021. Integration of Crop Growth Model and Random Forest for Winter Wheat Yield Estimation From UAV Hyperspectral Imagery. *IEEE Journal of Selected Topics in Applied Earth Observations and Remote Sensing,* vol. 14, pp. 6253-6269, 2021. DOI: 10.1109/JSTARS.2021.3089203.

Songlin, Y., Shanshan, L., Bing, Z., Ruyi, Y., Cunjun, L., Jinkang, H., Shengwei, L., Enhui, C., Zihang, L., and Dailiang, P., 2023. Accurate estimation of fractional vegetation cover for winter wheat by integrated unmanned aerial systems and satellite images. *Front. Plant Sci.,* 27 September 2023 Sec. Technical Advances in Plant Science, Volume 14 – 2023. DOI:10.3389/fpls.2023.1220137.

Sumanta, D., Jack, C., Armando, A., Malini, R. C., Scott, C., Neal, W. M., Yash, P. D., 2021. Evaluation of water status of wheat genotypes to aid prediction of yield on sodic soils using UAV-thermal imaging and machine learning. *Agricultural and Forest Meteorology,* 307 (2021) 108477. DOI:10.1016/j.agrformet.2021.108477.

Tadesse, W., Halila, H., Jamal, M., El-Hanafi, S., Assefa, S., Oweis, T.., Baum, M., 2017. Role of sustainable wheat production to ensure food security in the cwana

region. *Journal of Experimental Biology and Agricultural Sciences,* August - 2017; Volume – 5(Spl-1- SAFSAW). https://hdl.handle.net/20.500.11766/8067.

Tanzeel U. R., Md. S. M., Young K. C., Jian J., 2019. Jaemyung S., Current and future applications of statistical machine learning algorithms for agricultural machine vision systems. *Computers and Electronics in Agriculture,* Volume 156, 2019, Pages 585-605, ISSN 0168-1699, DOI:10.1016/j.compag.2018.12.006.

Thenkabail, P. S., Lyon, J. G., 2016. *Hyperspectral indices and image classifications for agriculture and vegetation.* CRC Press.

Tian H., Zhihua L., Rong H., Mi T., Zhiwei W., Ming L., Guanghui C., Guanghui C., 2024. Convolutional Neural Network-Based Estimation of Nitrogen Content in Regenerating Rice Leaves. *Agronomy,* 2024, 14(7), 1422. DOI:10.3390/agronomy14071422.

Tianxiang, Z., Jinya, S., Cunjia, L., Wen-Hua, C., 2019. Bayesian calibration of AquaCrop model for winter wheat by assimilating UAV multi-spectral images. *Computers and Electronics in Agriculture,* 167 (2019) 105052. DOI:10.1016/j.compag.2019.105052.

Tianxiang, Z., Jinya, S., Cunjia, L., Wen-Hua, C., 2021. State and parameter estimation of the AquaCrop model for winter wheat using sensitivity informed particle filter. *Computers and Electronics in Agriculture,* 180 (2021) 105909. DOI:10.1016/j.compag.2020.105909.

Tucker, C. J., 1979. Red and photographic infrared linear combinations for monitoring vegetation. *Remote Sensing of Environment,* 8(2), 127-150. DOI:10.1016/0034-4257(79)90013-0.

Tuia, D., Persello, C., & Bruzzone, L., 2016. Domain adaptation for the classification of remote sensing data: An overview of recent advances. *IEEE Geoscience and Remote Sensing Magazine,* 4(2), 41-57.

Wang, J., Yin, Q., Cao, L., Zhang, Y., Li, W., Wang, W., Zhou, G., Huo, Z., 2024. EnhancingWinter Wheat Soil–Plant Analysis Development Value Prediction through Evaluating Unmanned Aerial Vehicle Flight Altitudes, Predictor Variable Combinations, and Machine Learning Algorithms. *Plants,* 2024, 13, 1926. DOI:10.3390/plants13141926.

Wang, P., Wang, Y., Tian, H., Wang, J., Liu, J., Quan, W., 2023. Interpretability on Yield Estimation of Winter Wheat Based on LightGBM. *Transactions of the Chinese Society for Agricultural Machinery,* 2023,54(12):197-206. DOI:410.6041/j.issn.1000-1298.2023.12.018.

Waldner, F., Chen, Y., Lawes, R., & Hochman, Z., 2019. Needle in a haystack: mapping rare and infrequent crops using satellite imagery and data balancing methods. *Remote Sensing of Environment,* 233, 111375. DOI:10.1016/j.rse.2019.111375.

Wei, W., Yukun, C., Yi, R., Zhihui, Z. and Hongwei, G., 2022. Prediction of Chlorophyll Content in Multi-Temporal Winter Wheat Based on Multispectral

and Machine Learning. *Front. Plant Sci.,* 13:896408. DOI:10.3389/fpls.2022.896408.

Wei, W., Na, S., Bin, B., Hao, W., Yukun, C., Hongwei, G., JiKun, S., JinPing, Z., Zhiyuan, P., SongTing, Q., Wanyin, Z., 2024. Prediction of wheat SPAD using integrated multispectral and support vector machines. *Front. Plant Sci.,* 15:1405068. DOI:10.3389/fpls.2024.1405068.

Weilong, L., Jianjun, W., Yuting, Z., Quan, Y., Weiling, W., Guisheng, Z. and Zhongyang, H., 2023. Combining Texture, Color, and Vegetation Index from Unmanned Aerial Vehicle Multispectral Images to Estimate Winter Wheat Leaf Area Index during the Vegetative Growth Stage. *Remote Sens.,* 2023, 15(24), 5715. DOI:10.3390/rs15245715.

Weiss, M., Jacob, F., Duveiller, G., 2020. Remote sensing for agricultural applications: a meta‐review. *Remote Sensing of Environment,* 236, 111402. DOI:10.1016/j.rse.2019.111402.

WHO, 2023. *The state of food security and nutrition in the world 2023.* Available at: https://www.who.int/publications/m/item/the-state-of-food-security-and-nutrition-in-the-world-2023.

Worasit, S., Arron, H. C., Michael, O. P., Kyall, H., Vadim, J., Sindhuja, S., 2024. Effect of high-resolution satellite and UAV imagery plot pixel resolution in wheat crop yield prediction, *International Journal of Remote Sensing,* 45:5, 1678-1698, DOI: 10.1080/01431161.2024.2313997.

World Bank, 2020. *Deep Wells and Prudence: Towards Pragmatic Management of Groundwater in the North China Plain.* Washington, DC: World Bank Publications.

Xiaokai, C., Fenling, L., Botai, S. and Qingrui, C., 2023. Estimation of Winter Wheat Plant Nitrogen Concentration from UAV Hyperspectral Remote Sensing Combined with Machine Learning Methods. *Remote Sens.,* 2023, 15(11), 2831. DOI:10.3390/rs15112831

Xiaofeng, C., Yulin, L., Rui, Y., Dejun, H. and Baofeng, S., 2021 A Comparison of UAV RGB and Multispectral Imaging in Phenotyping for Stay Green of Wheat Population. *Remote Sens.,* 2021, 13(24), 5173. DOI:10.3390/rs13245173.

Xin, Z., Liangxiu, H., Yingying, D., Yue, S., Wenjiang, H., Lianghao, H., Pablo, G. M., Huiqin, M., Huichun, Y. and Tam, S., 2019. A Deep Learning-Based Approach for Automated Yellow Rust Disease Detection from High-Resolution Hyperspectral UAV Images. *Remote Sens.,* 2019, 11(13), 1554. DOI:10.3390/rs11131554.

Xiu, J., Tong, Z., Lianglong, W., Qing, L., Shaowen, L., Xiaodan, Z., Jie, L., Yuan, R., 2023. Using an optimised neural architecture search for predicting the quantum yield of photosynthesis of winter wheat. *Biosystems Engineering,* Volume 230, June 2023, Pages 442-457. DOI:10.1016/j.biosystemseng.2023.04.015.

Xu, J., Zhu, Y., Zhong, R., Lin, Z., Xu, J., Jiang, H., Huang, J., Li, H., Lin, T., 2020. DeepCropMapping: A multi-temporal deep learning approach with improved spatial generalizability for dynamic corn and soybean mapping. *Remote Sensing of Environment,* Volume 247, 2020, 111946, ISSN 0034-4257. DOI:10.1016/j.rse.2020.111946.

Xuguang, S., Baoyuan, Z., Menglei, D., Cuijiao, J., Kai, M., Boyi, T., Kejiang, L., Hongkai, D., Limin, G., Wenchao, Z., Xiaohe, G., 2024. Accurate irrigation decision-making of winter wheat at the filling stage based on UAV hyperspectral inversion of leaf water content, *Agricultural Water Management,* Volume 306, 2024, 109171, ISSN 0378-3774. DOI:10.1016/j.agwat.2024.109171.

Yafeng, L., Changchun, L., Qian, C., Li, C., Zongpeng, L., Weiguang, Z., Bohan, M., Zhen, C., 2024. Precision estimation of winter wheat crop height and above-ground biomass using unmanned aerial vehicle imagery and oblique photoghraphy point cloud data. *Front. Plant Sci.,* 15:1437350. DOI:10.3389/fpls.2024.1437350.

Yamashita, H., Sonobe, R., Hirono, Y.,2020. Dissection of hyperspectral reflectance to estimate nitrogen and chlorophyll contents in tea leaves based on machine learning algorithms. *Sci.,* Rep 10, 17360 (2020). DOI:10.1038/s41598-020-73745-2.

Yan, G., Jia, H., Jingyi, H., Yuhang, J., Shaobo, X., Laigang, W., Shimin, L. and Guoqing, Z., 2022. Effects of the Spatial Resolution of UAV Images on the Prediction and Transferability of Nitrogen Content Model for Winter Wheat. *Drones,* 2022, 6(10), 299. DOI:10.3390/drones6100299.

Yantong, W., Wenbo, X., Hai, H. and Jianxi, H., 2022. Bayesian Posterior-Based Winter Wheat Yield Estimation at the Field Scale through Assimilation of Sentinel-2 Data into WOFOST Model. *Remote Sens.,* 2022, 14(15), 3727. DOI:10.3390/rs14153727.

Yang, L., Bo, Z., Jizhong, W., Yanjun, L. and Yanwei, Y., 2023. Winter Wheat Yield Estimation Based on Multi-Temporal and Multi-Sensor Remote Sensing Data Fusion. *Agriculture,* 2023, 13(12), 2190. DOI:10.3390/agriculture13122190.

Yang, J., Wu, J., Liu, L., Zhou, H., Gong, A., Han, X., & Zhao, W., 2020. Responses of Winter Wheat Yield to Drought in the North China Plain: Spatial–Temporal Patterns and Climatic Drivers. *Water,* 12(11), 3094. DOI:10.3390/w12113094.

Yang, X., Gao, F., Yuan, H., Cao, X., 2024. Integrated UAV and Satellite Multi-Spectral for Agricultural Drought Monitoring of Winter Wheat in the Seedling Stage. *Sensors,* 2024, 24, 5715. DOI:10.3390/s24175715.

Yoseline, A. and Matthew, F. M., 2022. Machine Learning Strategies for the Retrieval of Leaf-Chlorophyll Dynamics: Model Choice, Sequential Versus Retraining Learning, and Hyperspectral Predictors. *Frontiers in Plant Science,* March 2022, Volume 13, Article 722442. DOI:10.3389/fpls.2022.722442.

Yu, K., Belwalkar, A., Wang, W., Hu, Y., Hunegnaw, A., Abdul, N., Thorsten, R., Li, F., Jia, L., Lammert, K., Miao, Y., Félicia N. T., 2025. UAV hyperspectral remote sensing for crop nitrogen monitoring: progress, challenges, and perspectives. *Smart Agricultural Technology,* Volume 12, 2025, 101507, ISSN 2772-3755. DOI:10.1016/j.atech.2025.101507.

Yu, Y., Si, X., Hu, C., Zhang, J., 2019. A Review of Recurrent Neural Networks: LSTM Cells and Network Architectures. *Neural Comput.,* 2019 Jul;31(7):1235-1270. DOI:10.1162/neco_a_01199.

Yuan W., Dejian W., Gang Z., Jun W., 2013. Estimating nitrogen status of rice using the image segmentation of G-R thresholding method. *Field Crops Research,* 149, 33-39. DOI:10.1016/j.fcr.2013.04.007.

Yuanyuan, T., Yuzhuang, Z., Minghan, C. and Chengming, S., 2023. Comprehensive Growth Index (CGI): A Comprehensive Indicator from UAV-Observed Data for Winter Wheat Growth Status Monitoring. *Agronomy,* 2023, 13(12), 2883. DOI:10.3390/agronomy13122883.

Yue, L., Yuxin, M., Jing, Z., Davide, C., Songyang, L., Xiaojun, L., Yongchao, T., Yan, Z., Weixing, C. and Qiang, C., 2022. Improving Estimation of Winter Wheat Nitrogen Status Using Random Forest by Integrating Multi-Source Data Across Different Agro-Ecological Zones. *Front. Plant Sci.,* 13:890892. DOI:10.3389/fpls.2022.890892.

Yuncai, H., Harald, H. and Urs, S., 2016. Comparative performance of spectral and thermographic properties of plants and physiological traits for phenotyping salinity tolerance of wheat cultivars under simulated field conditions. *Funct Plant Biol.,* 2016 Feb;44(1):134-142. DOI:10.1071/FP16217.

Zang, H., Su, X., Wang, Y., Li, G., Zhang, J., Zheng, G., Hu, W., Shen, H., 2024. Automatic grading evaluation of winter wheat lodging based on deep learning. *Front. Plant Sci.,* 15:1284861. DOI:10.3389/fpls.2024.1284861.

Zarco-Tejada, P. J., González-Dugo V., Berni J.A.J., 2019. Fluorescence, temperature and narrow-band indices acquired from a UAV platform for water stress detection using a micro-hyperspectral imager and a thermal camera. *Remote Sensing of Environment,* 117, 322-337. DOI:10.1016/j.rse.2011.10.007.

Zhang, C., Filella, I., Garbulsky, M. F., Peñuelas, J.,2016a. Affecting factors and recent improvements of the photochemical reflectance index (PRI) for remotely sensing foliar, canopy and ecosystemic radiation-use efficiencies. *Remote Sens.,* 2016, 8(9), 677. DOI:10.3390/rs8090677.

Zhang, L., Wang, X., Zhang, H., Zhang, B., Zhang, J., Hu, X., Du, X., Cai, J., Jia,W., Wu, C., 2024a. UAV-Based Multispectral Winter Wheat Growth Monitoring with Adaptive Weight Allocation. *Agriculture,* 2024, 14, 1900. DOI:10.3390/agriculture14111900.

Zhang, L., Wang, A., Zhang, H., Zhu, Q., Zhang, H., Sun,W., Niu, Y., 2024b. Estimating Leaf Chlorophyll Content of Winter Wheat from UAV Multispectral Images Using Machine Learning Algorithms under Different Species, Growth

Stages, and Nitrogen Stress Conditions. *Agriculture,* 2024, 14, 1064. https://doi.org/10.3390/agriculture14071064.

Zhang, SH., He, L., Duan, JZ. et al., 2024c. Aboveground wheat biomass estimation from a low-altitude UAV platform based on multimodal remote sensing data fusion with the introduction of terrain factors. *Precision Agric.,* 25, 119–145 (2024). DOI:10.1007/s11119-023-10062-4

Zhang, W., Cao, G., Li, X., Zhang, H., Wang, C., Liu, Q., Chen, X., Cui, Z., Shen, J., Jiang, R., Mi, G., Miao, Y., Zhang, F., Dou, Z., 2016b. Closing yield gaps in China by empowering smallholder farmers. *Nature,* 2016 Sep 29;537(7622):671-674. DOI:10.1038/nature19368.

Zhang, X., Chen, S., Sun, H., Pei, D., & Wang, Y. (2013). Dry matter, harvest index, grain yield and water use efficiency as affected by water supply in winter wheat. *Irrigation Science,* 31(3), 393-404. DOI:10.1007/s00271-011-0306-0.

Zhang Y., Yang, Q., 2022. A Survey on Multi-Task Learning. *IEEE Transactions on Knowledge and Data Engineering,* vol. 34, no. 12, pp. 5586-5609, 1 Dec. 2022. DOI: 10.1109/TKDE.2021.3070203.

Zhang Y, Yang Y, Zhang Q, et al., 2023. Toward Multi-Stage Phenotyping of Soybean with Multimodal UAV Sensor Data: A Comparison of Machine Learning Approaches for Leaf Area Index Estimation. *Remote Sens.,* 2023, 15, 7.

Zhang, Z., Dou, G., Zhao, X., Gao, Y., Liu, S., Qin, A., 2024d. Inversion of CropWater Content Using Multispectral Data and Machine Learning Algorithms in the North China Plain. *Agronomy,* 2024, 14, 2361. DOI:10.3390/agronomy14102361.

Zhao, G., Chang, X., Wang, D., Tao, Z., Wang, Y., Yang, Y., Zhu, Y., 2018. General Situation and Development of Wheat Production. *Crops,* 2018, (4): 1-7. DOI:10.16035/j.issn.1001-7283.2018.04.001.

Zhao, H., Wang, J., Guo, J., Hui, X., Wang, Y., Cai, D., Yan, H., 2024. Detecting Water Stress in Winter Wheat Based on Multifeature Fusion from UAV Remote Sensing and Stacking Ensemble Learning Method. *Remote Sens.,* 2024, 16, 4100. DOI:10.3390/rs16214100.

Zhengang, L., Ran, M., Jianguo, M., Linglin, Z., Meiyv, W., Binyuan, X., Renjie, G., Rui, S., Feng, Z., 2021. Modeling of winter wheat fAPAR by integrating Unmanned Aircraft Vehicle-based optical, structural and thermal measurement. *International Journal of Applied Earth Observations and Geoinformation,* 102 (2021) 102407. DOI:10.1016/j.jag.2021.102407.

Zhi-Hua, Z., 2017. A brief introduction to weakly supervised learning. *National Science* Review 5: 44–53, 20. DOI:10.1093/nsr/nwx106.

Zhikai, C., Xiaobo, G., Yadan, D., Zhihui, Z., Wenlong, L., Xiaobo, Z., Wenjing, C., Tian, C., 2024. Spectral purification improves monitoring accuracy of the comprehensive growth evaluation index for film-mulched winter wheat. *Journal*

of Integrative Agriculture 2024, 23(5): 1523–1540. DOI:10.1016/j.jia.2023.05.036.

Zongpeng, L., Xinguo, Z., Qian, C., Shuaipeng, F. and Zhen, C., 2023a. A Machine-Learning Model Based on the Fusion of Spectral and Textural Features from UAV Multi-Sensors to Analyse the Total Nitrogen Content in Winter Wheat. *Remote Sens.,* 2023, 15(8), 2152. DOI:10.3390/rs15082152.

Zongpeng, L., Zhen, C., Qian, C., Fuyi, D., Ruixiu, S., Xiuqiao, H. and Honggang, X., 2022. UAV-Based Hyperspectral and Ensemble Machine Learning for Predicting Yield in Winter Wheat. *Agronomy,* 2022, 12(1), 202. DOI:10.3390/agronomy12010202.

Zongpeng, L., Zhen, C., Qian, C., Shuaipeng, F. and Xinguo, Z., 2023b. Deep Learning Models Outperform Generalized Machine Learning Models in PredictingWinter Wheat Yield Based on Multispectral Data from Drones. *Drones,* 2023, 7(8), 505. DOI:10.3390/drones7080505.

Zu, J., Yang, H., Wang, J., Cai, W., Yang, Y., 2024. Inversion of winter wheat leaf area index from UAV multispectral images: classical vs. deep learning approaches. *Front. Plant Sci.,* 15:1367828. DOI:10.3389/fpls.2024.1367828.